A MODIFIED TUNED VIBRATION ABSORBER

FOR LIGHT SECONDARY STRUCTURES

A MODIFIED TUNED VIBRATION ABSORBER FOR LIGHT SECONDARY STRUCTURES

By

SHILIN (STEPHEN) MA, B. Sc.

A Thesis

Submitted to the School of Graduate Studies

in Partial Fulfilment of the Requirements

for the Degree

Master of Engineering

McMaster University

MASTER OF ENGINEERING — McMASTER UNIVERSITY

(Mechanical Engineering) — Hamilton, Ontario

TITLE: A Modified Tuned Vibration Absorber for Light Secondary Structures

AUTHOR: Shilin (Stephen) Ma, B. Sc.,

(Huazhong University of Science & Technology, China)

SUPERVISOR: Dr. S. E. Semercigil

NUMBER OF PAGES: xiii, 115

ABSTRACT

Secondary structures may have to endure severe vibration amplitudes under the influence of the primary structures on which they are mounted. A series of numerical case studies are presented in this thesis to investigate the effectiveness of a passive vibration controller which combines a conventional tuned absorber with an impact damper, to attenuate the excessive vibration amplitudes of light secondary structures. In addition, experimental measurements are reported for some selective cases and comparisons are made with numerical predictions. This suggested configuration seems to suit ideally as an add-on enhancer for existing conventional absorbers. Most of the Results are presented for random white noise excitation, and a few representative transient vibration cases are also studied.

ACKNOWLEDGMENTS

I would like to express my very sincere gratitude to my research supervisor Dr. S. E. Semercigil for his patient guidance and continuous encouragement throughout the entire course of this work.

This thesis is dedicated to my wife, Sherry, for giving me the support and for providing me the time required to accomplish it.

I would like to thank Mr. Joe Verhaeghe and Mr. Ron Lodewyks for their assistance in the experimental aspects of this project.

The financial support from the Mechanical Engineering Department is gratefully acknowledged.

TABLE OF CONTENTS

LIST OF FIGURES

CHAPTER 1

INTRODUCTION

A modified tuned vibration absorber is studied for the application on light secondary structures. The new passive vibration controller combines a conventional tuned absorber with an impact damper. The studies consist of dynamic modeling, numerical simulation and experimental verification.

Term "secondary structure" is used generically for light systems which are under some influence of larger primary systems. Therefore, response of a light secondary system is an indirect one through the dynamic response of the primary system to an external disturbance. Flexibly mounted machinery, transport of delicate cargo or the piping system in buildings may be envisaged as examples of secondary structures. Prediction and control of the excessive dynamic response of secondary structures have attracted significant attention in the literature [1-5]. A new approach of combining two conventional passive controllers is investigated in this thesis.

Tuned vibration absorbers have been used effectively to control excessive vibrations

of resonant systems [5,6]. A tuned absorber is an auxiliary oscillator added to the primary system to be controlled. The purpose here is to interact strongly with the primary system and to absorb the energy input from the external disturbance. Control is accomplished by tuning the parameters of the auxiliary oscillator so that an opposite force to the external disturbance is generated by intentionally resonating the absorber. Control may be very effective on restraining vibration amplitudes at the tuning frequency. However, effectiveness of a conventional tuned absorber deteriorates rapidly as the frequency of oscillations differs from this critical tuning frequency.

Many practical applications expose dynamic systems to wide-band excitations, rather than single-frequency excitations. Naturally, a passive conventional tuned absorber is inadequate for such cases. Some other means are required to improve the performance of the conventional tuned absorber. Active interference to maintain the resonance condition for the auxiliary absorber system promises to be effective for varying frequencies [7]. However, the approach taken in this study is to attempt to improve the performance by passive means only. Passive systems have the unquestionable advantage of simplicity and robustness, provided that they are effective. It has been demonstrated that the effectiveness of a passive tuned absorber could be enhanced significantly if another passive vibration controller, an impact damper, is used to complement the tuned absorber [8, 9].

An impact damper is a loose rigid mass placed in a container which is secured to a

resonant system to be controlled. The dimensions of the container are chosen so that there is an intentional clearance around the impact damper to allow intermittent collisions. Hence, an impact damper is another passive vibration controller which works on the principle of generating an intermittent control force through intentional collisions. Each collision dissipates some energy and imposes an exchange of momentum. As a result of this exchange of momentum, the smaller impact damper reverses its direction of motion. On the other hand, the larger primary mass only slows down due to the momentum lost to the damper. Control is the consequence of this slowing of the primary mass leading to a smaller excursion amplitude. An impact damper's effectiveness largely depends upon the proper choice of the clearance. Reference 10 outlines the general approach in designing an impact damper, presents information in the form of design charts and lists significant publications.

An impact damper is used in this study to enhance the vibration control ability of a tuned absorber. Impact damper is placed in the tuned absorber to control the secondary system. As mentioned earlier, the concept of using these two passive controllers to complement each other's deficiencies has been introduced in References 8 and 9. Therefore, the purpose of this thesis is to extend its use in secondary structures and to provide performance charts for potential practical applications.

The focus of Chapter 2, Chapter 3 and Chapter 4 is on secondary structures under wide band random excitation. Specifically, Chapter 2 presents the dynamic model and a series

of numerical results and Chapter 3 demonstrates the experimental results for one representative physical structure. In Chapter 4, the new controller is modified by tuning the natural frequency of the absorber, which is part of the new controller, off the natural frequency of the system to be controlled. Then the effects of off-tuning are presented for representative cases. Chapter 5 shows the performance of the new controller for secondary structures under transient excitation. Chapter 6 consists of the conclusions of this thesis and some recommendations for using the new controller. In addition, the computer program used for the numerical simulations in this thesis is listed in Appendix with input and output examples.

CHAPTER 2

AN NUMERICAL STUDY OF THE NEW VIBRATION CONTROLLER ON SECONDARY STRUCTURES UNDER RANDOM EXCITATION

2.1 INTRODUCTION

In this chapter, a 4 Degree-Of-Freedom (4DOF) dynamic model was developed to represent a secondary structure controlled by a new vibration controller which consisted of a conventional tuned absorber and an impact damper (a modified tuned vibration absorber). Based on this primary system - secondary system - absorber - impact damper model, a computer program (Appendix) was designed to simulate the dynamic responses of this model under wide band random excitation. A series of case studies were performed to investigate the effectiveness of the combined controller to the secondary system.

2.2 NUMERICAL SIMULATIONS

The model used in numerical simulations is shown in Figure 2.1 schematically. In this 4 Degree-Of-Freedom (4DOF) model, the first oscillator (m_1, c_1, k_1), represents the primary

system excited by the disturbance F(t). The smaller secondary system (m_2, c_2, k_2) is mounted on the primary system. Attention will be mostly focused on this secondary system to restrain its response as much as possible with the new controller (a combination of a tuned absorber and an impact damper). The tuned absorber (m_3, c_3, k_3) is the auxiliary oscillator attached to m_2. Finally, the rigid mass m_4 is the impact damper, which is placed in a cavity of m_3 with a total clearance of d.

The differential equations of motion of the 3DOF oscillator (m_1, m_2 and m_3) between collisions are

$$m_1\frac{d^2x_1}{dt^2}+(c_1+c_2)\frac{dx_1}{dt}+(k_1+k_2)x_1-c_2\frac{dx_2}{dt}-k_2x_2=F(t) \tag{1}$$

$$m_2\frac{d^2x_2}{dt^2}+(c_2+c_3)\frac{dx_2}{dt}+(k_2+k_3)x_2-c_2\frac{dx_1}{dt}-k_2x_1=0 \tag{2}$$

$$m_3\frac{d^2x_3}{dt^2}+c_3\frac{dx_3}{dt}+k_3x_3-c_3\frac{dx_2}{dt}-k_3x_2=0 \tag{3}$$

,whereas the impact damper experiences a constant velocity motion resulting

$$m_4 \frac{d^2 x_4}{dt^2} = 0 \quad . \tag{4}$$

Numerical procedure consisted of using a standard fourth order Runge-Kutta finite difference scheme to integrate all four equations of motion simultaneously until a contact between m_3 and m_4 was established. A time step of smaller than 1/100 of the natural period of the primary system was used to ensure the stability of integration. A collision was assumed to take place when the difference between the two coordinates $x_3(t)$ and $x_4(t)$, was obtained to be smaller than one millionth of the total clearance, d, in Figure 2.1. Iteration on the time step was performed by simple Bisection to locate the instant of contact.

Standard instantaneous collision assumption was used to implement the energy dissipation and momentum transfer [8]. Each collision resulted in an incremental change of velocities of the impact damper and the tuned absorber according to

$$\frac{dx_{3+}}{dt} = \frac{(1-\mu e)}{(1+\mu)} \frac{dx_{3-}}{dt} + \frac{\mu(1+e)}{(1+\mu)} \frac{dx_{4-}}{dt} \tag{5}$$

and

$$\frac{dx_{4+}}{dt} = \frac{(1+e)}{(1+\mu)} \frac{dx_{3-}}{dt} + \frac{(\mu-e)}{(1+\mu)} \frac{dx_{4-}}{dt} \quad , \tag{6}$$

where μ is the mass ratio (m_4/m_3) and e is the coefficient of restitution. Equations 5 and 6 may be obtained easily from the simultaneous solution of the conservation of linear momentum (before and after a collision) and from the definition of the coefficient of restitution:

$$e = -\frac{\frac{dx_{4+}}{dt} - \frac{dx_{3+}}{dt}}{\frac{dx_{4-}}{dt} - \frac{dx_{3-}}{dt}} \quad , \tag{7}$$

where subscripts - and + indicate the instances immediately before and after a collision. Consistent with the instantaneous collision assumption, the displacements of m_3 and m_4 were left unchanged. A collision caused no change in the primary and the secondary systems. Numerical integration always started with zero initial conditions. After every collision, integration resumed with new initial conditions until a new contact was located.

The random white noise excitation was approximated by using the expression suggested in reference 11, which can be expressed as

$$F(t) = \sqrt{2} \sum_{k=1}^{N} \left[S_o(\omega_k) \right]^{\frac{1}{2}} Cos\ (\omega_k' t + \Phi_k) \quad , \tag{8}$$

where $S_o(\omega_k)$ is the desired power spectral density of F(t) with N equally spaced spectral components, $\omega_k=\Delta\omega\ (\ k-1/2\ ),\ \ \Delta\omega=\ \omega_u/N,\ \ \omega_k^{/}=\omega_k+\delta\omega.$ $\delta\omega$ and Φ_k are random variables uniformly distributed over the ranges $\pm 0.05\ \Delta\omega$ and 0 to 2π, respectively. $S_o(\omega_k)$ was taken to be unity. The cut-off frequency of the excitation, ω_u, was set to be twice as large as the natural frequency of the uncontrolled primary system with 100 spectral components (N).

Performance of the new controller was evaluated by comparing the Root Mean Square (RMS) displacement of the secondary structure between the cases with and without the presence of the impact damper. In other words, the comparison was made between the secondary structure controlled by the new controller and that controlled by the conventional tuned absorber. Previous work [28] has shown that a conventional tuned absorber has positive, though limited, effect on the secondary structures under random excitation in terms of vibration reduction. Therefore, in this chapter, attention was focused on the investigation of the improvement of adding an impact damper.

RMS averages were calculated after every time step of integration until they were observed to reach stationary state. A 1000 second simulation was generally found to be long enough to obtain stationary RMS averages (where the fundamental frequency of the primary system was 1 rad./s). Hence, one 1000 second long sequence of values for F(t), was

generated from equation 8 and the same sequence was used invariably for each case of simulation, in order to maintain a consistent excitation for comparison purposes.

Case studies were performed for mass ratios between the secondary and the primary systems (m_1/m_2) ranging from 1 to 1000. Smaller ratios represented cases in which the primary and the secondary systems were comparable in size, whereas large ratios represented light resonant secondary structures in buildings. The fundamental frequency of the primary system $(k_1/m_1)^{1/2}$ was set to be unity (1 rad./s). The natural frequency of the secondary system $(k_2/m_2)^{1/2}$ was taken to be identical with that of the primary system, as this case represented the strongest interaction between these systems and hence the most critical case for the secondary structure [12,13]. The critical damping ratio of the primary system, $\xi_1 = c_1/(2\sqrt{m_1 k_1})$, was varied from 0 to 0.10. The secondary system was taken to be undamped (c_2=0.0).

A mass ratio (m_3/m_2) of 0.10 was maintained between the secondary system and the absorber. The absorber was tuned to the natural frequencies of the primary and the secondary systems, $(k_3/m_3)^{1/2} = (k_2/m_2)^{1/2} = (k_1/m_1)^{1/2} = 1$ rad./s, and assumed undamped (c_3=0.0). The mass ratio between the absorber and the impact damper, $\mu = m_4/m_3$, was kept at 0.25. Hence, although the value of μ was quite large, the addition of the impact damper raised the inertia of the secondary system only by a relatively insignificant factor of 1.025.

2.3 NUMERICAL RESULTS

In Figure 2.2, RMS displacement ratios, σ_{x2}/σ_{x20}, of the secondary system are presented for different non-dimensional clearances, d/σ_{x20}. Here, σ_{x2} and σ_{x20} represent the RMS displacement of the secondary system with and without the impact damper; and d is the total clearance of the impact damper. Hence, ratios smaller than unity represent attenuation, whereas a ratio of unity represents no change due to the impact damper.

Two different coefficients of restitution, e, were used for these simulations. A value of 0.3, for instance, represents contacts between hard neoprene and metal surfaces. These results are marked with (■) in Figure 2.2. A coefficient of restitution of 0.8, on the other hand, represents contacts between polished surfaces of hardened metals, such as tool steels. These results are marked with (□). For all cases presented in Figure 2.2, e = 0.3 (■) produced more effective attenuations than those of e = 0.8 (□). Hence, all further discussions will be limited to the smaller coefficient of restitution. This trend is in agreement with earlier findings reported for random excitations [9,14]. Different ratios of the primary mass to the secondary mass, m_1/m_2, are presented in each row in an ascending order from top to bottom, namely 1, 10, 100 and 1000. Each column corresponds to a critical damping ratio of the primary system, ξ_1, of 0.001, 0.01 and 0.05 from left to right.

Generally, all parameter combinations in Figure 2.2 show attenuations due to the

presence of the impact damper. These attenuations are quite marginal for cases with small d/σ_{x20}, producing values of σ_{x2}/σ_{x20} close to unity. Small d/σ_{x20} causes too many collisions which mostly occur with small relative approach speeds before contact. In turn, these slow speeds drastically inhibit the momentum exchange between the impact damper and the tuned absorber. When d/σ_{x20} is large, on the other hand, too few collisions occur. As a result, attenuations are again quite insignificant. Absence of collisions due to too large a clearance is always indicated with a σ_{x2}/σ_{x20} of unity for each case. Between too small and too large clearances, results for each set of parameters indicate an optimal clearance to produce the largest attenuations. These optimal clearances, produce relatively large approach speeds with an average frequency of two collisions per cycle. Term "cycle" is used loosely here due to the random nature of the disturbance.

In Figure 2.2, for $m_1/m_2 = 1$ and $m_1/m_2 = 10$ (in the first two rows), as the critical damping ratio of the primary system increases from 0.001 to 0.05 (from the first to the third column) effectiveness of the impact damper decreases. This trend is not surprising since any increase in damping will result in a smaller excursion amplitude in the absorber's oscillations. Effect of the impact damper on the secondary system is an indirect one through the response of the tuned absorber. Therefore, smaller excursion of the absorber gives the impact damper less of a chance to make a difference . Best attenuations are in the order of 50% for $m_1/m_2 = 1$ and 80% for $m_1/m_2 = 10$. These attenuations deteriorate to approximately 25% and 45%, respectively, in the third column of each row. The last two rows of Figure 2.2, for $m_1/m_2 =$

100 and $m_1/m_2 = 1000$ show a different trend than the first two rows. Particularly for $m_1/m_2 = 1000$, increasing values of ξ_1 produce more effective attenuations from approximately 50% in the first column to 80% in the third column. This drastic change may be attributed to the ratio of the primary and the secondary masses. When the secondary system's mass is 1000 fold smaller than that of the primary system, it is virtually impossible for the primary system to be affected by changes in the response of the secondary system. Hence, excitation applied on the primary system is in fact perceived as a moving base disturbance by the secondary system for control purposes, therefore, the "apparent" degree of freedom of the system is now reduced by one. Increasing damping in the primary system only enhances this apparent reduction phenomenon.

Dependence of the attenuations of the impact damper on m_1/m_2, is demonstrated further in Figures 2.3 and 2.4. In Figure 2.3, the RMS displacement ratios of the primary (□), secondary (*) and the tuned absorber (▲) systems are given for the same non-dimensional clearances as in Figure 2.2 but for a constant $m_1/m_2 = 10$ and again for $e = 0.3$. Each frame from Figure 2.3 (a) to 2.3 (e) corresponds to a ξ_1 of 0.0, 0.001, 0.01, 0.05 and 0.10. Hence, RMS displacement ratios of the secondary system (*) in the middle three frames are repeated from Figure 2.2. Because of the relatively strong interaction between the primary and the secondary systems for this $m_1/m_2 = 10$, as the damping in the primary system increases, the relative performance of the impact damper deteriorates from approximately 80% attenuation in frames Figure 2.3 (a) and 2.3 (b) to 30% in frame 3 (e). What is very interesting in Figure

2.3 is that, when the impact damper is effective, the attenuations are achieved in about the same order for all three of the primary, secondary and tuned absorber systems simultaneously. On the other hand, when the performance deteriorates, attenuations follow a reverse order depending on how large each system's mass is. They are most pronounced in the tuned absorber, then the secondary system and the primary system.

Results in Figure 2.4 are presented in an identical format to that of Figure 2.3, but this time for $m_1/m_2 = 1000$. As discussed briefly earlier, the effectiveness of control of the secondary system is particularly pronounced in Figures 2.4 (d) and 2.4 (e), for ξ_1 of 0.05 and 0.10, producing approximately 80% attenuation for non-dimensional clearances of 1.5 to 4. Best attenuations gradually deteriorate to approximately 65%, 50% and 40% as the value of ξ_1 changes to 0.01, 0.001 and 0.0, respectively. In Figures 2.4 (d) and 2.4 (e), the primary system's response remains unaffected for all clearances, whereas some marginal changes may be observed in Figures 2.4 (a) to 2.4 (c) due to the presence of the impact damper.

One of the drawbacks of a conventional tuned absorber is the large excursion amplitudes of the tuned absorber. Since the absorber is intentionally designed to resonate at the tuning frequency to be effective, resulting large amplitudes require sufficiently large space around the absorber and unavoidable maintenance or replacement of the absorber in time. Results presented so far invariably suggest that addition of the impact damper should negate this particular drawback of the tuned absorber.

Displacement histories of the primary (—) secondary (—) and the tuned absorber (.....) are shown in Figure 2.5 (a) for the system controlled by the conventional absorber with $m_1/m_2 = 10$ and $\xi_1 = 0$. In Figure 2 5 (b), the same system is shown with the addition of the impact damper at a non-dimensional clearance of $d/\sigma_{x20} = 2.17$. The first 150 s (second) period of the histories shows the process of gradually building of the excursion amplitudes starting from zero initial conditions. The last 150 s period, on the other hand, exhibits an almost perfectly periodic character in response to the random white noise excitation. This periodic character is not surprising considering that an oscillator is expected to respond in a narrow band of frequencies regardless of the frequency content of the excitation. However, this natural self-organization process of deliberately picking a narrow band of preferred frequencies is a gradual one. If a randomly excited response may be envisaged as a sequence of short transient disturbances, gradual building of significantly large oscillation amplitudes requires the presence of the preferred frequency components as initial conditions for each of these short transient disturbances. When this gradual building of the oscillation amplitudes is interrupted by discontinuities of the impact damper's collisions, the resulting response is somewhat disorganized and certainly smaller than the case without the impact damper [15]. Responses in both Figures 2.5 (a) and 2.5 (b) are identical until the first contact is established at about 50s. Differences start emerging towards the end of the initial 150 s period, though both cases are still quite similar. This similarity is due to the first few collisions having inevitably small approach speeds and being quite ineffective. However, displacement amplitudes with the new controller for the last 150 s are significantly smaller

than those of the displacements without the impact damper. Similar comparisons may be made between the displacement histories with and without the impact damper in Figures 2.6 (a) and 2.6 (b), this time for $m_1/m_2 = 1000$, $\xi_1 = 0.10$ and for $d/\sigma_{x20} = 2.95$. In Figure 2.6 (b), oscillation amplitudes of the primary system controlled by the new controller remain virtually unchanged due to its large inertia.

Figure 2.7 shows the Fast Fourier Transformation (FFT) of the displacement of the same secondary system in Figure 2.5. In this figure, the vertical axis represents the spectral amplitude, horizontal axis represents the frequency (in Hz) and the depth represents the starting time of a FFT snapshot (approximately 150s long each). The top half of Figure 2.7 is the response controlled by the conventional absorber (without the impact damper). The gradual building process discussed earlier, is displayed in this response without the impact damper, clearly emphasizing the exaggerated narrow band response after 600 s. For the first FFT, response with the impact damper, shown in the bottom half, has a very similar spectral distribution to that of the response without the impact damper. Starting from the second FFT, response's spectral amplitudes with the impact damper are significantly smaller with a wider frequency distribution. Figure 2.8 shows the same FFT histories in an identical format to that of Figure 2.7, but this time for the same parameters in Figure 2.6.

Figure 2.9 shows the effect of the clearance of the impact damper on the displacement of the secondary structure for $m_1/m_2 = 10$ and $\xi_1 = 0$. For comparison purposes, only the last

FFT snapshot (between 850 and 1000 s) of the displacement spectra of the secondary system are shown in Figure 2.9 (a). Some selective non-dimensional clearances, d/σ_{x20}, are marked along the depth axis. In Figure 2.9 (a), the second FFT corresponds to the best clearance case shown earlier in Figures 2.5 (b) and 2.7 (b). The clearance corresponding to the fifth FFT is deliberately chosen to be large enough to avoid collisions, and therefore to produce the response without the impact damper which is the same case shown in Figures 2.5 (a) and 2.7 (a). As may be noted easily in this figure, too small a clearance ($d/\sigma_{x20} = 0.54$) produces a spectral distribution with a smaller peak frequency but with a comparable spectral amplitude to that of the case without the impact damper ($d/\sigma_{x20} = 25.0$) due to having too frequent collisions. Larger clearances, on the other hand, are again ineffective due to too infrequent collisions. Example cases shown here correspond to σ_{x2}/σ_{x20} of approximately 0.37, 0.18, 0.32, 0.36 and 1.00 for d/σ_{x20} of 0.54, 2.17, 7.60, 12.49 and 25.0 (refer to Figure 2.3 (a)). Same information for clearance dependence is presented this time using the probability distribution in Figure 2.9 (b). The optimal clearance case ($d/\sigma_{x20} = 2.17$), which is cross hatched for easy comparison, suggests a three fold attenuation of the peak displacement as compared to the case when the impact damper is not active ($d/\sigma_{x20} = 25.0$). Other non-optimal clearances show similar attenuations in peak displacement to those of the corresponding RMS averages (refer to Figure 2.3 (a)).

In Figure 2.10, similar information to Figure 2.9 is presented in an identical format but for $m_1/m_2 = 1000$ and $\xi_1 = 0.10$. In Figure 2.10 (a), the comments made for Figure 2.9 (a)

are valid in general. The exception is that the spectral distribution of the components is significantly narrower this time due to an apparent loss of degree of freedom discussed earlier. This narrow band response leads to an almost perfectly periodic response which is reflected in the shape of the probability distribution of the case in Figure 2.10 (b) when the impact damper is not active. This resemblance of the probability distribution to a harmonic variation may also be noticed in the first ($d/\sigma_{x20} = 0.295$) and the fourth ($d/\sigma_{x20} = 16.20$) clearances at varying degrees as well.

Another look at the attenuation mechanism of the impact damper is presented in Figure 2.11, Figure 2.12 and Figure 2.13. In Figures 2.11 and 2.12, histories of the energy input to the primary system from the excitation for both cases without and with the impact damper (at optimal clearance) are presented. In addition, energy dissipated through collisions and the difference between the input and the dissipated energy (net-energy) are also marked for the case with the impact damper. In Figure 2.11, energy histories are given for $m_1/m_2 = 10$ and $\xi_1 = 0$ and $d/\sigma_{x20} = 2.17$. Energy input from the random excitation seems to produce rather large fluctuations due to large velocity fluctuations of the system without the impact damper. For the optimal impact damper, on the other hand, the input energy history is much smoother as compared to the case without the impact damper. This, of course, is due to the attenuations induced in the response of the primary system by the impact damper. Surprisingly, the cumulative energy input with the impact damper is larger than that of the case without the impact damper. Dissipated energy due to impacts, however, is just as large

as the input energy, leaving only a minimal net energy. In Figure 2.12, energy histories are presented in the same format as in Figure 2.11 but for $m_1/m_2 = 1000$, $\xi_1 = 0.10$ and $d/\sigma_{x20} = 2.95$. In this figure, energy histories without the impact damper, with the impact damper and net-energy with the impact damper seem very similar since the response of the primary system is virtually unaffected by any change in the secondary system. Histories in Figure 2.13 are for the same cases in Figure 2.12, but this time energy input to the secondary system rather than the primary system is plotted. Hence, this case is treated as if the primary system does not exist and the secondary system is given a base excitation. Trends in Figure 2.13 are very similar to those in Figure 2.11, leaving a minimal net-energy for the secondary system after the energy dissipation due to collisions subtracted from the energy input from the primary system.

2.4 CONCLUSIONS

A new passive vibration controller, which combines a tuned absorber with an impact damper, is investigated in this chapter for controlling excessive oscillations of light secondary structures. A numerical procedure is presented for predicting performance under random white noise disturbance. Addition of an impact damper provides significant improvement in the performance of the conventional absorber.

When the mass of the secondary system to be controlled is ten fold smaller than the mass of the primary system, $m_1/m_2 = 10$, impact damper is most effective when there is minimal damping in the system. Attenuations in the order of 80% are possible in the response of the secondary as well as the primary and the tuned absorber systems.

When the mass of the secondary system to be controlled is thousand fold smaller than the mass of the primary system, $m_1/m_2 = 1000$, impact damper is most effective when primary system has at least 5% critical damping. For this case, 80% attenuation is possible for both the secondary and the tuned absorber systems. No control is attainable for the primary system due to its large inertia.

CHAPTER 3

AN EXPERIMENTAL STUDY OF THE NEW VIBRATION CONTROLLER ON A SECONDARY STRUCTURE UNDER RANDOM EXCITATION

3.1 INTRODUCTION

A series of numerical case studies in Chapter 2 have shown that a new passive vibration controller combining a tuned absorber and an impact damper is effective on controlling a light secondary structure. In this chapter, the investigation of this new controller is continued with experimental observations. A prototype structure is built with selected parameters and tested under random excitation with the new controller as well as the conventional tuned absorber alone. Comparisons are made between the performances of the two controllers. In addition, measured results are compared with numerical predictions.

3.2 DETAILS OF THE EXPERIMENTS

A schematic drawing of the experimental model is shown in Figure 3.1. The design of the experimental rig is based on the 4 Degree-Of-Freedom (4DOF) model discussed in the previous chapter. The experimental structure consists of three mechanical oscillators and an impact damper. The primary structure is a rigid plate cantilevered from a fixed base by four

thin strips of steel. The strips act as the resilient elements, and in the mean time they also contribute to the equivalent mass. On top of the primary structure is another oscillator, the secondary structure, which is mounted on the primary structure by two similar steel strips. The equivalent mass of the secondary structure is approximately 1/10 of the primary mass. The third oscillator is mounted on the secondary structure with two thin strips. The mass of the third oscillator is approximately 1/10 of the secondary's. The third oscillator is designed as a conventional tuned absorber for the secondary system. Therefore, the natural frequency of the third structure is tuned to be the same as the secondary's. The impact damper is suspended into the cavity of the absorber as the mass of a simple pendulum. Hence, the impact damper's motion is free of all external forces between contacts with the walls of the cavity on the absorber. The radial clearance, d/2, between the damper and the absorber is indicated for clarity in Figure 3.1.

The parameters chosen for the experimental structure are listed in Table 3.1. Where K_{eq}, m_{eq} and ξ_{eq} represent the equivalent stiffness, critical viscous damping ratio and mass when each system is considered individually as SDOF oscillators. The dynamic response of the secondary system depends upon the level of interaction between the secondary system and the primary system. The parameters of the system were chosen so that the resulting uncontrolled combination (without the impact damper) would produce the largest response of the secondary system. Previous work has demonstrated that the largest response of the secondary system is produced when the natural frequencies of the primary and the secondary

systems are the same [12, 13]. Hence, the natural frequencies of all three structures in Figure 3.1 were tuned to be identical (within experimental variations) when they were tested as SDOF oscillators individually. The natural frequency of the simple pendulum which consists of the impact damper and a string was set to be approximately 0.6 Hz, much smaller than those of the primary, secondary and absorber systems.

Table 3.1 Parameters of the experimental structure

	Resonant Frequency† (Hz)	Stiffness‡ K_{eq} (10^3 N/m)	Mass‡ m_{eq} (kg)	Damping Ratio† ξ_{eq}
Primary System	25.17 ± 0.30	113.63	4.544	0.0053 ± 0.0002
Secondary System	24.67 ± 0.30	11.22	0.467	0.0026 ± 0.0002
Tuned Absorber	23.08 ± 0.30	1.22	0.058	0.0034 ± 0.0002
Impact Damper			0.011± 0.002	

† Measured ‡ Calculated

The experimental setup is shown in Figure 3.2. The primary system was randomly excited by an electromagnetic exciter. A soft spring was used between the exciter and the primary system to facilitate the excitation on the primary system from the motion of the coil of the exciter. The random signals were generated by an HP Spectrum Analyzer. The original signals were amplified by a power amplifier. Three accelerometers were placed on

the primary system, secondary system and the absorber to measure the responses. The signals collected by the accelerometers were amplified by another amplifier, then sent to the HP Analyzer for data processing. In the analyzer, first the low frequency noise below 5 Hz was filtered by built-in filters. Power spectra of the accelerations were measured by averaging 32 samples to obtain a reliable average. Then by using built-in integrators, acceleration spectra were converted to those of the displacements. Finally, the Root Mean Square (RMS) averages of the displacements were calculated. A printer was connected to the analyzer to obtain hard copies when needed.

During the experiment, the RMS displacement amplitudes of the primary system, the secondary system and the absorber, were measured both with and without the impact damper at each level of random excitation. Again, the attention was focused on the investigation of the improvement of adding an impact damper, since previous work [28] had shown that a conventional tuned absorber had positive, though limited, effect on the secondary structures under random excitation in terms of vibration reduction. Measurements were performed over a frequency span from 0 to 50 Hz, whereas the natural frequencies of the primary, secondary and the absorber were tuned to be around 25 Hz. The dimensionless variable d/σ_{x20} was chosen to represent the change of the clearance of the impact damper, where d was the measured value of the clearance and σ_{x20} represents the RMS displacement of the secondary system without the impact damper (with the absorber alone). d was kept constant throughout the experiments. The variations of the clearance d/σ_{x20}, were obtained by gradually adjusting

the excitation level, and therefore changing σ_{x20} values. The clearance was measured to be 1.44±0.02 mm. The coefficient of restitution between the damper and the neoprene-lined walls of the tuned absorber was measured to be 0.34±0.05 [9].

3.3 RESULTS

Figure 3.3 shows the measured displacement spectrum of the electromagnetic exciter's moving coil within the 50 Hz frequency span. This random signal was assumed to be close to a theoretical white noise for a 25 Hz natural frequency and was used as the excitation of the primary system.

The representative frequency spectra of the displacements of the secondary system are shown in Figure 3.4 for increasing levels of excitation from the first row to the fourth row. The left column represents the spectra with the conventional tuned absorber, whereas the right column represents the spectra with the new combined controller. The Root-Mean-Square (RMS) values are obtained by integrating these displacement spectra to evaluate the performance of the new combined controller on the experimental structure. The RMS displacement value of the secondary system controlled by the new controller is denoted as σ_{x2}. The RMS displacement value of the secondary system controlled by the conventional tuned absorber is denoted as σ_{x20} here. The ratio of σ_{x2}/σ_{x20} is used here to indicate the effectiveness of the new controller comparing with the conventional tuned absorber. Hence, a value of

σ_{x2}/σ_{x20} less than unity represents an additional attenuation of the RMS displacement of the secondary system for each level of excitation. As we mentioned in the previous section, changing the excitation level is equivalent to changing the clearance of the impact damper in this experiment. A non-dimensional variable d/σ_{x20}, where d is the measured value of the clearance of the impact damper, is used to represent the clearance. Because d remains constant (1.44 mm), the non-dimensional clearance d/σ_{x20} decreases when the excitation (σ_{x20}) increases.

The spectra in Figure 3.4 from frames (a), (c), (e) to (g) in the first column, and from frames (b), (d), (f) and (h) in the second column correspond to d/σ_{x20} of 45.7, 30.9, 10.2 and 4.7, respectively. From the spectra in the first column of Figure 3.4, it can be seen that the RMS of the secondary system controlled by the conventional absorber increases steadily with increasing excitation (decreasing of d/σ_{x20}). Each spectrum shows three peaks around the original natural frequency of the secondary system (25 Hz). In the second column of this figure, the spectral responses, with the help of adding an impact damper, are flatter and the peak values are much smaller than those in the first column. The variation of the effectiveness of the new controller with different excitation levels reflects the dependence of the impact damper to its clearance. For d/σ_{x20}=45.7, the ratio between the RMS displacement of the secondary system with the new controller (Figure 3.4 (b)) and that with the conventional absorber (Figure 3.4 (a)), σ_{x2}/σ_{x20}, is about 86%. It indicates about 14% RMS reduction for adding the impact damper. As the non-dimensional clearance d/σ_{x20} decreases to 30.9 in

Figure 3.4 (c) and (d), the RMS displacement reduction increases to 34% with the help of the impact damper. The best RMS attenuation for the secondary system was obtained at d/σ_{x20}=10.2 (Figure 3.4 (f) comparing with Figure 3.4 (e)), where the RMS reduction is about 57%. As the clearance continue to decrease, the effectiveness of the impact damper starts to decrease. For d/σ_{x20} of 4.7 in Figure 3.4 (g) and (h), the RMS displacement reduction is about 53% with the impact damper.

Very similar to the frequency spectra of the secondary system, Figures 3.5 and 3.6 present the frequency spectra of the displacement of the primary system and the absorber system. For both Figure 3.5 and 3.6, Frames (a), (c), (e) and (g) in the first column, and frame (b), (d), (f) and (h) in the second column correspond to d/σ_{x20} of 45.7, 30.9, 10.2 and 4.7, which are the same cases listed in Figure 3.4. Figure 3.5 and Figure 3.6 show that the addition of the impact damper to the conventional tuned absorber also helps reducing the displacements of the primary system and that of the absorber system. This trend is in agreement with the findings of the previous chapter. Comparing Figures 3.5 (b), (d), (f) and (h) with Figures 3.5 (a), (c), (e) and (g), the obtained RMS displacement reductions for the primary system are 6%, 30%, 56% and 55%. The RMS displacement reductions are 14%, 38%, 53% and 59% for the absorber system in Figures 3.6 (b), (d), (f) and (h) as compared with that in Figures 3.6 (a), (c), (e) and (g). The vibration reduction achieved for the primary system is especially significant considering that the mass ratio of the primary system over the impact damper is approximately 400. The vibration reduction to the absorber is also useful

in practice at the situation where space is limited for adding an absorber on a system.

Both numerically predicted and experimentally observed RMS displacement ratios of the primary, secondary and tuned absorber systems are shown in Figures 3.7 (a), (b) and (c). Vertical axis of each frame represents the corresponding non-dimensional displacement ratio (σ_{x1}/σ_{x10} or σ_{x2}/σ_{x20} or σ_{x3}/σ_{x30}), whereas the horizontal axes indicate the clearance non-dimensionalised with the RMS displacement of the secondary system (d/σ_{x20}).

Two sets of numerical predictions are presented in this figure, considering the variation of the experimentally measured coefficient of restitution. Results for e=0.3 are shown with (○), whereas (□) represents results for e=0.4. Experimentally measured ratios are marked with (▲). Changing the coefficient of restitution between 0.3 and 0.4, produces quite insignificant differences. Generally, overall agreement between the numerical predictions and measurements is quite close for all three coordinates, particularly when the attenuations of the impact damper are most effective. This close agreement slowly deteriorates as the value of the non-dimensional clearance d/σ_{x20} increases to values greater than 13. Here, it must be kept in mind that an experimental value of the non-dimensional clearance d/σ_{x20}, is varied by keeping the clearance constant and changing the level of excitation (whereas changing the clearance is a more practical approach in numerical simulations). Hence, a large d/σ_{x20} is only possible by lowering the level of excitation. At these low levels, it was found to be practically impossible to avoid the effects of small amplitude building vibrations. These structural

vibrations were confounded with the practical impossibility of centering the impact damper perfectly in its cavity. Hence, at low excitation levels, more frequent collisions were observed in the experiments as compared to what could be predicted in numerical simulations. As a result, these more frequent collisions at large d/σ_{x20} produced larger attenuations. For small d/σ_{x20}, experimental imperfections were largely overwhelmed by high excitation levels.

Figure 3.8 presents a set of acceleration spectra and histories for the secondary and the primary systems for a representative case. The non-dimensional clearance d/σ_{x20} in this case is 8.6. On the left side of Figure 3.8, frames (a) and (e) show the acceleration spectra of the secondary system and the primary system with the tuned absorber alone, whereas frames (c) and (g) show the corresponding spectra with the new controller for the secondary system and the primary system. On the right side of Figure 3.8, frames (b), (d), (f) and (h) present the histories of the acceleration corresponding to frames (a), (c), (e) and (f), respectively. Figure 3.8 indicates that the new controller is effective on reducing not only the displacements but also the accelerations of the system. The RMS acceleration attenuations are 35% for the secondary system and 21% for the primary system.

The ability of reducing the accelerations as well as displacements of the system is one of the advantages of the new controller over the conventional impact damper. Using the conventional impact damper as a vibration controller results in relatively large contact forces due to intermittent rigid body collisions. These collisions, when utilized properly, may control

the displacement excursions of a resonant system effectively. However, the acceleration amplitudes of the system may in fact be exaggerated as a result of the contact forces [30]. Placing the impact damper within the absorber mass, rather than in direct contact with the secondary system helps alleviating this problem.

3.4 CONCLUSIONS

In this chapter, the experiments are detailed to demonstrate that using an impact damper as a supplementary controller for a conventional tuned vibration absorber enhances the vibration control significantly. The new controller, which combines an impact damper with a tuned absorber, is effective for both the primary system and the secondary system. For the experimental structure under a random white noise excitation, the best result for the secondary system is obtained at d/σ_{x20} =10.2 with 57% RMS displacement attenuation as compared with the result of the conventional tuned absorber. At the mean time, the RMS displacement attenuation to the primary system and the absorber system are 56% and 53%. In addition to the displacement attenuation, the new controller also reduces the acceleration of the controlled system, which overcomes the inherent disadvantages of using the impact damper alone. An overall agreement between the experiment and the simulation is achieved with the exception of low levels of excitation. At these low levels, experimental model performs better than the numerical model.

CHAPTER 4

THE EFFECTS OF AN OFF-TUNED ABSORBER ON SECONDARY STRUCTURES UNDER RANDOM EXCITATION

4.1 INTRODUCTION

In previous chapters, a new passive vibration controller combining a tuned absorber and an impact damper has been discussed for controlling a secondary structure under random excitation. In this treatment, the natural frequency of the absorber has always been assumed to be exactly the same as the natural frequency of the secondary system to be controlled. However, there might be difficulties in practice to obtain a precise tuning due to inaccuracies of measurement, manufacturing and assembly. In some other situations, the resonant frequency of the system might shift after the absorber is installed. In other words, it is possible that the natural frequency of the absorber is off tuned to that of the system.

Another reason for the investigation presented in this chapter, is to observe the possibility of improving the new controller by off-tuning its absorber. Such an observation may lead to a recommendation of deliberately designing an off-tuned absorber with the impact

damper.

In this chapter, performance of an off-tuned absorber is investigated to control the secondary system under random excitation. The corresponding responses of the primary system are also presented. The investigation is conducted for the new vibration controller (with an impact damper and an absorber) as well as for the conventional absorber.

4.2 NUMERICAL APPROACH

The basic numerical approach used in this chapter is very similar to that in Chapter 2. The simulation is still based on the model illustrated in Figure 2.1. The system is configured as the 4DOF system discussed in previous chapters. As a quick reminder, this system consists of a primary system (m_1, c_1, k_1), a secondary system (m_2, c_2, k_2), an absorber (m_3, c_3, k_3) and an impact damper (m_4).

An off-tuned absorber was obtained by adjusting the stiffness of the absorber (k_3). The mass of the absorber (m_3) and the undamped natural frequency of the secondary system ($f_2 = (k_2/m_2)^{1/2}/(2\pi)$) remained constant throughout. The natural frequency of the absorber ($f_3 = (k_3/m_3)^{1/2}/(2\pi)$) was tuned to be up to 20% off the natural frequency of the secondary system (f_2). Therefore, the tuning ratio, f_3/f_2, ranged from 0.8 to 1.2. The natural frequency of the primary system ($f_1 = (k_1/m_1)^{1/2}/(2\pi)$) was taken to be identical to the natural frequency

of the secondary system, f_2, to represent the strongest interaction between these systems [12, 13].

The investigation still concentrated on the effectiveness of the control of a light resonant structure. Two representative cases were studied in details, one with mass ratio m1/m2 = 10 and $\xi_1 = \xi_2 = 0$, the other with mass ratio m1/m2 = 1000, $\xi_1 = 0.1$ and $\xi_2 = 0$. From previous finding in Chapter 2, these two represented the cases in which the new controller was most effective. A mass ratio of 0.10 was maintained between the secondary system and the absorber (m_3/m_2) and the mass ratio between the absorber and the impact damper (m_4/m_3) was kept constant at 0.25. In addition, the absorber was taken to be undamped ($\xi_3 = 0.0$). The coefficient of restitution, e, between the impact damper and its container was kept to be 0.3 in this chapter. The random white noise excitation described in Chapter 2 was employed to excite the primary mass (m_1). The critical system parameters investigated were the clearance between the impact damper and the container, d, the mass ratio between the primary system and the secondary system, m_1/m_2, and the tuning ratio, f_3/f_2.

For comparison purposes, the dynamic model in Figure 2.1 was also configured as a 2DOF system, only the primary and secondary systems, by simply setting k_3 and c_3 to be zero. This system represented the original uncontrolled structure, before a tuned absorber was introduced. Then the comparison of the effectiveness of off-tuning was made between the system controlled by the new controller and that controlled only by the absorber.

4.3 NUMERICAL RESULTS

Figure 4.1 demonstrates the influence of off-tuning the absorber on the performance of the impact damper as part of the new controller for the case of $m_1/m_2 = 10$. In this figure, RMS displacement ratios between the system controlled by the combined new controller and that controlled by an absorber alone are presented for different non-dimensional clearances, d/σ_{x20}. In each frame of Figure 4.1, (□) represents the RMS ratio of the displacement of the primary system, σ_{x1}/σ_{x10}. The RMS ratio of the displacement of the secondary system, σ_{x2}/σ_{x20}, is represented by (×). Again, σ_{x1} and σ_{x2} represent the RMS displacements of the primary and secondary systems controlled by the new controller. σ_{x10} and σ_{x20} represent the RMS displacements of the primary and secondary systems controlled by the conventional tuned absorber. Frames (a), (b), (c), (d) and (e) in Figure 4.1 correspond to the tuning ratios, f_3/f_2, of 0.8, 0.9, 1.0, 1.1 and 1.2. Where f_3/f_2=1.0 is the same case as that discussed in Figure 2.3 (a) of Chapter 2, where the absorber is tuned to the resonant frequency of the secondary system.

Rather significant attenuations are suggested in Figure 4.1 due to the presence of the impact damper, even when the absorber is tuned 20% off the resonant frequency of the secondary system. From frame (a) to (e), the best RMS reductions for the secondary system are 55%, 77%, 79%, 67% and 75%, which are obtained at d/σ_{x20} of 3.24, 2.69, 2.72, 4.46 and 1.10, respectively. The best RMS reductions of the primary system are 57%, 79%, 82%,

86% and 72%, corresponding to d/σ_{x20} of 3.24, 2.69, 2.17, 4.46 and 1.10. Comparing with each case, the best RMS reduction of x_2 is obtained at f_3/f_2=1.0 and it decreases when the tuning is off the center. However, the best RMS reduction for x_1 happens at f_3/f_2=1.1 and the attenuation decreases when f_3/f_2 changes from this point. Considering the secondary system is the major object to be protected, the best overall performance of the impact damper can be considered at f_3/f_2=1.0 (Figure 4.1 (c)), where the RMS reductions are 79% and 82% for x_2 and x_1. Generally, off-tuning the absorber reduces the effectiveness of the impact damper.

The overall performance of the new controller and the conventional absorber to the off-tuning is summarized in Figure 4.2. In each frame, the horizontal axis is the tuning ratio f_3/f_2. Figure 4.2 (a) shows the performance of the conventional absorber on the secondary system. In this frame, the vertical axis is the RMS displacement ratio σ_{x20}/S_{x2}. Here, S_{x2} is the RMS displacement of the secondary system of the original 2DOF system without the absorber. Similarly, Figure 4.2 (b) presents the performance of the conventional absorber on the primary system. The vertical axis in this frame is σ_{x10}/S_{x1}, where S_{x1} is the RMS displacement of the primary system of the original 2DOF system. The overall performance of the new controller is demonstrated in Figure 4.2 (c) to (f) with two different approaches. As discussed earlier in this section, the best performance of the impact damper is obtained at different clearances (d/σ_{x20}) for different tuning conditions. In Figure 4.2 (c), the RMS displacement ratio of the secondary system (σ_{x2}/S_{x2}) is obtained by assuming that the impact damper works at its best clearance values for all off-tuning conditions. In other words, Figure

4.2 (c) shows the best results of the new controller. Figure 4.2 (d) shows the corresponding RMS displacement ratio of the primary system (σ_{x1}/S_{x1}). This approach is used to investigate the possibility of getting better performance from off tuning. The second approach is used to investigate the sensitivity of the new controller with a fixed clearance (d/σ_{x20}) when the tuned frequency of the absorber is shifted. Therefore, in Figure 4.2 (e), the RMS displacement ratio of the secondary system (σ_{x2}/S_{x2}) is obtained by assuming the clearance of the impact damper (d/σ_{x20}) is fixed at 2.72 which is the best clearance for $f_3/f_2 = 1.0$ (refer to Figure 4.1 (c)). Figure 4.2 (f) shows the RMS displacement ratio of the primary system (σ_{x1}/S_{x1}) corresponding to this clearance.

In Figures 4.2 (a) and (b), the RMS ratio with the absorber alone shows large fluctuations. When f_3/f_2 changes from 0.8 to 1.2, σ_{x20}/S_{x2} varies from 0.41 to 0.97, whereas σ_{x10}/S_{x1} varies from 0.68 to 0.99. This is not surprising, considering the extreme sensitivity of the undamped system to any significant presence of a frequency component in the excitation close to a resonance frequency.

Figures 4.2 (c) and (d) show that the new controller provides much larger and stable reductions on the RMS displacements of the structure when working at its best clearance. When f_3/f_2 changes from 0.8 to 1.2, σ_{x2}/S_{x2} ranges from 0.09 to 0.32, and σ_{x1}/S_{x1} ranges from 0.14 to 0.43. Figures 4.2 (c) and (d) show very clearly that the performance of the new controller decreases with off-tuning. The best performance of the new controller is obtained

at $f_3/f_2 = 1.0$ for both the secondary system and the primary system. Therefore, off-tuning can not be used to improve the performance of the new controller for this case.

With the clearance (d/σ_{x20}) fixed at 2.72, the new controller has slightly less performance for both the secondary and primary systems when the frequency of the absorber is shifted from its center. In Figures 4.2 (e) and (f), σ_{x2}/S_{x2} ranges from 0.09 to 0.43, and σ_{x1}/S_{x1} ranges from 0.14 to 0.52, while f_3/f_2 changing from 0.8 to 1.2. Within 10% of off-tuning range ($f_3/f_2 = 0.9$ to 1.1), σ_{x2}/S_{x2} variation is only about 15%, whereas σ_{x1}/S_{x1} variation is only about 5%. Comparing with the conventional absorber in Figures 4.2 (a) and (b), the new controller provides better RMS displacement performance, and it is less sensitive to off-tuning.

The effect of off-tuning on the performance of the impact damper for a large mass ratio (m_1/m_2) structure is demonstrated in Figure 4.3. This time m_1/m_2 is set to be 1000, and $\xi_1 = 0.1$ and $\xi_2 = 0$. It is one of the best cases discussed in Chapter 2. In Figure 4.3 the RMS displacement ratio variations of the secondary system (×), σ_{x2}/σ_{x20}, and the primary system (□), σ_{x1}/σ_{x10}, are presented in an identical format to those in Figure 4.1. The horizontal axes are the non-dimensional clearance, d/σ_{x20}. Again, in this figure, frames (a), (b), (c), (d) and (e) correspond to the off-tuning ratios of 0.8, 0.9, 1.0, 1.1 and 1.2.

The primary system with 1000 mass ratio shown in Figure 4.3 has a very different

response to the tuning of the absorber as compared with the 10 mass ratio case in Figure 4.1. Due to the large mass ratio between m_1 and m_2, the impact damper has almost no effect on the primary system when f_3/f_2 changing from 0.8 to 1.1. Further simulation results show that both the new controller and the conventional absorber have simply no effect on the primary system for this case. This is due to the large mass ratio of the structure. As discussed in Chapter 2, when the secondary system's mass is 1000 fold smaller than that of the primary system, it is virtually impossible for the primary system to be affected by changes in the response of the secondary system.

On the other hand, the response of the secondary system shows very similar trend to that of the 10 mass ratio case illustrated in Figure 4.1. From frames (a) to (e), the best RMS displacement reductions for the secondary system are 72%, 81%, 82%, 77% and 73%, which are obtained at d/σ_{x20} of 2.82, 3.18, 2.95, 2.25, and 2.17, respectively. It is obvious that the impact damper is still in favor of f_3/f_2=1.0, at which the best RMS reduction (82%) is obtained.

The overall performance of the new combined controller and the conventional absorber under off-tuning condition for the secondary system is summarized for this 1000 mass ratio case in Figure 4.4. The comparison in Figure 4.4 is made only for the secondary system since both of the controllers do not have any effect on the primary system.

In the same format as that used in the first column of Figure 4.2, Figure 4.4 (a) shows the RMS displacement ratio of the secondary system (σ_{x20}/S_{x2}) with the conventional absorber. Figure 4.4 (b) presents the RMS displacement ratio of the secondary system (σ_{x2}/S_{x2}) with the new controller when the impact damper is assumed working at its best clearances under off-tuning conditions. In Figure 4.4 (c), the RMS displacement ratio, σ_{x2}/S_{x2}, is obtained at a fixed impact clearance. This time the clearance, d/σ_{x20}, is set at 2.95 which is the best clearance value for the secondary system at $f_3/f_2=1.0$.

In Figure 4.4 (a), while f_3/f_2 changing from 0.8 to 1.2, σ_{x20}/S_{x2} varies between 0.56 to 0.98. At $f_3/f_2=1.0$, σ_{x20}/S_{x2} is 0.78. The conventional absorber shows its best performance at $f_3/f_2=1.1$ on the secondary system with σ_{x20}/S_{x2} of 0.56 (about 44% total reduction).

The presence of the impact damper provides large additional attenuation to the secondary system. In Figure 4.4 (b), while the impact damper working at its best clearances within 20% off-tuning, σ_{x2}/S_{x2} ranges from 0.13 to 0.28, which indicates about 87 - 72% total reduction. However, the best RMS reduction of the secondary system is obtained still around f_3/f_2 of 1.0. There is no improvement of the performance obtained when f_3/f_2 is off its center. Therefore, off-tuning the absorber is not an effective way to improve the performance of the new controller in this large mass ratio case either.

With the clearance (d/σ_{x20}) fixed at 2.95, Figure 4.4 (c) is essentially very similar to

Figure 4.4 (b). The new controller keeps very good performance when f_3/f_2 shifting between 0.8 to 1.2. It has its best performance within 10% of off-tuning range (f_3/f_2= 0.9 to 1.1).

4.4 CONCLUSIONS

In this chapter, the effect of tuning an absorber is investigated. Comparisons are presented between performances of the new controller and the conventional absorber. For the range of parameters investigated, the new controller shows much better performance than the absorber alone. Presence of the impact damper always contributes additional displacement attenuation to the system. However, no significant improvement has been observed by tuning the absorber of the new controller off the natural frequency of the secondary system. In addition, it has been found that the performance of the new controller is not a strong function of the tuning of its absorber. Especially within 10% of off-tuning, the new controller may be able to remain in its best effectiveness range. The insensitivity to absorber's frequency shifting of the new controller may be useful in applying the new controller for practical problems.

CHAPTER 5

EFFECTIVENESS OF THE NEW VIBRATION CONTROLLER FOR TRANSIENT OSCILLATIONS OF SECONDARY STRUCTURES

5.1 INTRODUCTION

In this chapter, the new passive vibration controller combining a tuned absorber and an impact damper will be studied further for the applications of secondary structures. A parametric study will be presented to determine the capabilities of this new controller in attenuating the excessive transient vibrations of a resonant secondary structure in response to an initial velocity. Comparisons will be made among the new controller, the conventional impact damper and the conventional tuned absorber. Next, the numerical approach will be discussed along with the system parameters chosen for numerical simulations.

5.2 NUMERICAL APPROACH

The basic numerical approach followed in this chapter is very similar to that in Chapter 2. Again, the attention in this chapter will be still focused on the response of the secondary

system. The response of the primary system will be discussed briefly. The effectiveness of the new vibration controller to attenuate the transient oscillations of a secondary structure will be investigated by comparing its response with those of : (1) the uncontrolled secondary structure; (2) the structure controlled by a conventional tuned absorber; (3) the structure controlled by an impact damper alone. The 4DOF model in Figure 2.1 was designed to be flexible enough to simulate the dynamic responses of these four different configurations. The details of the parameter setting are as following:

(1) *The uncontrolled secondary structure* is obtained by setting k_3 and c_3 in Figure 2.1 to zero. Where m_1, k_1, c_1 and m_2, k_2, c_2 constitute the primary system and the secondary system.

(2) *The secondary structure controlled by a conventional tuned absorber* is obtained by choosing the clearance, d, to be very large to avoid collisions between m_4 and its container. Here m_3, k_3, and c_3 constitute the tuned absorber.

(3) *The secondary structure controlled by a conventional impact damper* is obtained by setting m_1 to be very large so that it will be virtually motionless. This time, m_2, k_2 and c_2 will represent the primary system and m_3, k_3 and c_3 will represent the secondary system. The impact damper is m_4.

(4) *The secondary structure controlled by the new controller* is the original 4DOF system. The new controller is represented by the combination of m_3, k_3, c_3 and m_4.

The differential equations of motion of the 4DOF oscillator have been discussed in Chapter 2 and will not be repeated here. In the case studies of this chapter, the external force F(t) in equation 1 of Chapter 2 is set to zero. A non-zero V_{10}, initial velocity of the primary system, is imposed as the disturbance. All other initial conditions of the system are zero.

Similar to Chapters 2 and 4, the case studies in this chapter are performed for mass ratios of 10 and 1000 between the secondary and the primary systems (m_1/m_2). The natural frequency of the secondary system $(k_2/m_2)^{1/2}$ and the primary system $(k_1/m_1)^{1/2}$ are taken to be identical to represent the most critical case for the secondary system. The studies are focused on light damped resonant structures, therefore the critical damping ratios of the primary system, ξ_1, and the secondary system, ξ_2, are set to be 0.01 and 0.0 throughout.

The absorber is tuned to the natural frequencies of the primary and the secondary systems and assumed undamped. That is $(k_3/m_3)^{1/2} = (k_2/m_2)^{1/2} = (k_1/m_1)^{1/2}$ and $c_3 = 0.0$. The coefficient of restitution of the impact damper, e, will be kept at 0.3.

The ratio of the controller's total mass over the secondary system's mass, μc, is kept constant for the three controlled configurations. For the structure controlled by the

conventional absorber, the mass ratio μc is equal to m_3/m_2. For the structure controlled by the conventional impact damper, the mass ratio μc is equal to m_4/m_3, where m_3 becomes the secondary mass for this configuration. For the structure controlled by the new combined controller, the mass ratio μc is taken to be $(m_3+m_4)/m_2$ while maintaining $m_4/m_3 = 0.25$ throughout.

Before performing the parametric case studies, the validity of the computer code was tested extensively by using previously published data [8, 10, 28]. No experimental verification will be sought in this study, since the model presented in Figure 2.1 has been demonstrated to be an accurate representation of the impact process in references 8 and 28.

5.3 NUMERICAL RESULTS

Figure 5.1 shows the time histories of the secondary system (x_2), for the case of mass ratio $m_1/m_2 = 10$ and $\xi_1 = 0.01$, in response to an initial velocity V_{10} imposed on the primary system. Figure 5.1(a) represents the response of the uncontrolled secondary system, whereas Figure 5.1(b) shows the response of the system controlled by a conventional tuned absorber. Starting from the second row, the first column represents the representative responses of the system controlled by a conventional impact damper with different clearances. On the other hand, the second column shows the results of the system controlled by the new controller corresponding to the same clearances. The clearance of the impact damper is taken to be

non-dimensional as $d/(V_{10}/\omega_d)$, where d is the absolute clearance, V_{10} is the initial velocity of the primary system and ω_d is the damped natural frequency of the SDOF primary system. As mentioned in previous section, the ratio of the total mass of the controller over the secondary system, μc, is kept to be 0.10 for all the controlled cases in Figure 5.1.

To evaluate the performance of the three different controllers, two kinds of performance indicators are used, namely the maximum displacement amplitude (x_{max}) and the duration required for this displacement amplitude to decay to an acceptably small value. Although the first criterion is quite intuitive, the second requires some elaboration. Two different settling times are used in the studies. A 10% settling time (t_{10}) represents the time required for the displacement amplitude to decay within ±10% of the uncontrolled displacement peak of the original 2DOF secondary structure in response to the same initial velocity. A 5% (t_5) settling time has the same definition for ±5% of the uncontrolled peak.

As suggested in Figures 5.1(c) and (e), for the structure with mass ratio of 10 (m_1/m_2=10), the response of the secondary system controlled by the conventional impact damper decays much faster than that of the uncontrolled secondary system. For $d/(V_{10}/\omega_d)$=2.0 in Figure 5.1(c), the 10% settling time, $t_{10,}$ is reduced by 65% as compared with the uncontrolled case in Figure 5.1(a), whereas the 5% settling time, $t_{5,}$ has 58% reduction, which are the best results in this group as far as the settling time is concerned. For $d/(V_{10}/\omega_d)$=4.0 in Figure 5.1(e), t_{10} and t_5 reductions are 57% and 48%. In Figure 5.1(g), for

$d/(V_{10}/\omega_d)$=6.0, the impact damper has no effect on the system, because the clearance is too large for the impact damper to have any collisions. Although the effectiveness of the impact damper is always clearance dependent, further simulation shows that for $1.0 < d/(V_{10}/\omega_d) < 5.8$, at least 40% reduction of t_{10} and t_5 can be obtained. However, the impact damper shows little effect on the maximum amplitude (x_{max}) of the system. The best reduction of x_{max} from the impact damper is only 12% of the uncontrolled peak, which shows in Figure 5.1(c).

Unlike the impact damper, the conventional tuned absorber (Figure 5.1(b)) does not reduce the settling time of the secondary system, but it reduces the maximum amplitudes (x_{max}) by about 24%. Comparing the absorber controlled response in Figure 5.1(b) with the uncontrolled response in Figure 5.1(a), after 75 seconds the amplitudes of the controlled response are even larger than those of the uncontrolled response. The system controlled by the conventional absorber will need longer settling time. Hence, the classical tuned absorber is not at all an effective controller of transient vibrations.

The new controller as a combination of a tuned absorber and an impact damper retains the advantages of both of its individual components. As shown in Figures 5.1 (d), (f), (h) with $d/(V_{10}/\omega_d)$ of 2.0, 4.0 and 6.0, the responses of the secondary system under the control of the new controller show both reduction on settling time and maximum displacement amplitudes. Comparing with the uncontrolled case, the t_{10} and t_5 reductions corresponding to Figures 5.1(d), (f), (h) are 55%, 68%, 74% and 66%, 61%, 62%, respectively. The x_{max}

reductions for all three cases are about 24%, which are very close to the attenuations obtained with the tuned absorber alone. Comparing with the conventional impact damper, the new controller not only provides better attenuation to x_{max} but also has further reduction to t_{10} and t_5. In addition, the new controller works in a wider range of clearance.

The comparison between the conventional impact damper and the new controller for $m_1/m_2=10$, is summarized in the first column of Figure 5.3. In these figures, the horizontal axes represent the non-dimensional clearance $d/(V_{10}/\omega_d)$, while the vertical axes represent x_{max} ratio (Figure 5.3(a)), t_{10} ratio (Figure 5.3(c)) and t_5 ratio (Figure 5.3(e)) of the controlled over the uncontrolled response, respectively. The performance of the conventional impact damper is denoted by the curves with (Δ), and the performance of the new controller is denoted by the curves with ($\square$). For the structure controlled by the conventional impact damper, when $d/(V_{10}/\omega_d)$ increases beyond 6.0, the clearance becomes too large for the impact damper to establish contact. Hence, beyond the point $d/(V_{10}/\omega_d)$ of 6.0, the curves become horizontal lines with unity value. Similarly, the new controller starts working as a conventional tuned absorber after $d/(V_{10}/\omega_d)$ of 20.0.

In Figure 5.3(a), the system with the new controller ($\square$) shows almost a horizontal line at 0.76, which indicates its stable attenuation of x_{max} (about 24% reduction), over a wide range of clearances. On the other hand, the system with the conventional impact damper (Δ) provides only small attenuations of x_{max} (0-12%) in a smaller range of clearances. In Figures

5.3 (c) and (e), the conventional impact damper shows good attenuation of the settling time in its effective clearance range. However, the new controller has either comparable or better attenuations of the settling time with wider effective clearance range.

Figure 5.2 presents the time history of the displacement of the primary system (x_1) for the case of $m_1/m_2 = 10$ with the same format as that used in Figure 5.1. Comparing with the uncontrolled case in Figure 5.2 (a), the case controlled by the conventional absorber in Figure 5.2(b) shows no attenuation for x_{max} and even longer settling time. Starting from the second row, Figures 5.2 (c), (e) and (f) on the left side show the effects of the conventional impact damper for $d/(V_{10}/\omega_d)$ of 2.0, 4.0 and 6.0, whereas Figure 5.2 (d), (f) and (h) demonstrate the effects of the new controller. It can be easily observed that both the conventional impact damper and the new controller reduce the settling time of the primary system during their effective clearance ranges. However, they have no effect on the maximum displacement of the primary system. For $d/(V_{10}/\omega_d)$ of 2.0 and 4.0 in Figure 5.2 (c) and (e), the conventional impact damper has 66% and 67% reductions for t_{10}, 51% and 43% for t_5. For $d/(V_{10}/\omega_d)$ of 6.0 in Figure 5.2 (g) the clearance is out of the effective range of the conventional impact damper. Corresponding to $d/(V_{10}/\omega_d)$ of 2.0, 4.0 and 6.0, the new controller has 55%, 69% and 82% reductions for t_{10}, 69%, 65% and 68% for t_5.

The comparison between the conventional impact damper and the new controller on the primary system of these 10 mass ratio cases is summarized in the second column of Figure

5.3. Very similar to the first column, frames (b), (d) and (f) in Figure 5.3 show the x_{max}, t_{10} and t_5 ratios with different clearances $d/(V_{10}/\omega_d)$. There are two overlapped horizontal lines (symbol Δ and $\square$) at x_{max} ratio of 1.0, because there is no attenuation on x_{max} for both controllers. In Figures 5.3 (d) and (f), for both t_{10} and t_5 the new controller ($\square$) shows better attenuation and wider effective clearance range than the conventional impact damper does (Δ).

Figures 5.4 presents the time histories of the secondary system (x_2) of m_1/m_2=1000 and ξ_1 = 0.01, responding to an initial velocity of the primary system. The results are arranged with the same format as in Figure 5.1 to compare the performance of the three controllers.

As shown in Figure 5.4(b), the conventional tuned absorber reduces the maximum displacement amplitudes of the secondary system (x_{max}) by an impressive 74% comparing with the uncontrolled case in Figure 5.4(a). However, similar to Figure 5.1(b), the conventional absorber is relatively less effective on the settling time, producing attenuations of 34% and 0% for t_{10} and t_5 , respectively.

Figures 5.4 (c), (e) and (g) show the effect of the conventional impact damper on the displacement of the secondary system x_2 for $d/(V_{10}/\omega_d)$ of 1.8, 3.6 and 25.0. In these 1000 mass ratio cases, the impact damper provides larger reduction on the maximum displacement

amplitudes than that of the 10 mass ratio cases except the too large clearance case in Figure 5.4 (g). The peak displacement amplitudes also decay sooner comparing with the uncontrolled time history in Figure 5.4 (a). In each case with the impact damper, however, a relatively large amplitude residual vibrations remain for a long period of time, after the initial decay. Hence, t_{10} and t_5 reductions are not very impressive for most of the cases with the conventional impact damper.

The histories of the displacement of the secondary system (1000 mass ratio) with the new controller are shown in Figures 5.4(d), (f) and (h) for $d/(V_{10}/\omega_d)$ of 1.8, 3.6 and 25.0. The new controller provides smaller maximum displacement amplitudes and shorter settling time in most of the cases, than those of the conventional impact damper.

The x_{max} ratio, t_{10} and t_5 ratios to the uncontrolled values are demonstrated in Figures 5.6(a), (b) and (c) for the new controller (□) and the conventional impact damper (Δ), for different non-dimensional clearances $d/(V_{10}/\omega_d)$. For a wide range of clearances ($2<d/(V_{10}/\omega_d)<27$) the new controller has consistent attenuations to x_{max}, t_{10} and t_5. The overall best reduction for x_{max}, t_{10} and t_5 are 74%, 69% and 43% at $d/(V_{10}/\omega_d)=25.0$. On the other hand, the conventional impact damper has only slight reduction for t_5 in a small range of clearances ($1.0\leq d/(V_{10}/\omega_d)\leq 2.0$), even producing amplifications of t_5 for some other clearances. Also, the conventional impact damper is generally less effective on x_{max} and t_{10}.

Figure 5.5 presents the time histories of the primary system for the same cases listed in Figure 5.4 with the same format. The responses of the primary systems controlled by the conventional absorber (Figure 5.5 (b)), the impact damper (Figures 5.5 (c), (e)) and the new controller (Figures 5.5 (d), (f) and (h)) are surprisingly very similar, except the response in Figure 5.5 (g) which is identical to the uncontrolled case in Figure 5.5 (a) since the impact damper is out of its working range at this clearance ($d/(V_{10}/\omega_d) = 25.0$) . On the other hand, it is not surprising that all the three controllers do not work well on the primary system for such large mass ratio cases. For all the controlled cases, x_{max} and t_5 remain almost unchanged as compared with the uncontrolled values in Figure 5.5 (a). The systems controlled by the conventional absorber (Figure 5.5 (b)) and the impact damper (Figures 5.5 (c), (e)) have about 80% longer t_{10}, while those controlled by the new controller (Figures 5.5 (d), (f) and (h)) have 110% increase in t_{10}. For both the conventional impact damper and the new controller, changing the clearance $d/(V_{10}/\omega_d)$ makes almost no difference on their performance. Therefore, the x_{max} ratio, t_{10} and t_5 ratios versus $d/(V_{10}/\omega_d)$ would be almost horizontal lines if they were plotted.

Generally, for a system with a mass ratio (m_1/m_2) as large as 1000, all the controllers which has been discussed (including the new controller) have no effect on the maximum displacement on the primary system, and they make the primary system need longer time to settle down. This drawback shows the limitation of these passive controllers for this large mass ratio case. But this does not offset the impressive positive effect of the new controller

on the secondary system which is the major object to be protected.

Comparing the 10 mass ratio structure with the 1000 mass ratio structure, as far as the secondary system is concerned, the first one has better settling time attenuation with both the conventional impact damper and the new controller, and the second one has better maximum amplitude reduction. It is found that the impact damper is more effective on reducing settling time for small m_1/m_2 ratio, and it is more effective on reducing the maximum displacement amplitudes for large m_1/m_2. For the primary system, both the conventional impact damper and the new controller work better for small m_1/m_2 ratio.

5.4 CONCLUSIONS

In this chapter, the effectiveness of the new passive vibration controller combined with a tuned absorber and an impact damper to the secondary structures under transient vibration is investigated and compared with that of the conventional tuned absorber and the conventional impact damper.

The investigation is focused on protecting the secondary system (m_2, k_2, and c_2) from excessive vibration. It has been found that the conventional tuned absorber mostly contributes to the attenuation of the maximum displacement amplitudes of the secondary system (x_2), it has less effect on the settling time. Generally, the conventional impact damper

can be effective on both the maximum displacement amplitudes and the settling time, but the effectiveness is limited on the maximum displacement amplitudes for a system with small m_1/m_2 ratio, and it is also limited on the settling time for a system with large m_1/m_2 ratio.

As a combination of a tuned absorber and an impact damper, the new controller takes the advantageous features of both the conventional tuned absorber and the impact damper, and it produces larger attenuations for both the maximum displacement amplitudes and the settling times on the secondary system as compared to those of its individual components. As the indirect application of the impact damper, the new controller works effectively in a wider range of clearances than the conventional impact damper. Generally, the maximum amplitudes of the secondary system with the new controller are largely determined by the absorber and have little change with the clearance variation. On the other hand, the settling time is mostly determined by the impact damper. Settling time is more sensitive to the clearance variation than the maximum displacement.

For the structure with $m_1/m_2=10$, the new combined controller also provides the best vibration attenuation on the primary system comparing with the conventional impact damper and the conventional tuned absorber. However, for the structure with a mass ratio as large as 1000, the primary system controlled by any of the three controllers requires longer settling time as compared with the uncontrolled system.

CHAPTER 6

CONCLUSIONS

In this study, a new passive vibration controller which combines a tuned absorber and an impact damper was investigated for controlling the vibrations of light secondary structures. A series of parametric studies were conducted by computer simulation. Experiments were performed along with numerical predictions. Most of the studies were based on random excitation. Some representative transient vibration cases were also investigated. Following are the major conclusions of this study.

For a light secondary structure under random vibration, adding an impact damper on the conventional tuned absorber may provide significant improvements in controlling the excessive vibrations of the secondary system as well as those of the primary system. In addition, the displacement of the absorber itself as part of the new controller is smaller than that of the absorber when working alone.

When the mass ratio between the primary system and the secondary system (m_1/m_2) is 10, the impact damper as part of the new controller is most effective for system with

minimal damping. RMS displacement attenuations in the order of 80% based on the effectiveness of a conventional absorber are possible in the responses of the secondary, the primary, and the tuned absorber systems. This indirect benefit of controlling the primary system through the controlled response of the secondary system, may prove particularly useful for practical applications.

For the structures with m_1/m_2=1000, the impact damper as part of the controller is most effective when primary system has at least 5% critical damping. The impact damper can provide about 80% further RMS displacement attenuation for both the secondary and the tuned absorber systems. No control is attainable for the primary system due to its large inertia.

For the experimental structure (m_1/m_2=10, ξ_1=0.0053, ξ_2=0.0026) under a random white noise excitation, the best result for the secondary system was measured at d/σ_{x20} =10.2 with 57% RMS displacement attenuation as compared with the result of the conventional tuned absorber, whereas the RMS displacement attenuations to the primary system and the absorber system are 56% and 53%.

Tuning the natural frequency of the absorber off the natural frequency of the secondary system to be controlled is found to be ineffective to further improve the performance of the new controller. Keeping the absorber within 10% off-tuning (f3/f2

ranging from 0.9 to 1.1) will ensure that the new controller works in its most effective range.

For secondary structures under transient vibration, the new controller takes the advantageous features of both the conventional tuned absorber and the impact damper. It produces larger attenuations, for both the maximum displacement amplitudes and the settling times on the secondary system, than those of the two conventional controllers when they are used individually. In addition, as the indirect application of the impact damper, the new controller works effectively in a wider range of clearances than the conventional impact damper does.

For transient vibrations, the new controller also provides large vibration attenuation to the primary system with $m_1/m_2=10$, as it does to the secondary system. For the primary system with $m_1/m_2=1000$, the new controller has no effect on the maximum displacement and some negative effect on the settling time though its performance on the secondary system is quite impressive.

REFERENCES

1. A. G. HERNRIED and J. L. SACKMAN 1984 *Earthquake Engineering and Structural Dynamics*, vol. 12, 737-748. Response of Secondary Systems in Structures Subjected to Transient Excitation.

2. Y. CHEN and T. T. SOONG 1988 *Engineering Structures*. vol. 10, 218-228. State of the Art Review: Seismic Response of Secondary Systems.

3. J. M. KELLY and H. C. TSAI 1985 *Earthquake Engineering and Structural Dynamics* vol. 13, 711-732. Seismic Response of Light Internal Equipment in Base-Isolated Structures.

4. N. D. EBRAHIMI 1988, *Journal of Sound and Vibration*, 120(3),445-455. Optimum Secondary Dampers for Free Response of Underdamped Systems.

5. J. B. HUNT 1979 *Dynamic Vibration Absorbers*. Letchworth, London: The Garden City Limited.

6. J. C. SNOWDON 1968 *Vibration and Shock in Damped Mechanical Systems.* New York: John Wiley & Sons.

7. N. OLGAC and B. T. HOL-HANSEN 1994 *Journal of Sound and Vibration* 176(1), 93-104. A Novel Active Vibration Absorption Technique: Delayed Resonator.

8. S. E. SEMERCIGIL, D. LAMMERS and Z. YING 1992 *Journal of Sound and Vibration* 156(3), 445-459. A New Tuned Vibration Absorber for Wide-Band Excitations.

9. Z. YING and S. E. SEMERCIGIL 1995 *Journal of Sound and Vibration* in press. A Critical Look at a New Tuned Absorber.

10. C. N. BAPAT and S. SANKAR 1985 *Journal of Sound and Vibration* 99(1), 85-94. Single Unit Impact Damper in Free and Forced Vibration.

11. C. H. LEE and K. P. BYRNE 1987 *Journal of Sound and Vibration* 119(3), 529-543. Impact Statistics for a Random Rattling System.

12. L. H. V. BERKEL and S. E. SEMERCIGIL 1991 *Journal of Sound and Vibration* 150(2), 322-329. Tuned Vibration Absorber for Secondary Structures.

13. A. B. SCHRIVER and A. C. HEIDEBRECHT 1989 *Proceedings of the Canadian Congress of Applied Mechanics*, 420-421. Damping and Secondary System Response.

14. S. F. MASRI and A. M. IBRAHIM 1973 *The Journal of the Acoustical Society of America* 53(1), 200-211. Response of the Impact Damper to Stationary Random Excitation.

15. S. F. MASRI, R. K. MILLER, T. J. DEGHANYAR and T. K. CAUGHEY 1989 *Transactions of the American Society of Mechanical Engineers, Journal of Applied Mechanics* 56, 658-666. Active Parameter Control of Nonlinear Vibrating Structures.

16. K. G. BEAUCHAMP 1973 *Signal Processing Using Analog and Digital Techniques.* London: Allen and Unwin.

17. M. M. NIGM and A. A. SHABANA 1983 *Journal of Sound and Vibration* 89(4), 541-557. Effect of an Impact Damper on a Multi-Degree of Freedom System.

18. R. K. ROY, R. D. ROCKE and J. E. FOSTER 1975 *Journal of Engineering for Industry*, November, 1317 - 1324. The Application of Impact Dampers to Continuous Systems.

19. C. N. BAPAT and S. SANKAR 1985 *Journal of Sound and Vibration* 99(1), 85 - 94. Single Unit Impact Damper in Free and Forced Vibration.

20. C. PANG, N. POPPLEWELL and S. E. SEMERCIGIL 1989 *Journal of Sound and Vibration* 133(2), 359 - 363. An Overview of A Bean Bag Damper's Effectiveness.

21. M. M. SADEK and B. MILLS 1970 *Journal Mechanical Engineering Science*, Vol 12 No 4. Effect of Gravity on the Performance of an Impact Damper: Part 1. Steady-State Motion.

22. M. M. SADEK and B. MILLS 1970 *Journal Mechanical Engineering Science*, Vol 12 No 4. Effect of Gravity on the Performance of an Impact Damper: Part 2. Stability of Vibration.

23. H. G. DAVIES 1980 *Journal of Sound and Vibration* 68(4), 479 - 487. Random Vibration of a Beam Impacting Stops.

24. M. KATO, M. DAZAI and H. TAKASE 1976 *Bulletin of the JSME.* Vol. 19, No. 128. Study on Impact Damper Having a Spring-supported Additional Mass.

25. M. D. THOMAS and M. M. SADEK 1974 *Journal of Mechanical Engineering*

Science, Vol 16 No 2. The Effectiveness of the Impact Damper With a Spring-Supported Auxiliary Mass.

26. J. D. RIERA 1980 *Nuclear Engineering and Design* 57, 193 - 206. A Critical Reappraisal of Nuclear Power Plant Safety Against Accidental Aircraft Impact.

27. S. S. RAO 1986 *Mechanical Vibration*, Addison Wesley, Massachusetts.

28. Z. YING 1992 *Passive Vibration Control of Resonant Systems and Vibration Prediction at Inaccessible Points*, M. Eng. thesis, Mechanical Engineering Department, McMaster University.

29. L. H. Van BERKEL 1991 *Spreadsheet Solutions for Vibration Analysis and Modeling*, M. Eng. thesis, Mechanical Engineering Department, McMaster University.

30. S. E. SEMERCIGIL, N. POPPLEWELL and R. TYC 1988 *Journal of Sound and Vibration* 121(1), 178-184, Impact Damping Random Vibrations.

31. M. LEONARD 1975 *Elements of Vibration Analysis*, New York, McGill-Hill.

32. L. H. Van BERKEL, 1991 *Spreadsheet Solutions for Vibration Analysis and Modeling, Thesis for Master of Engineering*, Department of Mechanical Engineering, McMaster University.

33. T. THOMSON, 1981 *Theory of Vibration with Applications*, Prentice-Hall Englewood Cliffs.

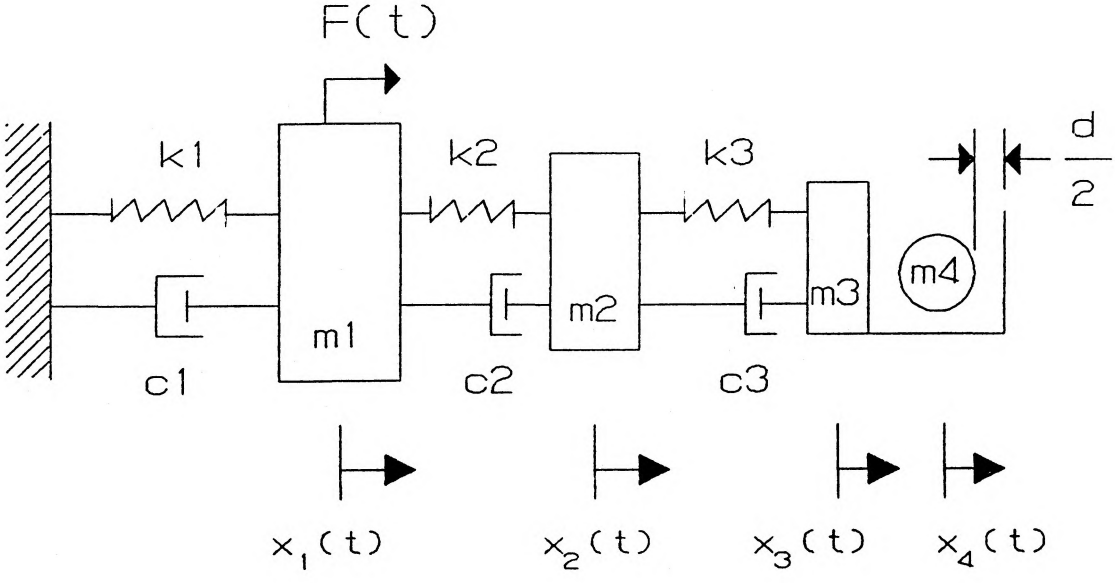

Figure 2.1 The Four Degree-Of-Freedom model to represent a secondary structure controlled by a tuned absorber and an impact damper.

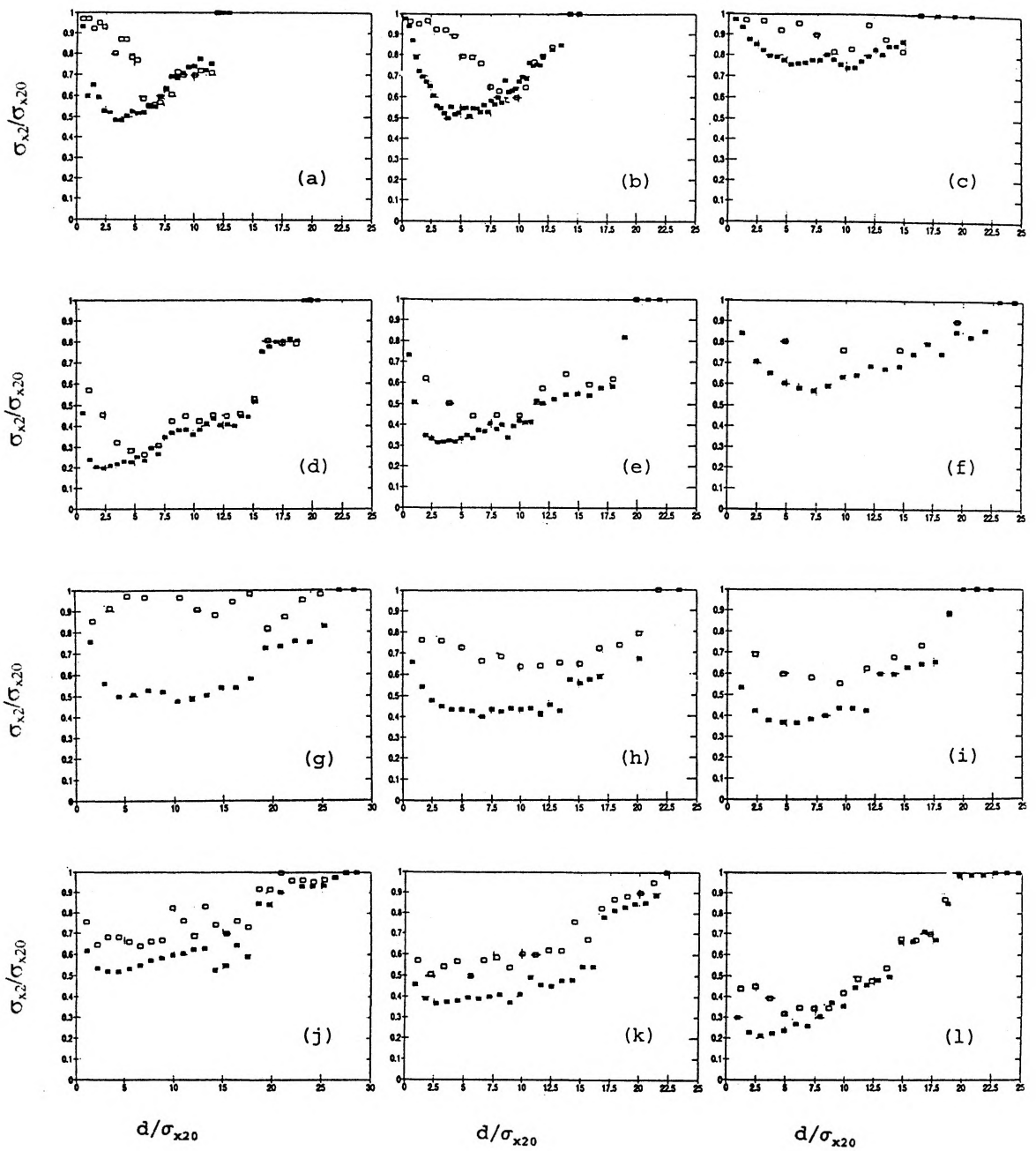

Figure 2.2 Variation of RMS displacement ratios of the secondary structure with clearance d/σ_{x20} for e=0.3 (■) and e=0.8 (□) and

for $m_1/m_2 = 1$ (a) ξ_1=0.001, (b) ξ_1=0.01, (c) ξ_1=0.05;
for $m_1/m_2 = 10$ (d) ξ_1=0.001, (e) ξ_1=0.01, (f) ξ_1=0.05;
for $m_1/m_2 = 100$ (g) ξ_1=0.001, (h) ξ_1=0.01, (i) ξ_1=0.05;
for $m_1/m_2 = 1000$ (j) ξ_1=0.001, (k) ξ_1=0.01, (l) ξ_1=0.05.

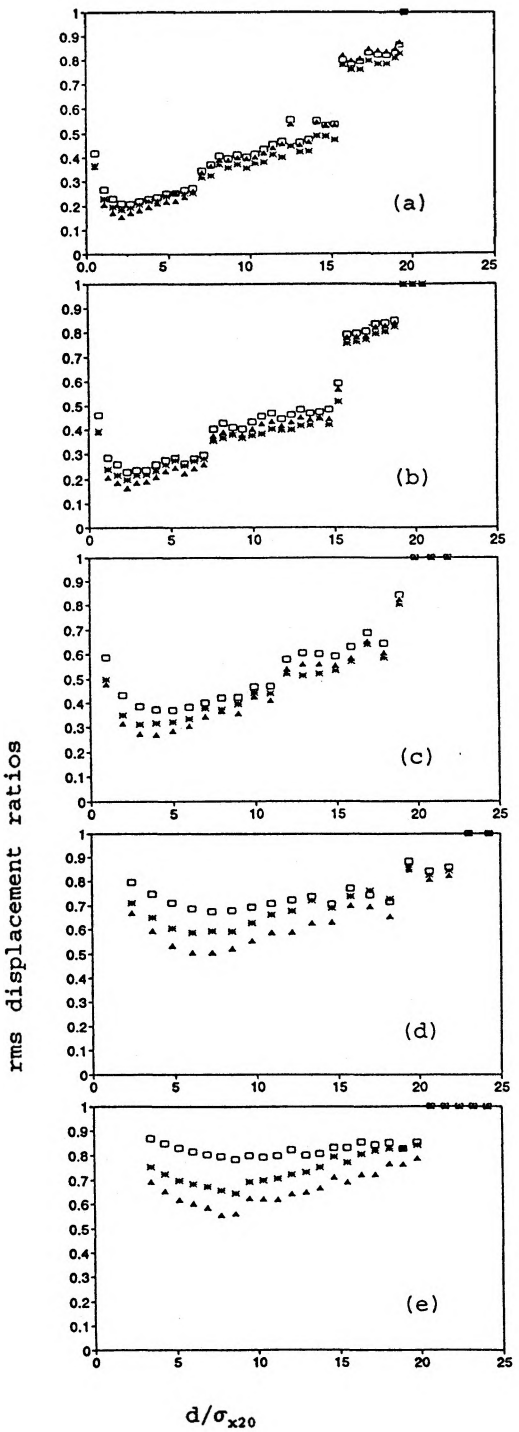

Figure 2.3 Variation of RMS displacement ratios of the primary system (□),secondary system (*) and the absorber (▲) for e=0.3 and for m_1/m_2=10 and (a) ξ_1=0, (b) ξ_1=0.001, (c) ξ_1=0.01, (d) ξ_1=0.05 and (e) ξ_1=0.10.

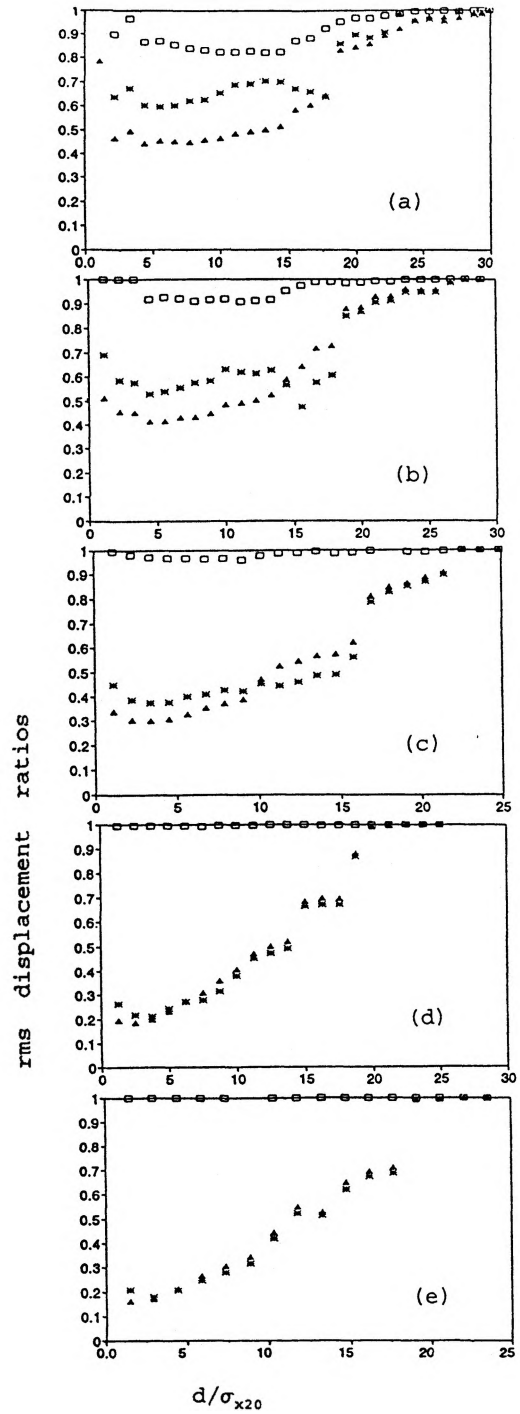

Figure 2.4 Variation of RMS displacement ratios of the primary system (□),secondary system (*) and the absorber (▲) for e=0.3 and for m_1/m_2=1000 and (a) ξ_1=0, (b) ξ_1=0.001, (c) ξ_1=0.01, (d) ξ_1=0.05 and (e) ξ_1=0.10.

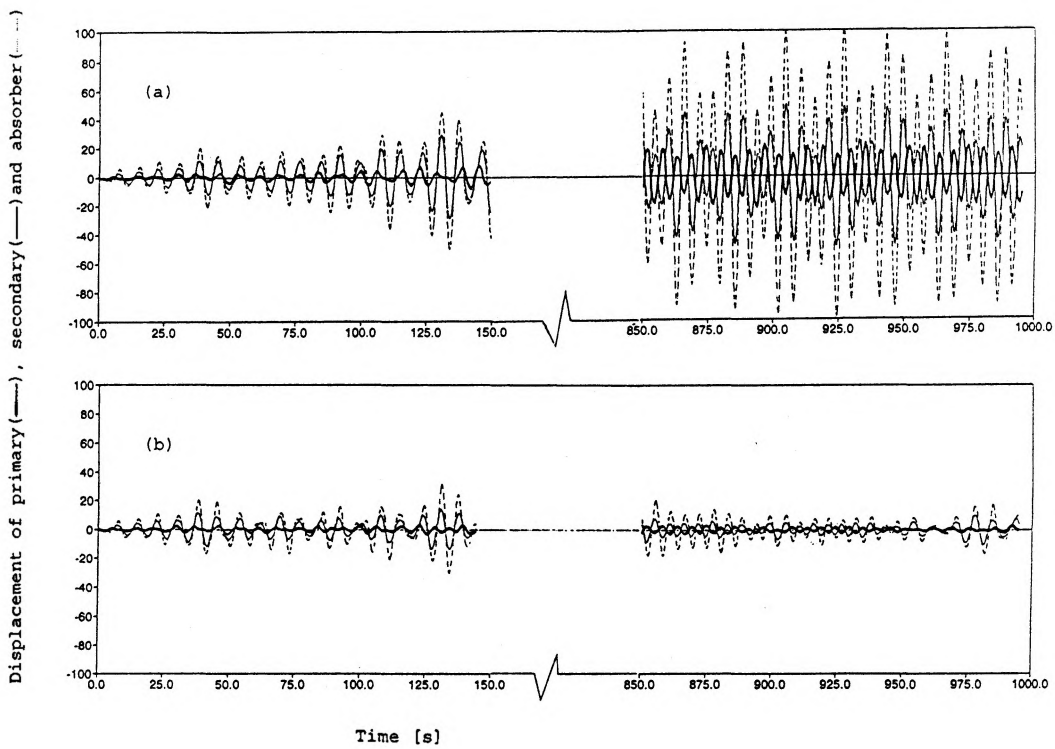

Figure 2.5 Time History of the primary (▬), secondary (—) and absorber (----) displacement for the system controlled by (a) the absorber alone, (b) the new controller at $d/\sigma_{x20} = 2.17$. $m_1/m_2 = 10$ and $\xi_1 = 0$.

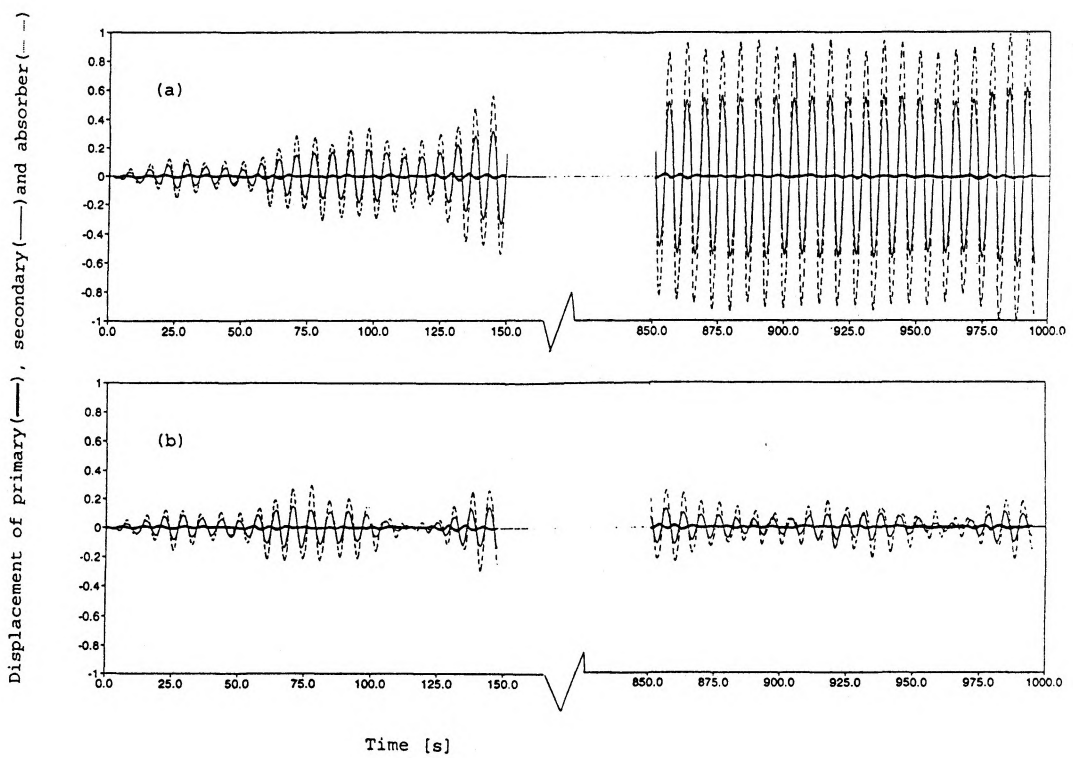

Figure 2.6 Time History of the primary (—), secondary (—) and absorber (----) displacement for the system controlled by (a) the absorber alone, (b) the new controller at $d/\sigma_{x20} = 2.95$. $m_1/m_2 = 1000$ and $\xi_1 = 0.10$.

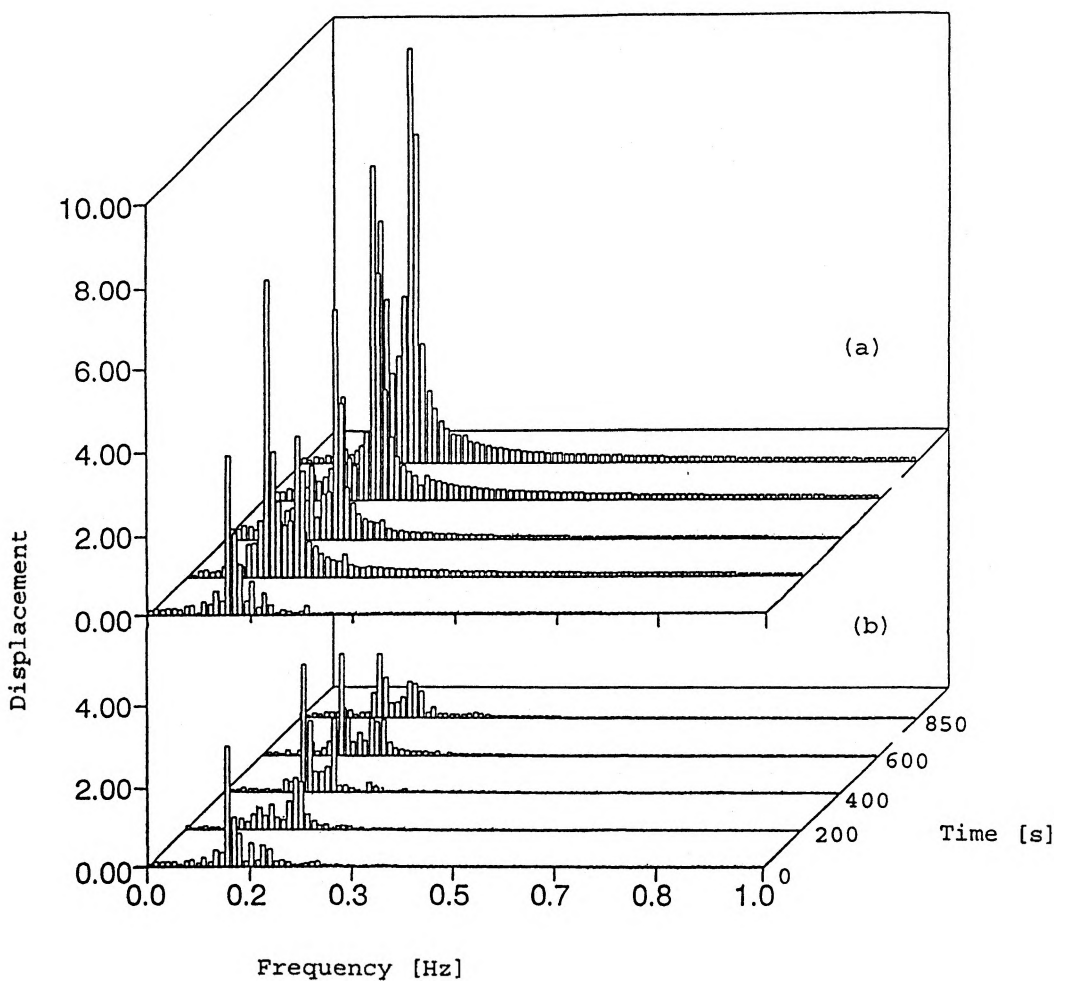

Figure 2.7 Variation of FFT of the displacement of the secondary system with time for the system controlled by (a) the absorber alone, (b) the new controller at $d/\sigma_{x20} = 2.17$. $m_1/m_2 = 10$ and $\xi_1 = 0$.

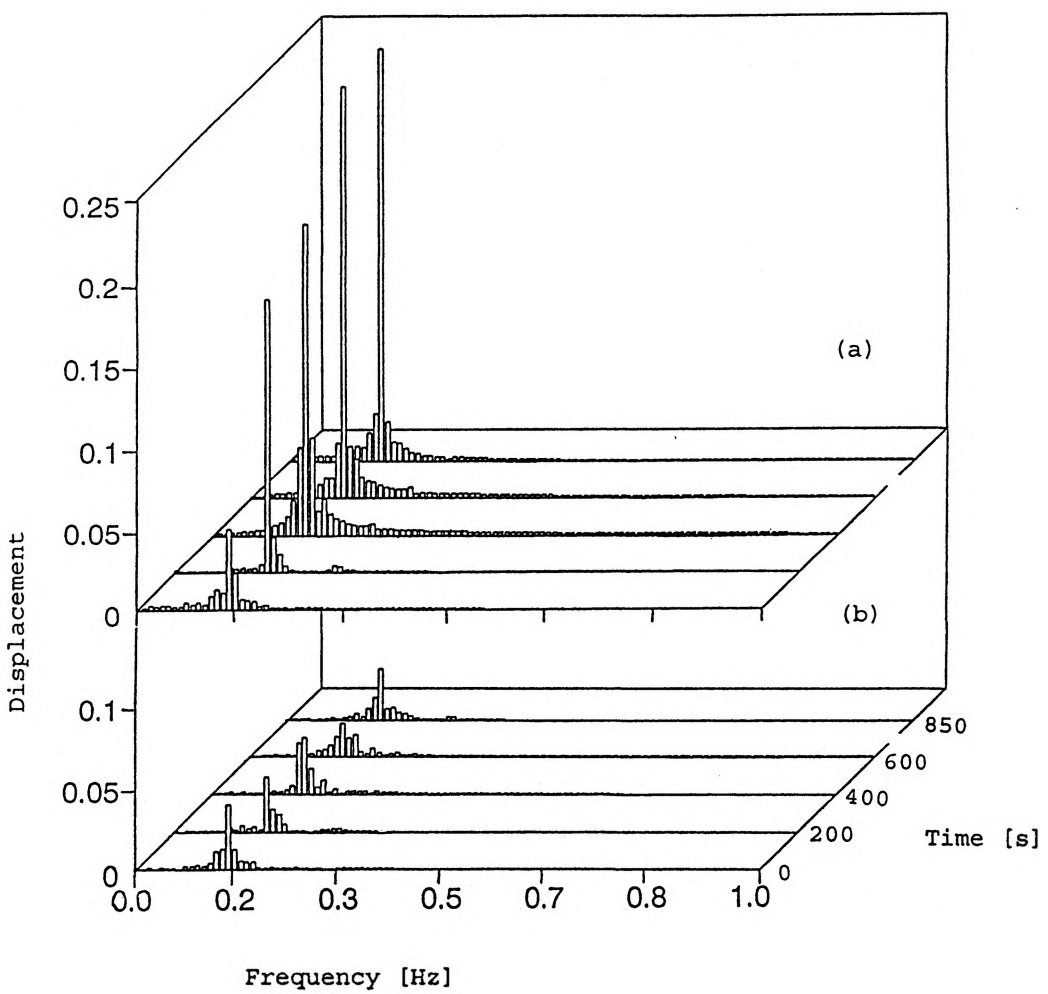

Figure 2.8 Variation of FFT of the displacement of the secondary system with time for the system controlled by (a) the absorber alone, (b) the new controller at $d/\sigma_{x20} = 2.95$. $m_1/m_2 = 1000$ and $\xi_1 = 0.10$.

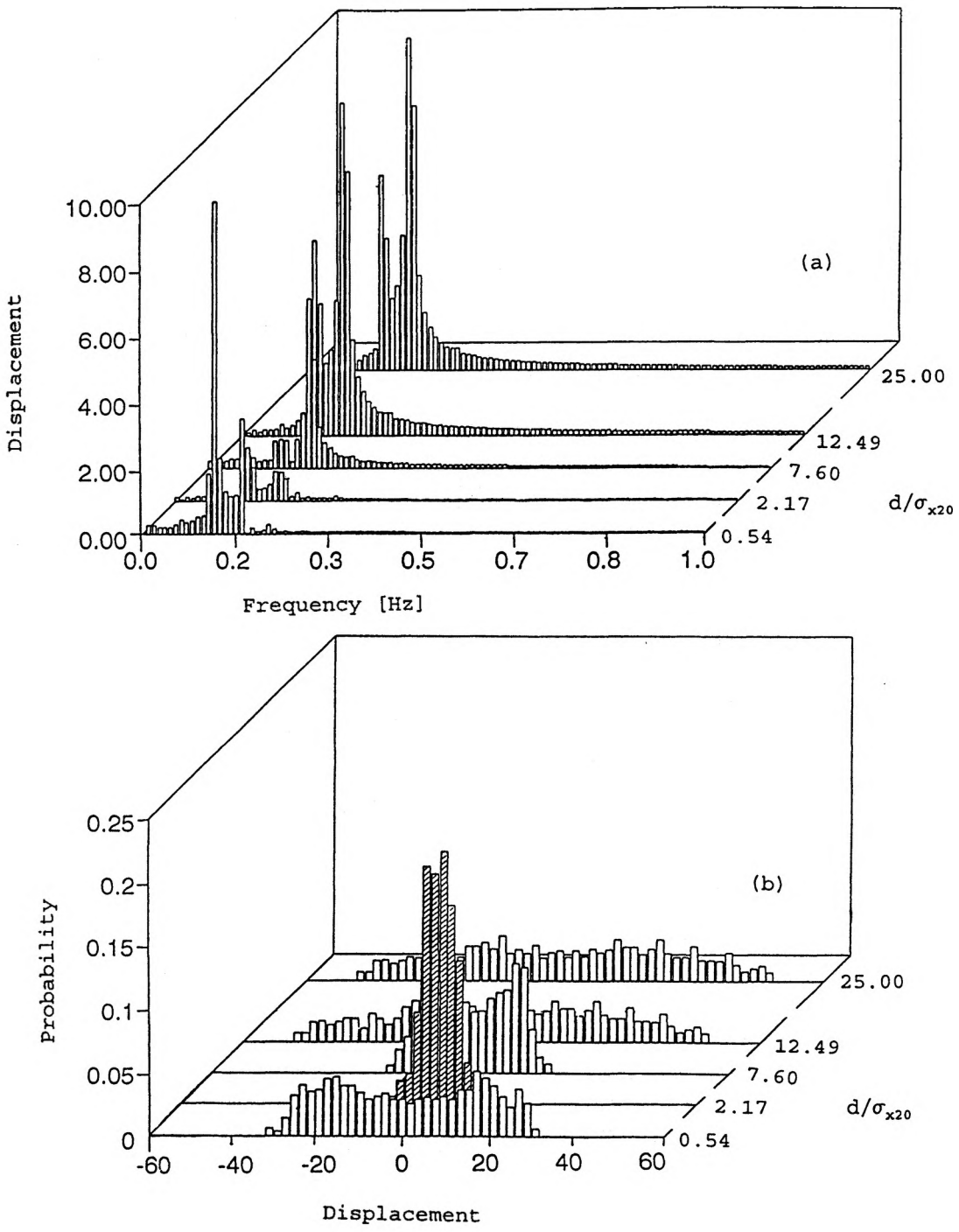

Figure 2.9 Variation of (a) FFT and (b) probability distribution of the displacement of the secondary system with clearance. $m_1/m_2=10$ and $\xi_1=0$.

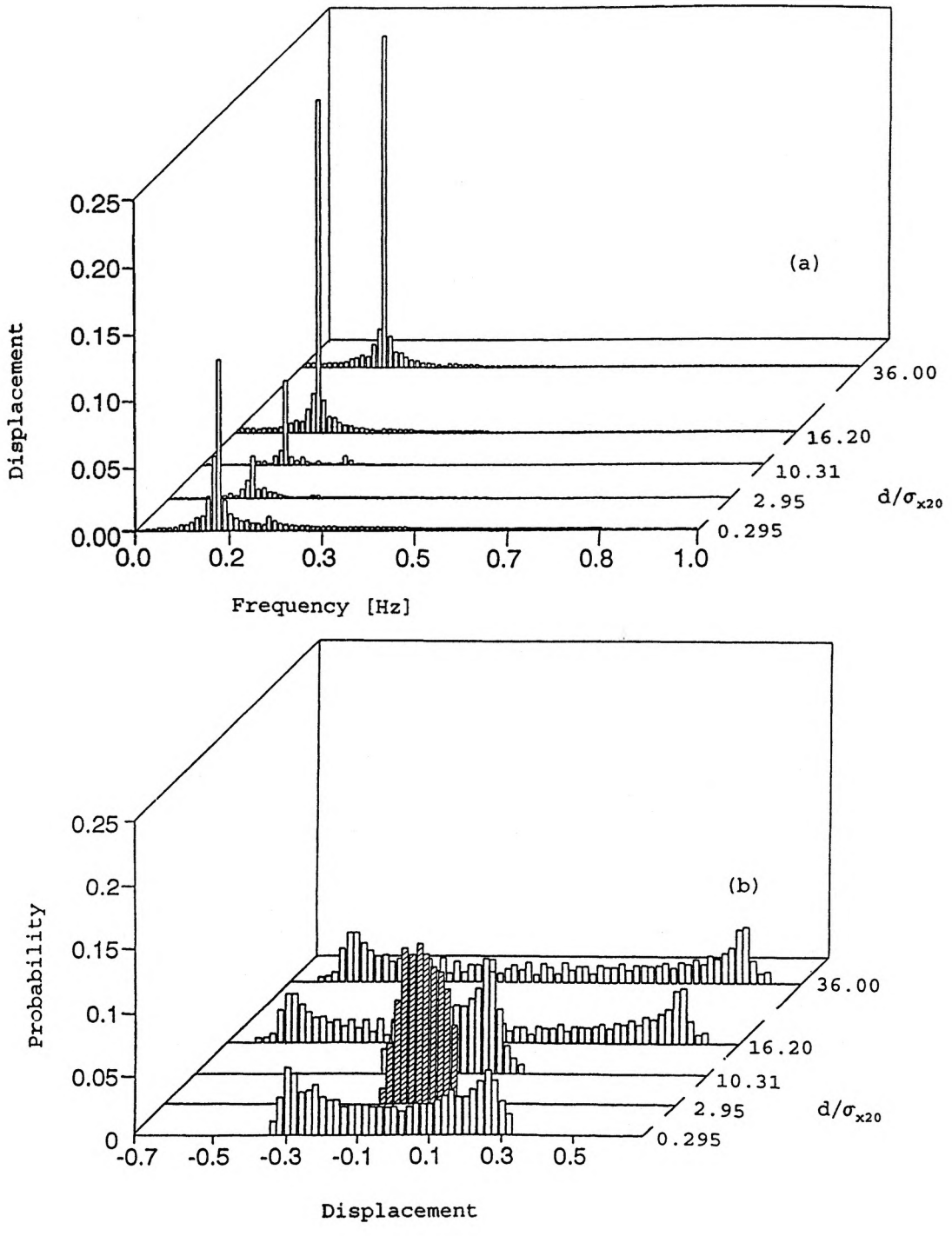

Figure 2.10 Variation of (a) FFT and (b) probability distribution of the displacement of the secondary system with clearance. m_1/m_2=1000 and ξ_1=0.10.

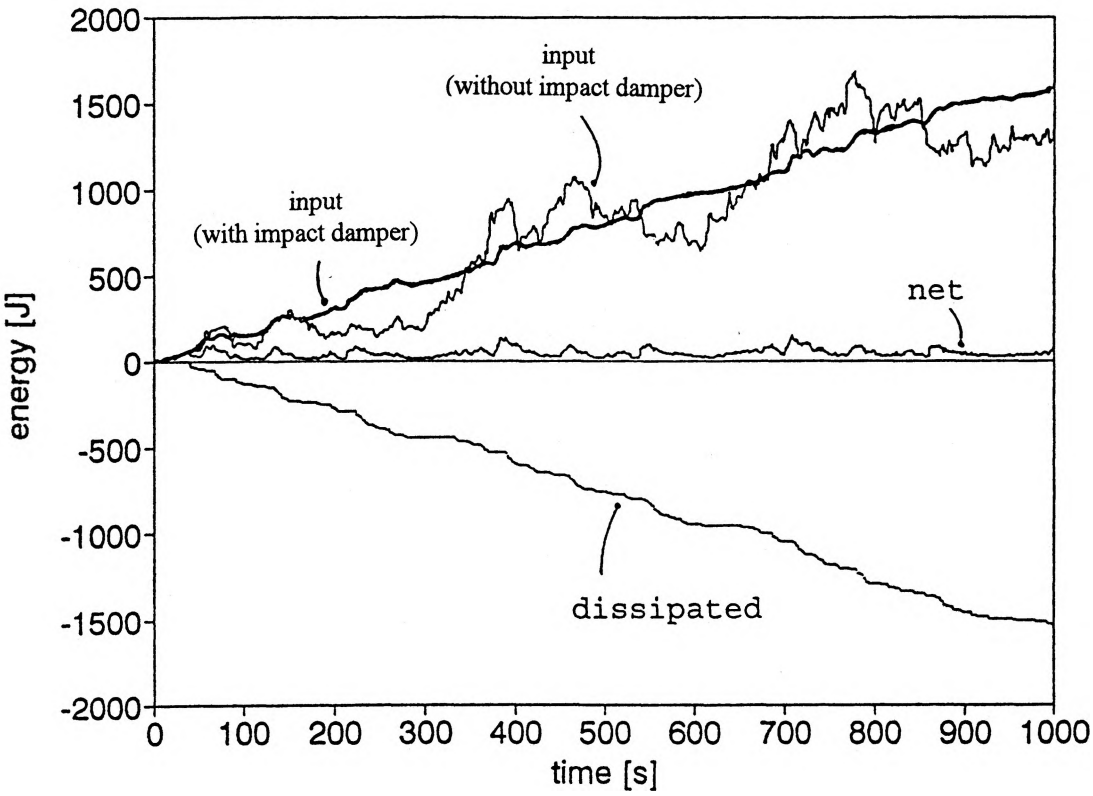

Figure 2.11 History of the input energy to the primary system, dissipated energy and net energy for $m_1/m_2=10$ and $\xi_1=0$.

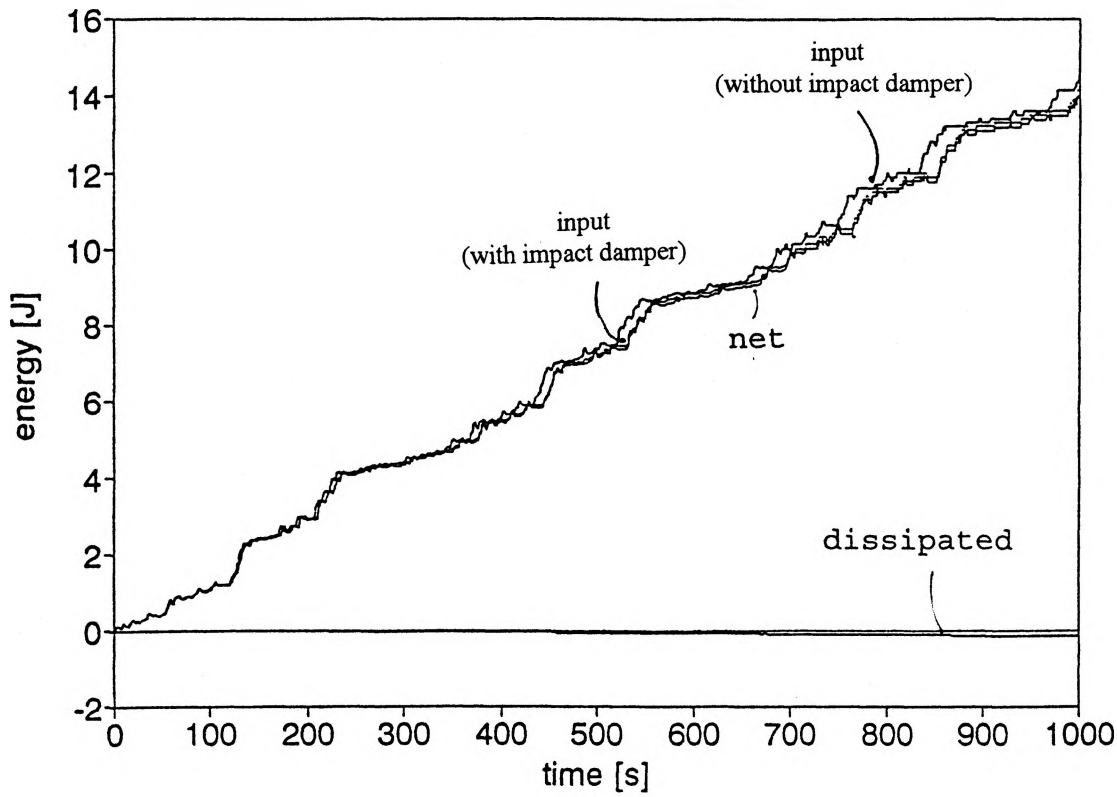

Figure 2.12 History of the input energy to the primary system, dissipated energy and net energy for $m_1/m_2=1000$ and $\xi_1=0.10$.

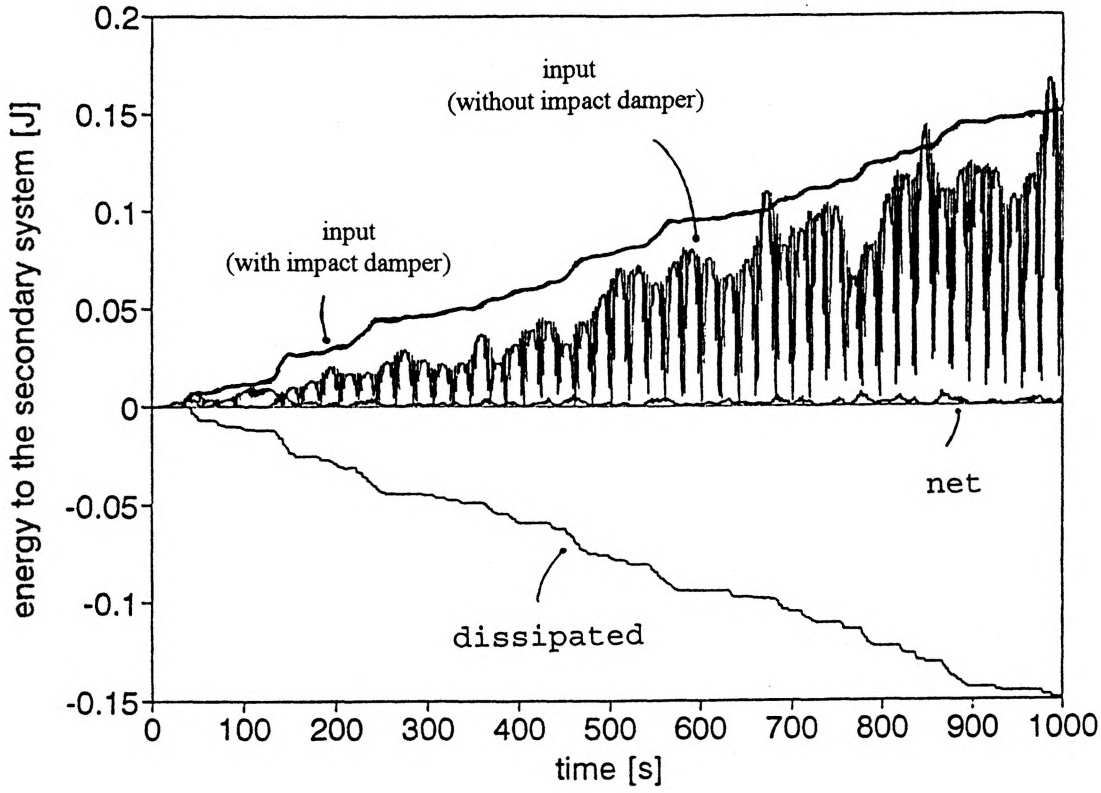

Figure 2.13 History of the input energy to the secondary system, dissipated energy and net energy for m_1/m_2=1000 and ξ_1=0.10.

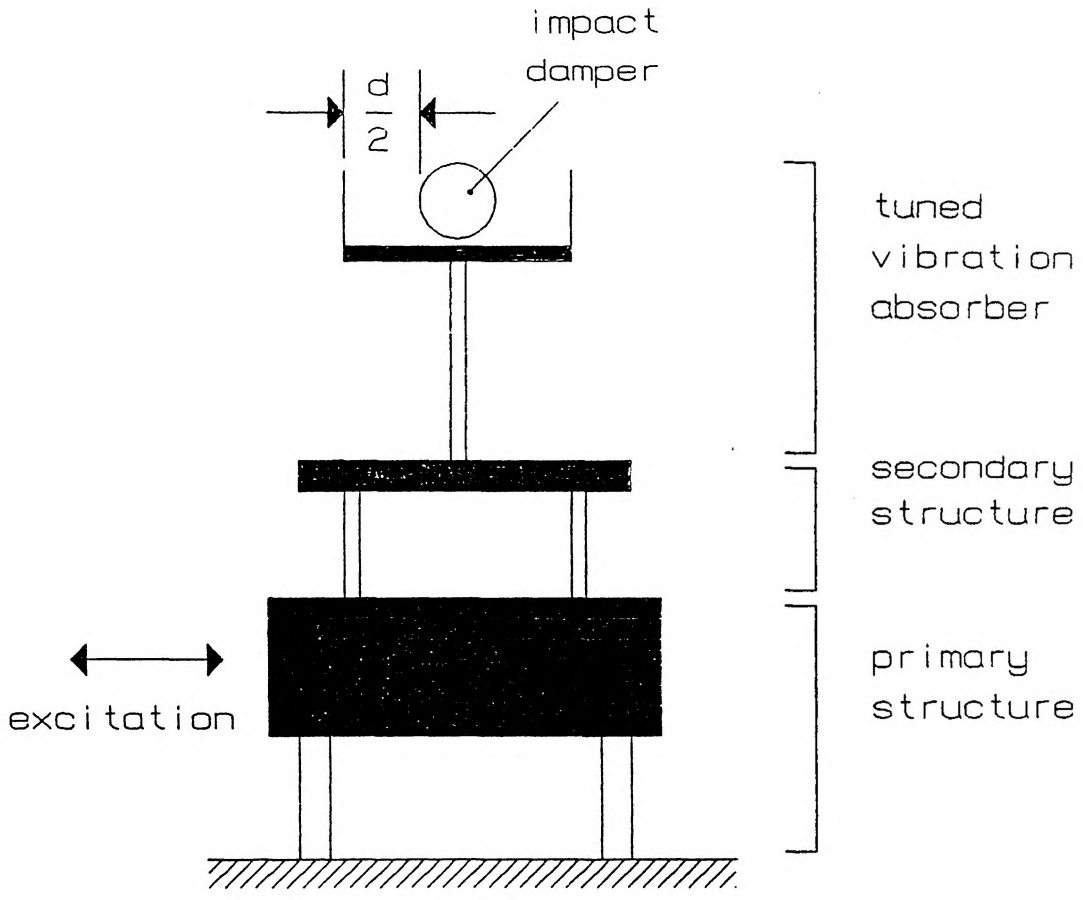

Figure 3.1 Schematic drawing of the experimental structure

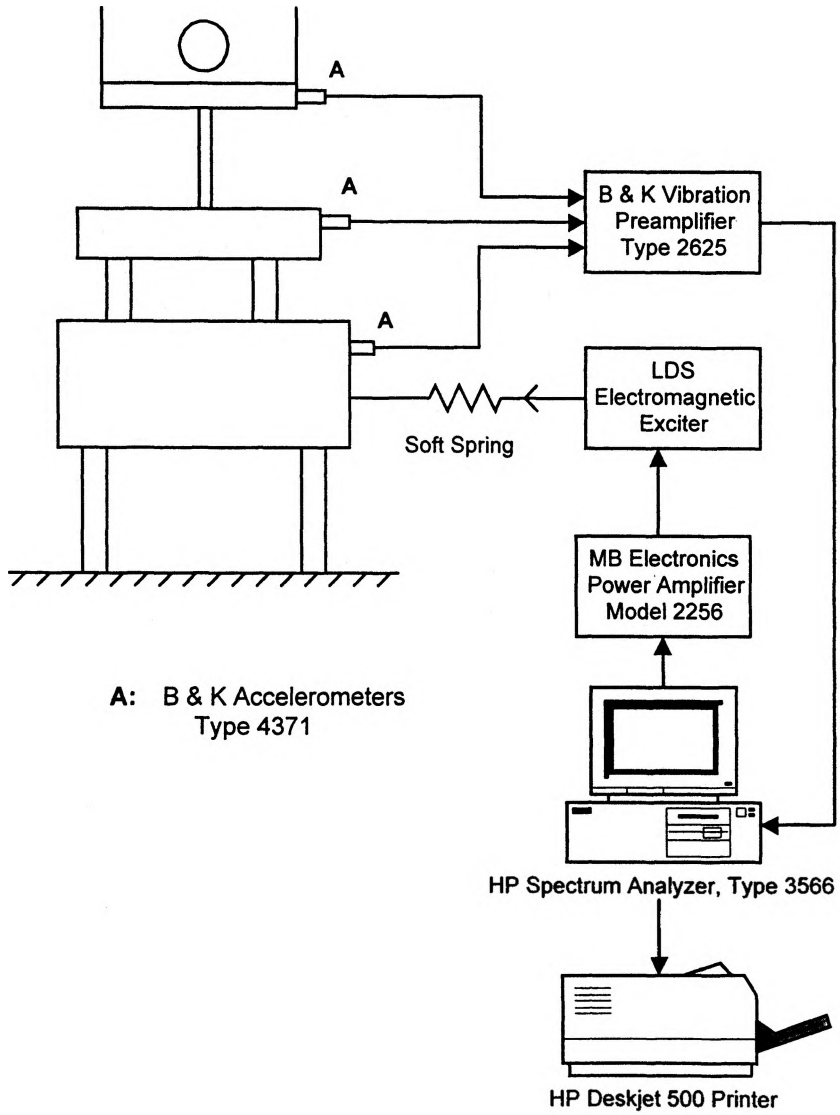

Figure 3.2 Experimental setup and instrumentation.

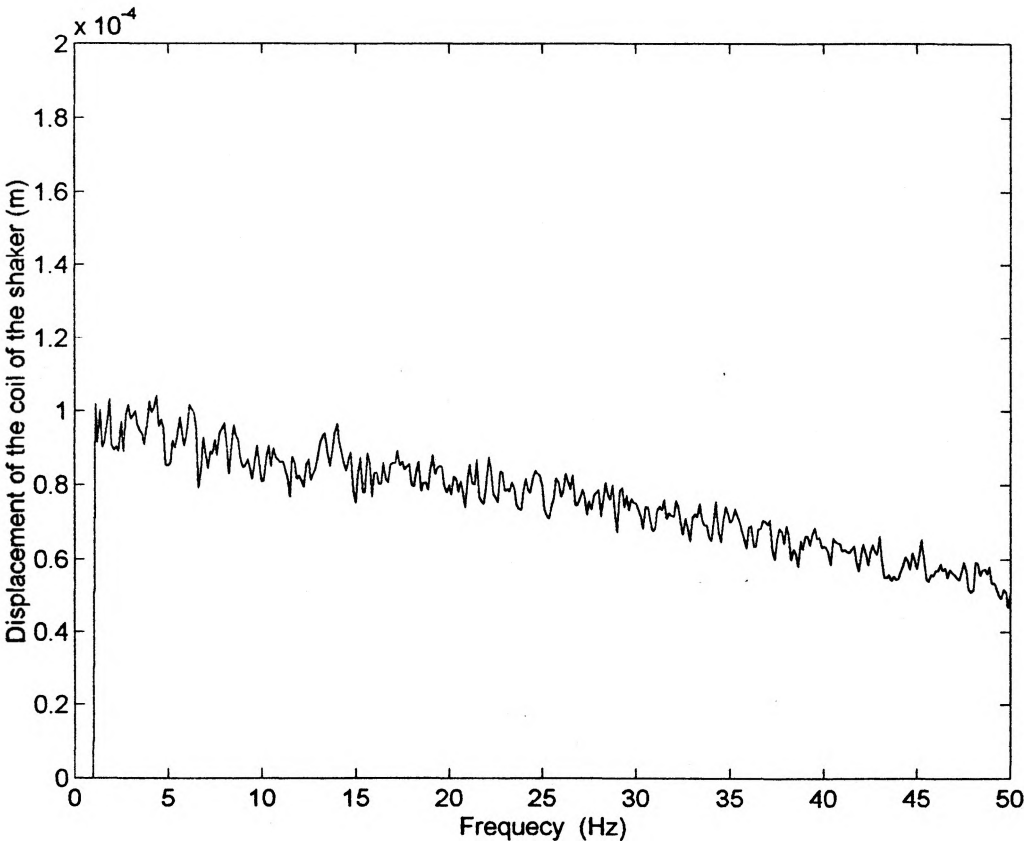

Figure 3.3 Frequency spectrum of the moving coil of the magnetic shaker.

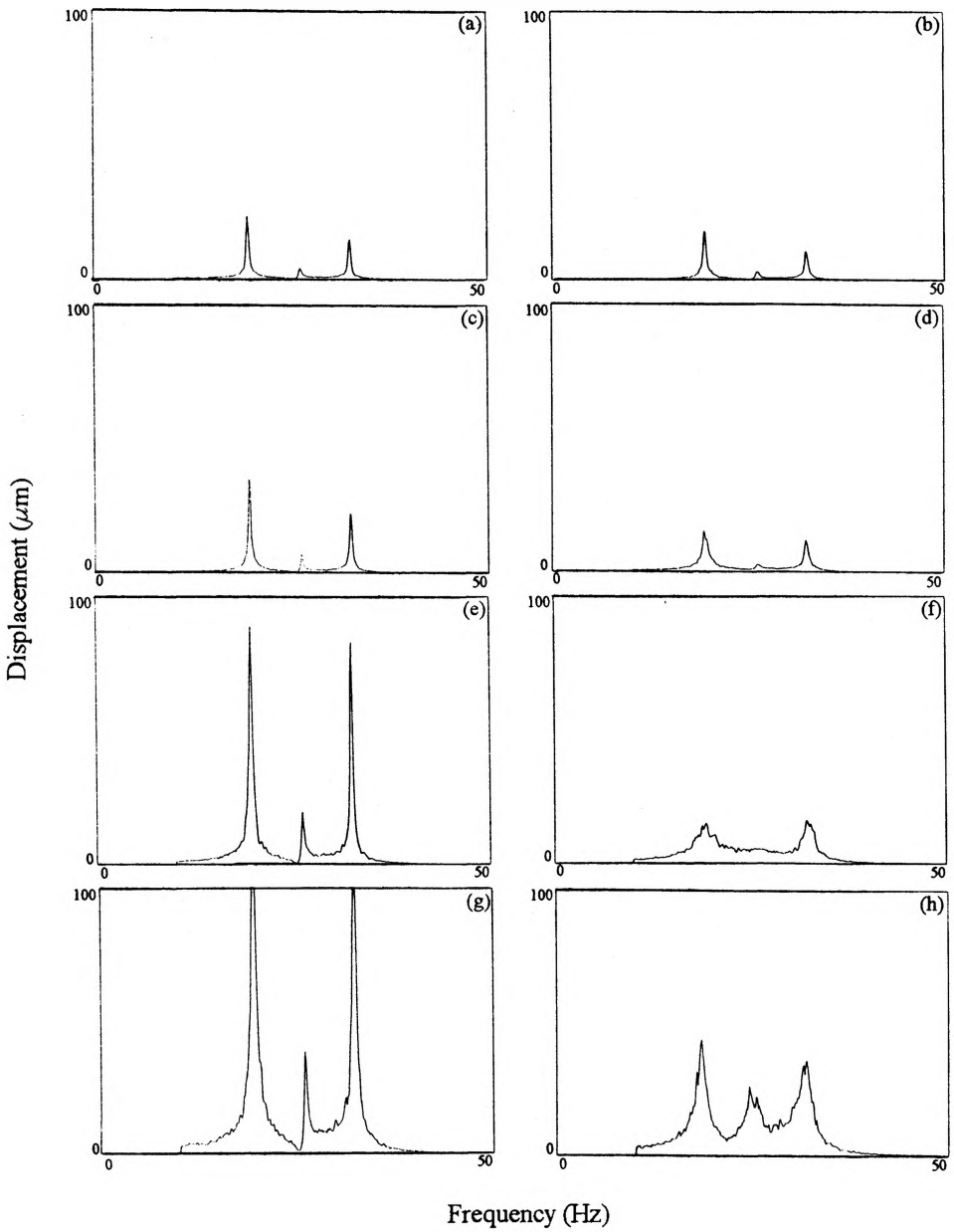

Figure 3.4 Displacement spectra of the secondary system controlled by the conventional absorber (the first column) and the new controller (the second column) for d/σ_{x20} of (a), (b) 45.7; (c), (d) 30.9; (e), (f) 10.2; and (g), (h) 4.7.

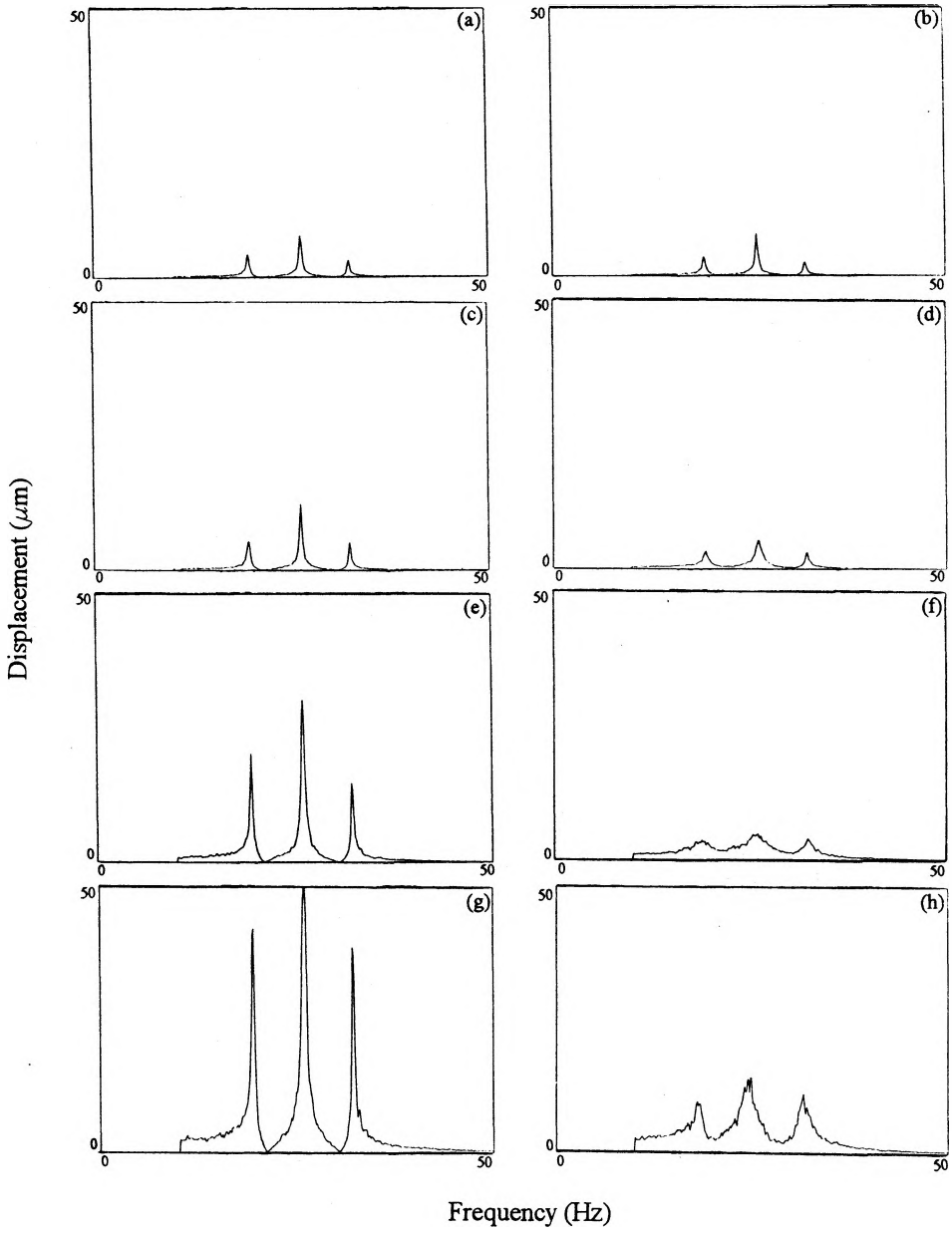

Figure 3.5 Displacement spectra of the primary system controlled by the conventional absorber (the first column) and the new controller (the second column) for d/σ_{x20} of (a), (b) 45.7; (c), (d) 30.9; (e), (f) 10.2; and (g), (h) 4.7.

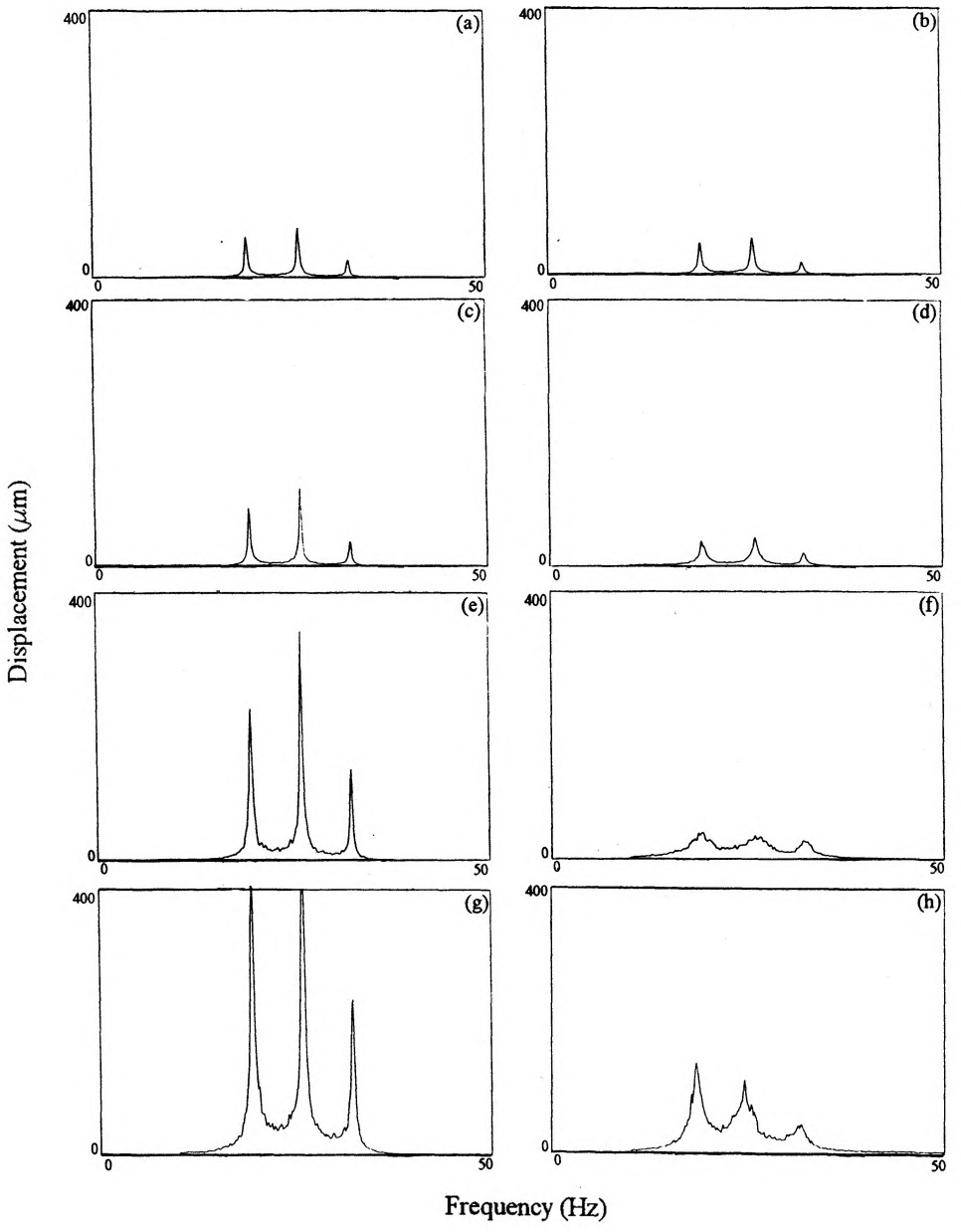

Figure 3.6 Displacement spectra of the absorber system when it works alone (the first column) and when it works as part of the new controller (the second column) for d/σ_{x20} of (a), (b) 45.7; (c), (d) 30.9; (e), (f) 10.2; and (g), (h) 4.7.

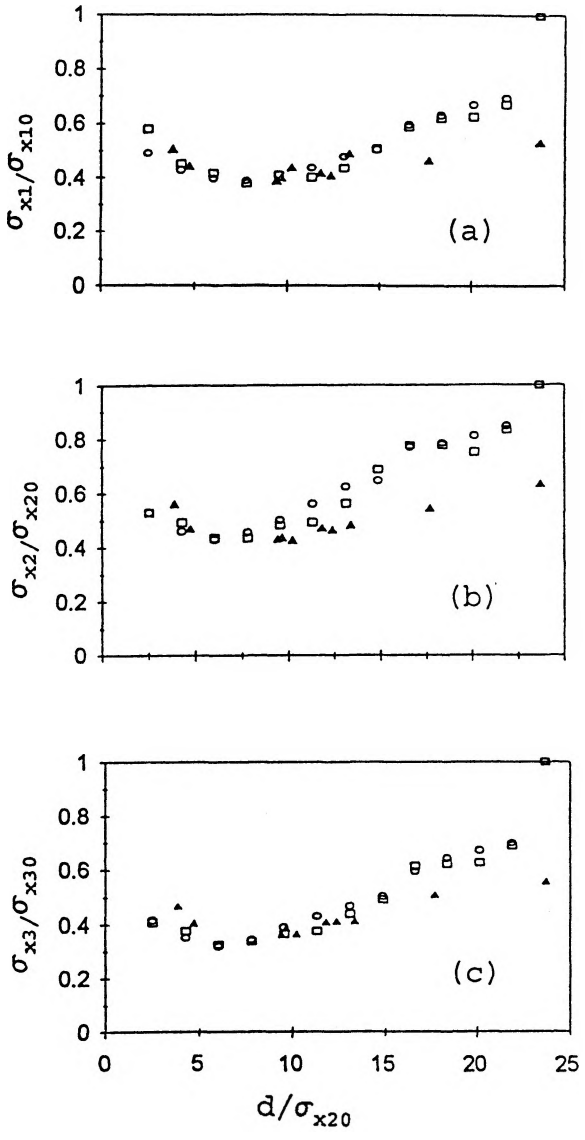

Figure 3.7 RMS displacement variation of: (○) the simulation results of e=0.3, (□) the simulation results of e=0.4; and (▲) the experiment results for (a) the primary system (σ_{x1}/σ_{x10}); (b) the secondary system (σ_{x2}/σ_{x20}); (c) the absorber (σ_{x3}/σ_{x30}) versus the non-dimensional clearance d/σ_{x20}.

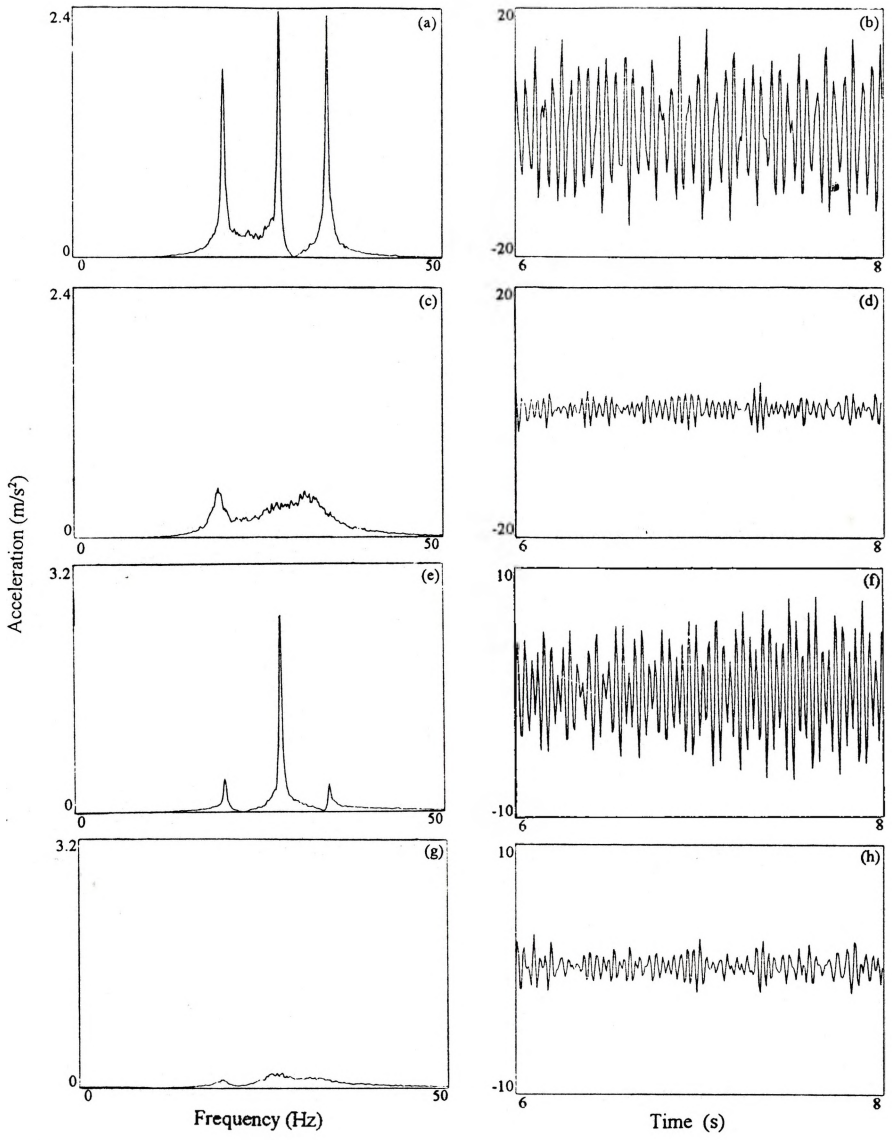

Figure 3.8 Acceleration spectra (the first column) and the corresponding time histories (the second column) for d/σ_{x20}=8.6. (a), (b): The secondary system with the absorber ; (c), (d): the secondary system with the new controller; (e), (f): the primary system with the absorber; (g), (h) the primary system with the new controller.

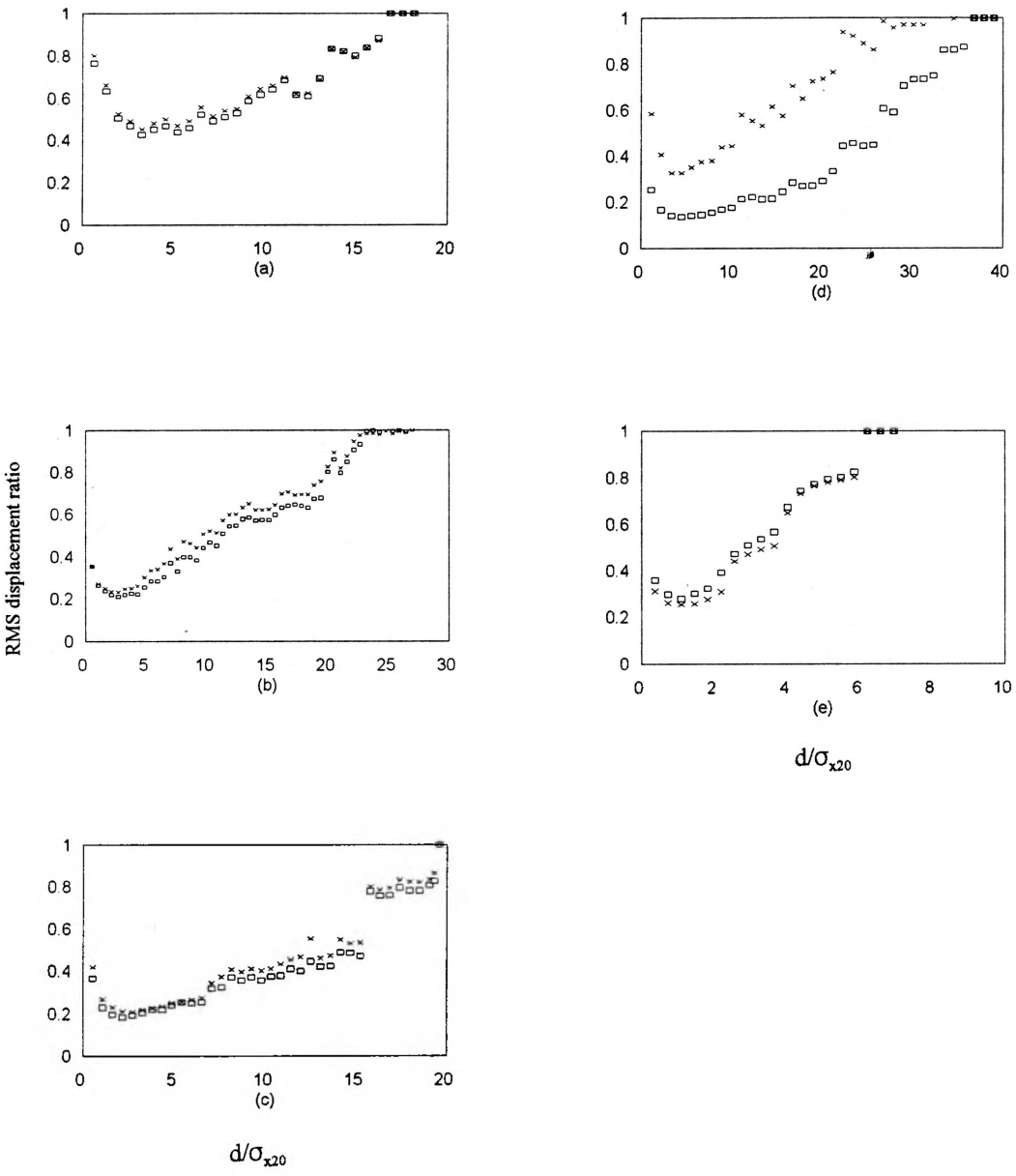

Figure 4.1 variation of the RMS displacement ratios (σ_x/σ_{x0}) of the primary system (□) and the secondary system (×) versus the non-dimensional clearance (d/σ_{x20}) for the cases of m_1/m_2=10, $\xi_1=\xi_2$=0.0 and the off-tuning ratio (f_3/f_2) of (a) 0.8; (b) 0.9; (c) 1.0; (d) 1.1 and (e) 1.2.

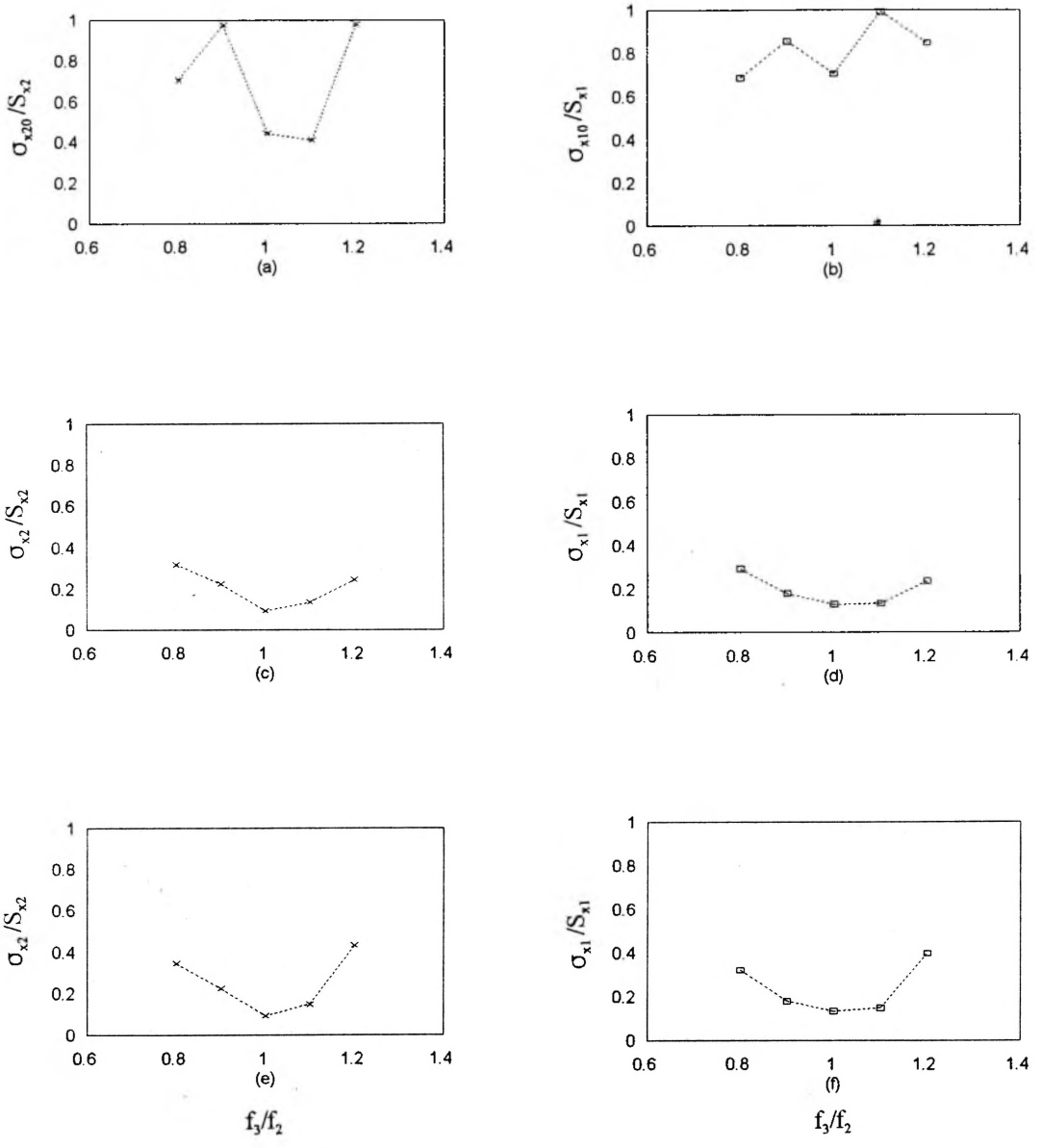

Figure 4.2 RMS displacement ratios of the secondary system (the first column) and the corresponding primary system (the second column) versus the off-tuning ratio (f_3/f_2) for the case of $m_1/m_2=10$, $\xi_1=\xi_2=0.0$. (a) and (b): system controlled by absorber alone; (c) and (d): system controlled by new controller working at the best clearances; (e) and (f): system controlled by new controller working at a fixed clearance ($d/\sigma_{x20}=2.72$).

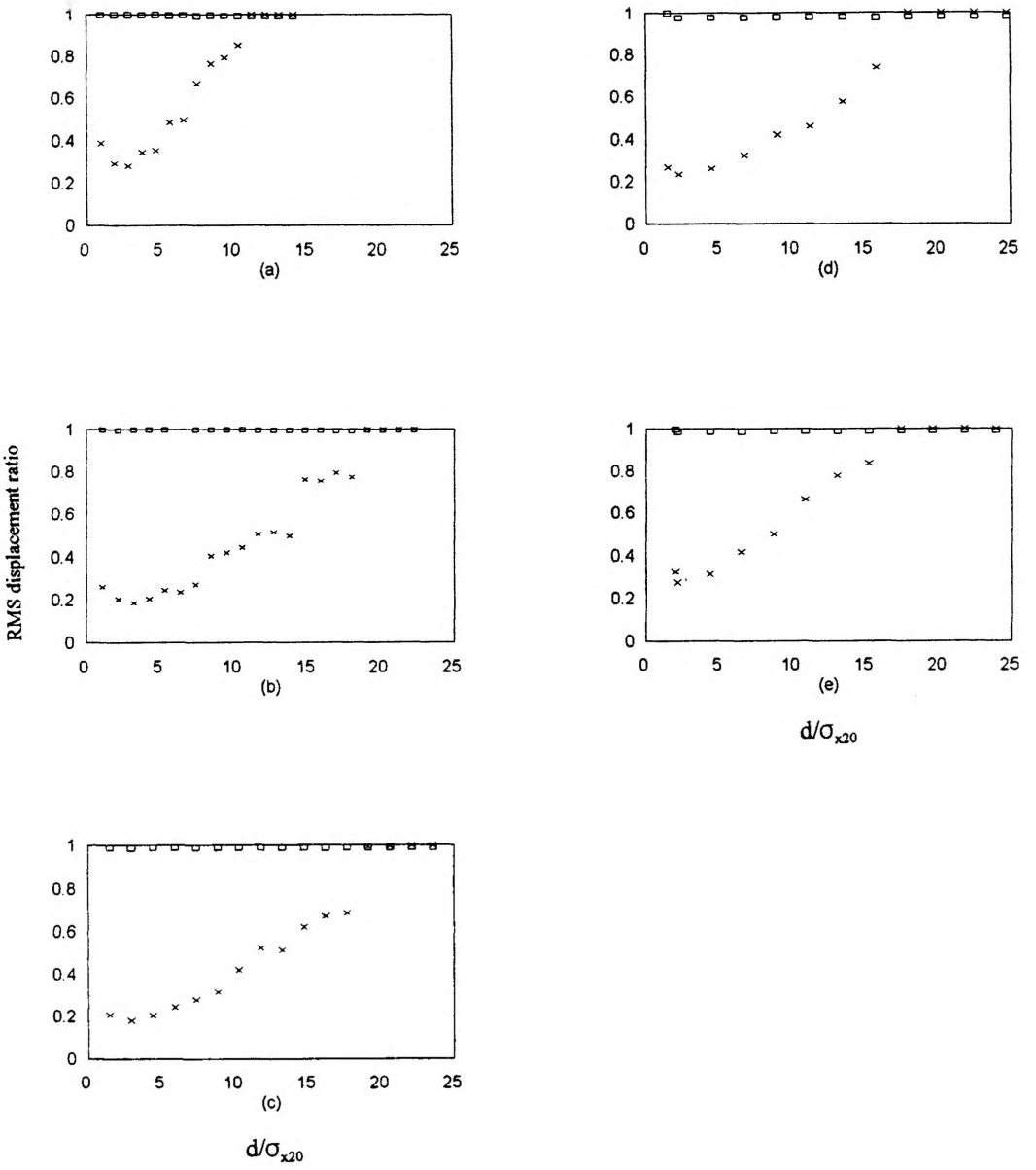

Figure 4.3 Variation of the RMS displacement ratios (σ_x/σ_{x0}) of the primary system (□) and the secondary system (×) versus the non-dimensional clearance (d/σ_{x20}) for the cases of m_1/m_2=1000, ξ_1=0.10, ξ_2=0.0 and the off-tuning ratio (f_3/f_2) of (a) 0.8; (b) 0.9; (c) 1.0; (d) 1.1 and (e) 1.2.

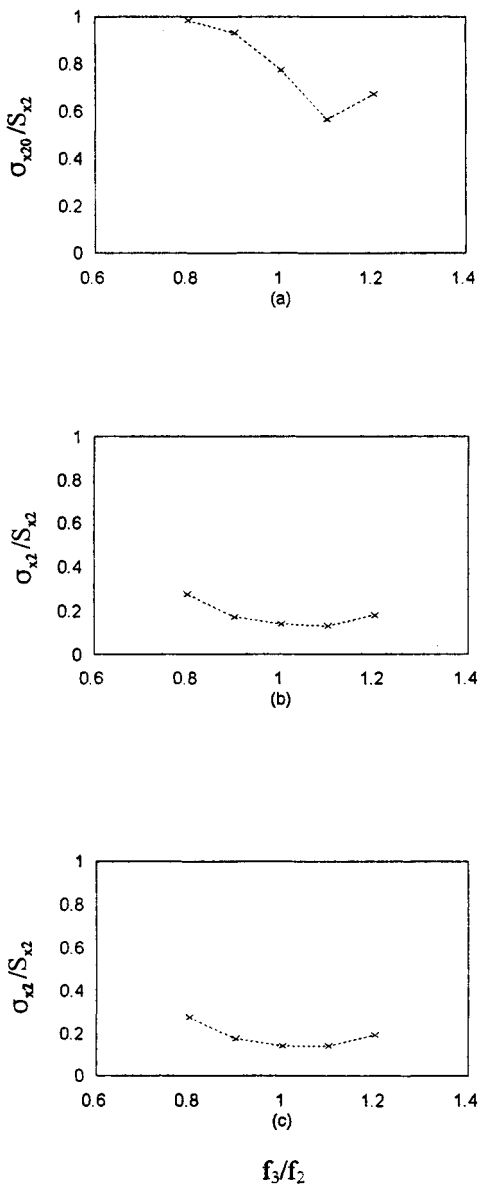

Figure 4.4 RMS displacement ratios of the secondary system versus the off-tuning ratio (f_3/f_2) for the case of m_1/m_2=1000, ξ_1=0.10, ξ_2=0.0. (a) : system controlled by absorber alone; (b): system controlled by new controller working at the best clearances; (c): system controlled by new controller working at a fixed clearance (d/σ_{x20}=2.95).

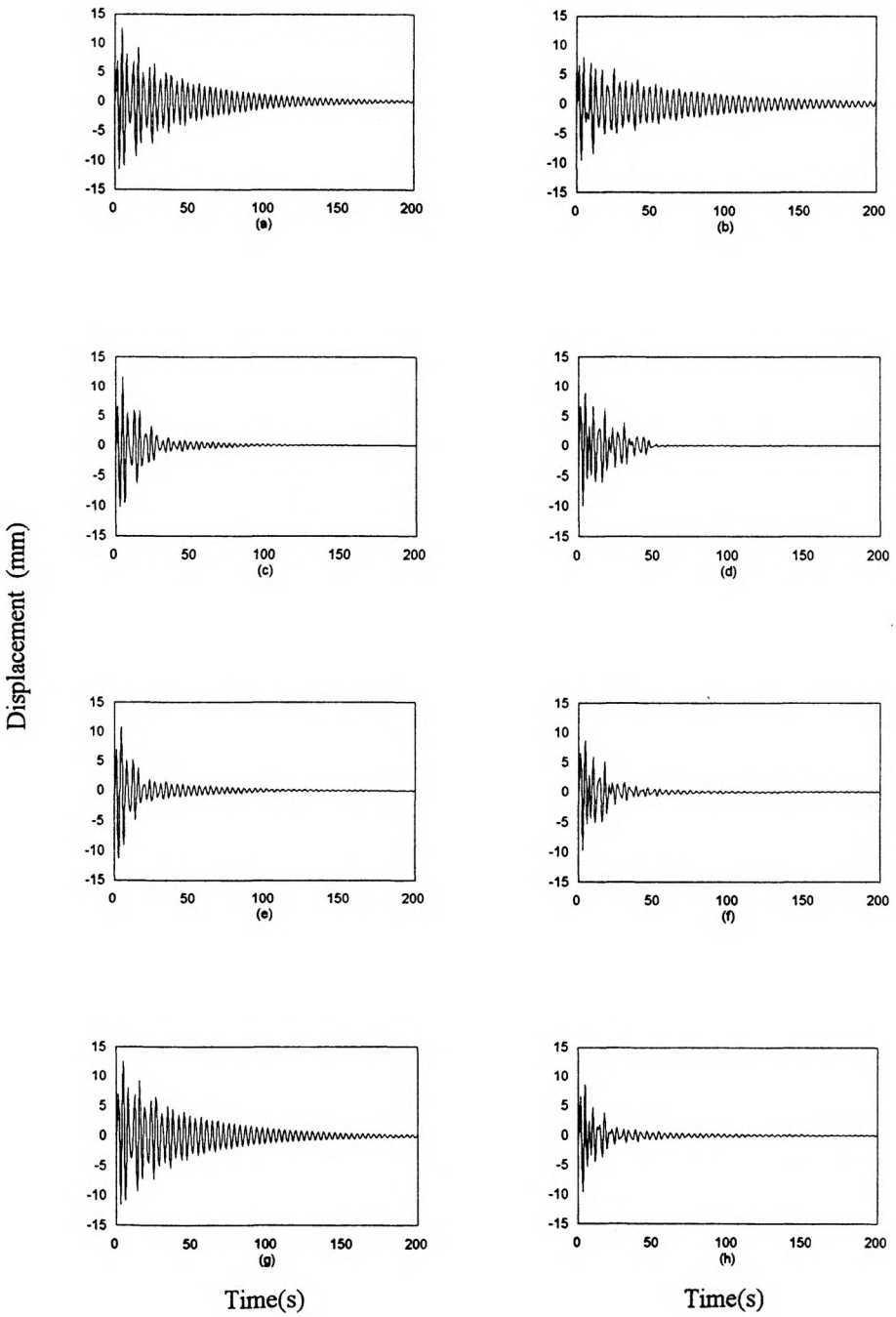

Figure 5.1 Time histories of the secondary system for the structure with $m_1/m_2=10$, $\xi_1=0.01$, and $\xi_2=0$, while the structure is (a): uncontrolled; (b): controlled by absorber alone; (c), (e) and (g): controlled by impact damper with $d/(v_{10}/\omega_d)$ of 2.0, 4.0 and 6.0; (d), (f) and (h): controlled by new controller with $d/(v_{10}/\omega_d)$ of 2.0, 4.0 and 6.0.

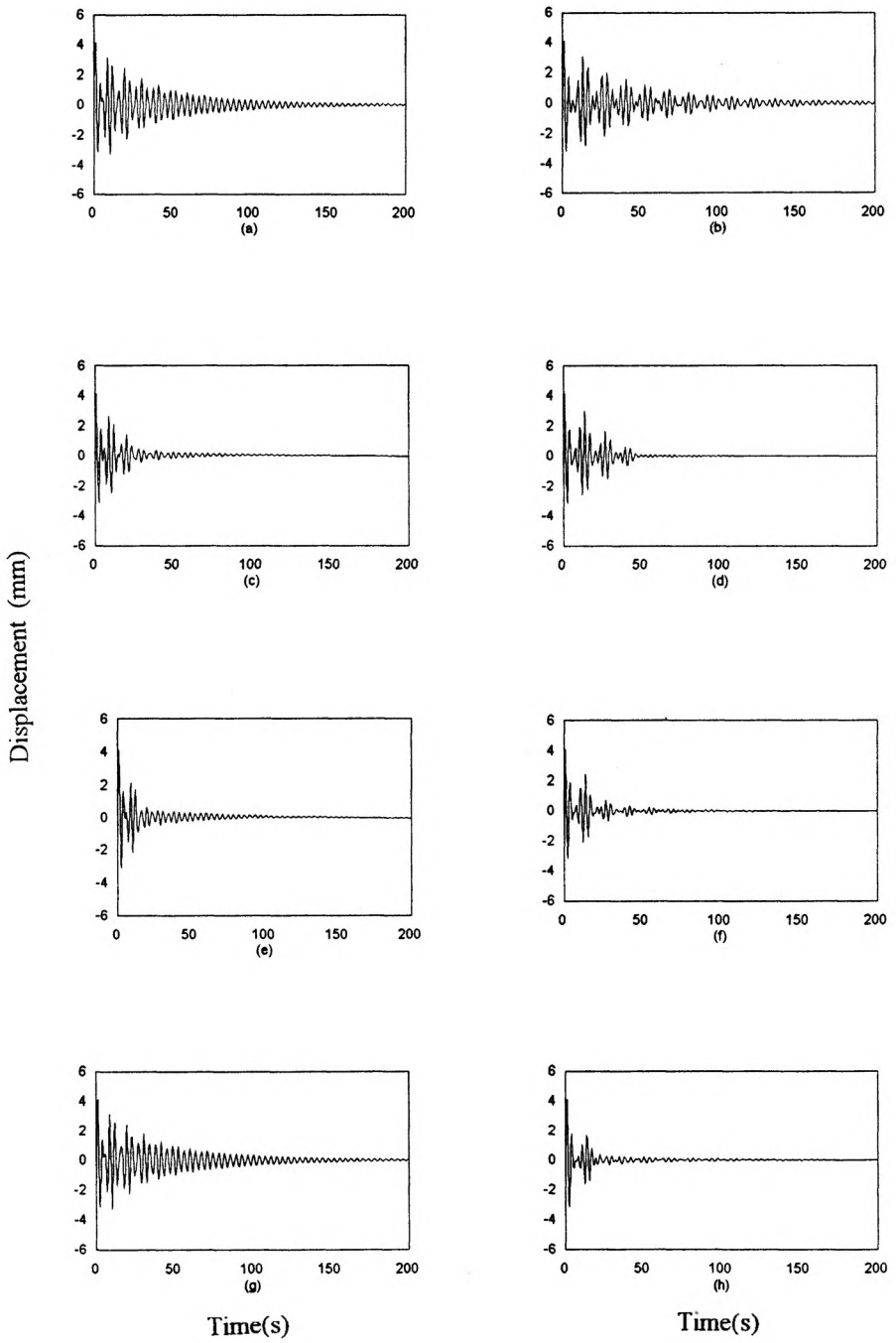

Figure 5.2 Time histories of the primary system for the structure with $m_1/m_2=10$, $\xi_1 = 0.01$, and $\xi_2=0$, while the structure is (a): uncontrolled; (b): controlled by absorber alone; (c), (e) and (g): controlled by impact damper with $d/(v_{10}/\omega_d)$ of 2.0, 4.0 and 6.0; (d), (f) and (h): controlled by new controller with $d/(v_{10}/\omega_d)$ of 2.0, 4.0 and 6.0.

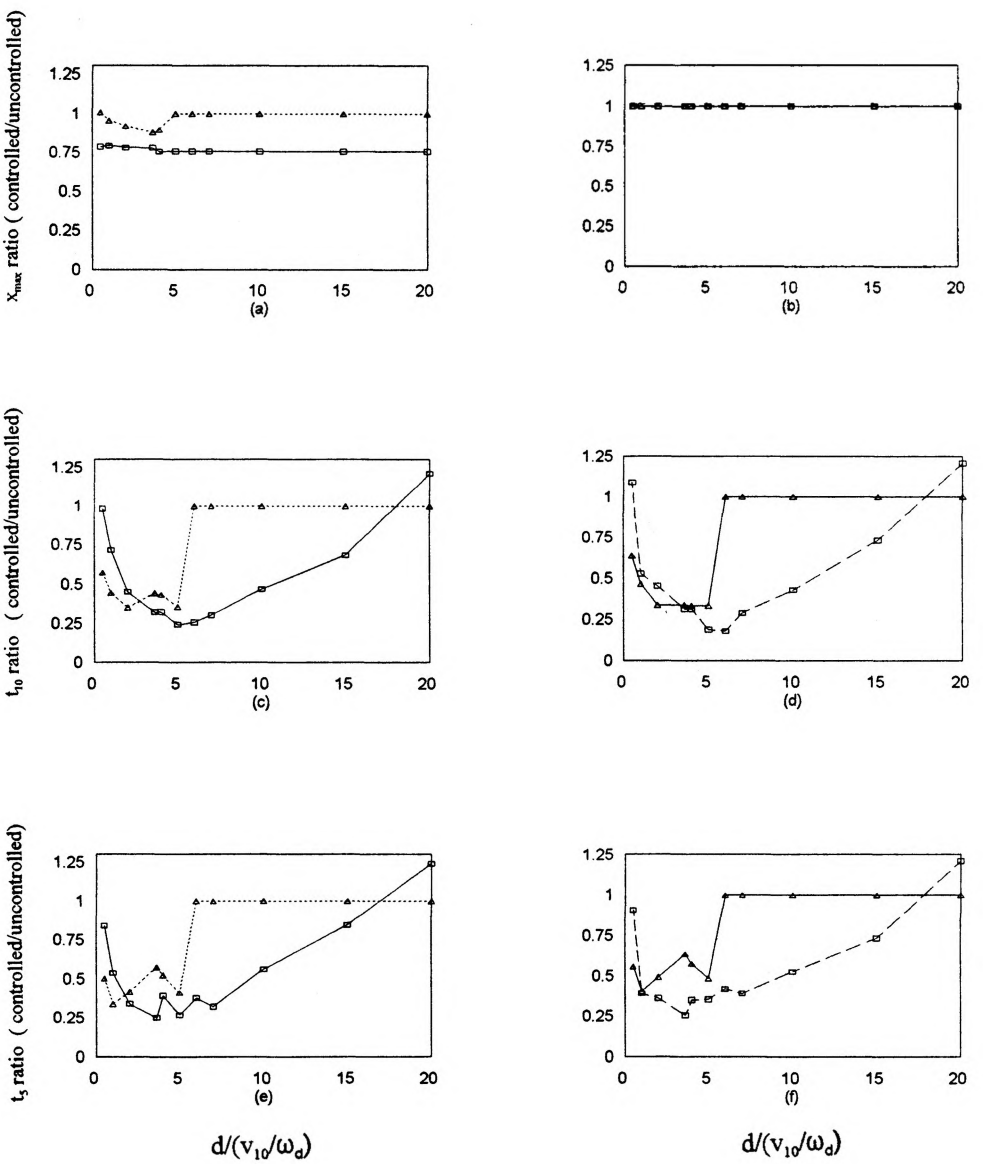

Figure 5.3 Comparison of (a), (b): the maximum displacement ratio; (c), (d): 10% settling time ratio; (e) (f): 5% settling time ratio between the structure controlled by the new controller (□) and that controlled by the conventional impact damper (Δ) versus the non-dimensional clearance $d/(v_{10}/\omega_d)$ for the case of $m_1/m_2=10$, $\xi_1=0.01$ and $\xi_2=0$. The first column is the secondary system, and the second column is the primary system.

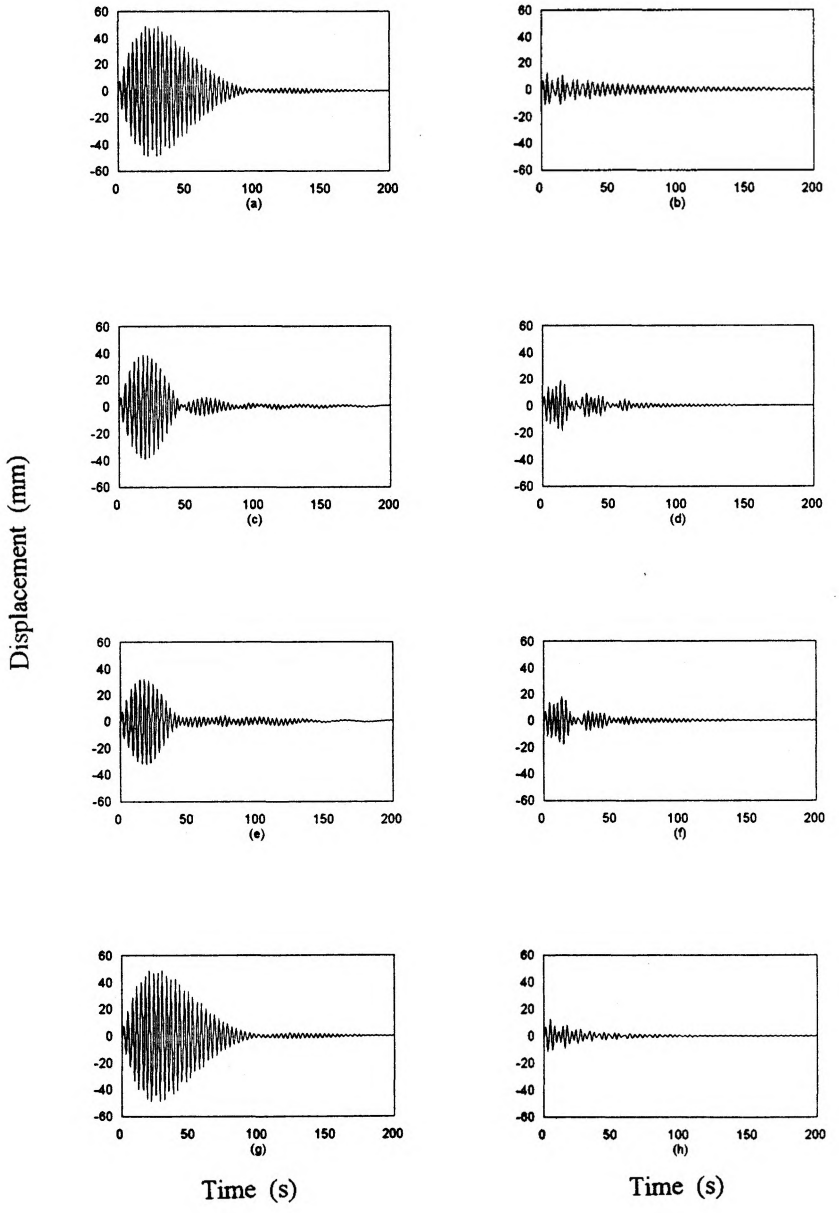

Figure 5.4 Time histories of the secondary system for the structure with m_1/m_2=1000, ξ_1=0.01, and ξ_2=0, while the structure is (a): uncontrolled;(b): controlled by absorber alone; (c), (e) and (g): controlled by impact damper with $d/(v_{10}/\omega_d)$ of 1.8, 3.6, and 25.0; (d), (f) and (h): controlled by new controller with $d/(v_{10}/\omega_d)$ of 1.8, 3.6 and 25.0.

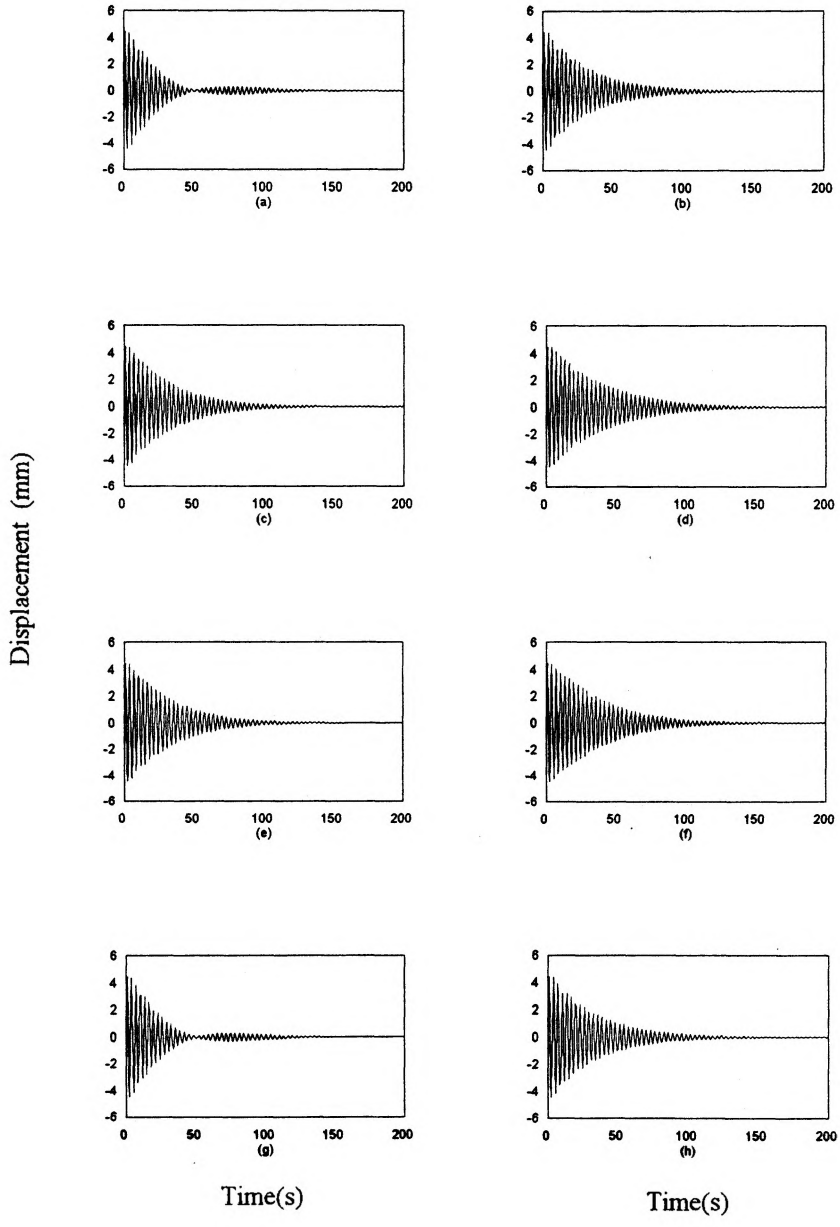

Figure 5.5 Time histories of the primary system for the structure with m_1/m_2=1000, ξ_1 = 0.01, and ξ_2=0, while the structure is (a): uncontrolled; (b): controlled by absorber alone; (c), (e) and (g): controlled by impact damper with $d/(v_{10}/\omega_d)$ of 1.8, 3.6 and 25.0; (d), (f) and (h): controlled by new controller with $d/(v_{10}/\omega_d)$ of 1.8, 3.6 and 25.0.

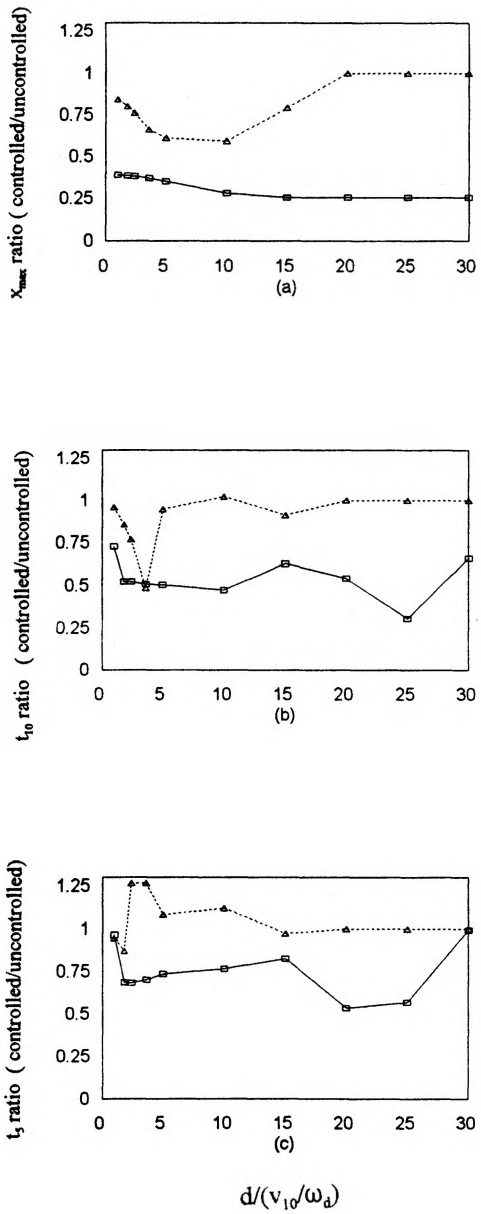

Figure 5.6 Comparison of (a): the maximum displacement ratio; (b): 10% settling time ratio; (c): 5% settling time ratio of the secondary system between the structure controlled by the new controller (□) and that controlled by the conventional impact damper (Δ) versus the non dimensional clearance $d/(v_{10}/\omega_d)$ for the case of m_1/m_2 =1000, ξ_1=0.01 and ξ_2=0.0.

APPENDIX

THE PROGRAM USED FOR THE NUMERICAL STUDIES

1. PROGRAM LIST

```
                                PROGRAM FOUR

C   THIS FORTRAN PROGRAM IS DESIGNED TO SOLVE THE COUPLED
C   SYSTEM OF EQUATIONS FOR A 3DOF SYSTEM WITH AN IMPACT[1]
C   DAMPER USING A FOURTH ORDER RUNGE-KUTTA METHOD.
C   m1 : primary mass
C   m2 : secondary mass
C   m3 : mass of the vibration absorber
C   m4 : mass of the impact damper (interacting with m3)
C   k1 : primary stiffness
C   k2 : secondary stiffness
C   k3 : stiffness of the vibration absorber
C   k4 : optional stiffness of the vibration absorber
C   b  : distance from centre of impact damper to the left wall
C   c  : distance from centre of impact damper to the right wall
C   c1 : viscous damping coefficient for the primary system
C   c2 : viscous damping coefficient of the secondary system
C   c3 : viscous damping coefficient of the vibration absorber
C   c4 ; optional viscous damping coefficient of the vibration absorber
C   d  : diameter of spherical impact damper
C   e : coefficient of restitution
C   T0 : time
C   Ttotal     : total time
C   h          : time step of integration
C   K1Z1...K4X3 : coefficients needed for integration
C   SIDE       : variable to flag impact - right/left indicator
C   X1,Z1      : displacement and the velocity of the primary system
C              ( at t = T0 + H )
C   X2,Z2      : displacement and the velocity of the secondary system
C              ( at t = T0 + H )
C   X3,Z3      : displacement and the velocity of the vibration absorber
C              ( at t = T0 + H )
```

---

[1]Refer to Figure 2.1 for the mathematical model and variables.

```
C    X10,Z10    : initial conditions at t = T0
C    X20,Z20    : initial conditions at t = T0
C    X30,Z30    : initial conditions at t = T0
C
C    FORCE(IFORC) : VECTOR CONTAINING THE RANDOM FORCE
C                   READ FROM AN INPUT DATA FILE FFORCE
C
C    OPTION ADDED FOR CHATTER DETECTION.  IF THERE ARE > 20
C    COLLISIONS DETECTED DURING THE LAST TIME INCREMENT 'H' THE
C    EXECUTION IS TERMINATED THROUGH CCOUNT AND DCOUNT.
C
C    declare variable status
C
     IMPLICIT REAL*8 (A-H,O-Z)
     REAL*8 M1,M2,M3,M4,K1,K2,K3,K4
     INTEGER CCOUNT,DCOUNT
     DIMENSION FORCE(20000)
     CHARACTER*20 FILE1,FILE2,FFORCE
     CHARACTER*1 SIDE
     COMMON FORCE, IFORC
     COMMON FOLD,FNEW,FNOW
     COMMON RMSX1,RMSV1,RMSX2,RMSV2,RMSX3,RMSV3
     COMMON RMSF,RMSA1,RMSA2
     COMMON RMSX4,RMSV4,RMSA3,XMAX4
     COMMON XMAX1,XMAX2,XMAX3,XMAXF
C
C       INITIALIZE THE COUNTER TO DETERMINE THE # OF IMPACTS IN ONE
C       TIME STEP
C    COUNT=0
C
     WRITE(*,'(A)') ' ENTER THE NAME OF THE INPUT DATA FILE :'
     READ(*,'(A)') FILE1
C
C        set the output option
C
     WRITE(*,'(A)') ' ENTER 1 FOR SCREEN OUTPUT ',
    $' ENTER 2 FOR SAVING THE OUTPUT IN A DATA FILE :'
     READ(*,'(I1)') IOUT
     IF(IOUT.EQ.2) THEN
     WRITE(*,'(A)') ' ENTER THE NAME OF THE OUTPUT DATA FILE :'
     READ(*,'(A)') FILE2
     OPEN(6,FILE=FILE2,STATUS='new')
     END IF
C
C       read in parameters from data file
C
C*********************
```

```
IMASS=1
     id=0
9  CONTINUE
OPEN(5,FILE=FILE1,STATUS='old')
     READ(5,10)FFORCE,M1,M2,M3,C1,C2,C3,C4,K1,K2,K3,K4,T0,H,TTOTAL,
    $X10,Z10,X20,Z20,X30,Z30,e,dmin,dmax,dinc,m4
     READ(5,'(I2)') IPRINT,IFORCE
   10 FORMAT(A,/,(e14.7))
     CLOSE (5)
     if(dmin.lt.0.0) id=1

C     IF(IFORCE.NE.0) OPEN(7,FILE=FFORCE,STATUS='OLD')
C
C**********************
C
C     INCREMENT FOR DIFFERENT MASS RATIOS FROM 1 TO 1000 IN
C     FOUR STEPS :

     M1=M1*10**(IMASS-1)
     K1=K1*10**(IMASS-1)
     C1=C1*10**(IMASS-1)

     IF(IMASS.EQ.1.AND.ID.EQ.1) THEN
     DMIN=1000.0
     DMAX=700.0
     DINC=50.0

     ELSE IF(IMASS.EQ.2.AND.ID.EQ.1) THEN
     DMIN=1000.0
     DMAX=120.0
     DINC=10.0

     ELSE IF(IMASS.EQ.3.AND.ID.EQ.1) THEN
     DMIN=1000.0
     DMAX=25.0
     DINC=2.5

     ELSE IF(ID.EQ.1) THEN
     DMIN=1000.0
     DMAX=5.00
     DINC=0.25
     END IF

C*****************************************************
C
C      echo input
write(6,'(a,2x,e14.7)')'m1',m1,'m2',m2,'m3',m3,'k1',k1,'k2',k2,

          AMMA4=0.0
```

```
    $'k3',k3,'k4',k4,'c1',c1,'c2',c2,'c3',c3,'c4',c4,'t0',t0,'ttotal',
    $ttotal,'H  ',h,'x10',x10,'x20',x20,'v10',z10,'v20',z20,'x30',x30,
    $'v30',z30,'e  ',e,'dia',d,'c  ',c,'b  ',b,'m4 ',m4
     write(6,'(a,i2)') 'IPRINT ',iprint,'IFORCE ',iforce
     IF(IPRINT.EQ.1.OR.IPRINT.EQ.2) THEN
     WRITE(6,'(A,A)')
    $'     t       x1       x2',
    $'       x3       x4       v4       F(t)'
           WRITE(6,'(A,A)')
    $'-------------------------------------------------------'
END IF

C         set the values of d,c and b for the desired clearance
d=0.05
  11 b=dmin/2.0+d/2.0
     c=dmin/2.0+d/2.0
C
C     open the data file to input the random force
IF(IFORCE.NE.0) OPEN(7,FILE=FFORCE,STATUS='OLD')
C
C       set initial conditions of impact damper to x=0, z=0
          Z4=0.0
          X40=0.0
          TINC=H
          HOLD=H
          IFLAG=0
          SIDE=' '
          IFORC=1
          FOLD=0.0
          FNOW=0.0
          FNEW=0.0
          RMSX1=0.0
          RMSV1=0.0
          RMSX2=0.0
          RMSV2=0.0
          RMSX3=0.0
          RMSV3=0.0
          RMSX4=0.0
          RMSV4=0.0
          RMSF =0.0
          RMSA1=0.0
          RMSA2=0.0
          RMSA3=0.0
          XMAX1=0.0
          XMAX2=0.0
          XMAX3=0.0
          XMAX4=0.0
```

```
        XMAXF=0.0
15  CONTINUE
C
C    Accelerations
A10=F1(M1,K1,K2,C1,C2,T0,Z10,X10,Z20,X20,
   $4,IFLAG,TINC,H,IFORCE)
    A20=F3(M2,K2,K3,C2,C3,T0,Z10,X10,Z20,X20,Z30,X30,
   $4,IFLAG,TINC,H,IFORCE)
    A30=F5(M3,K3,K4,C3,C4,T0,Z20,X20,Z30,X30,
   $4,IFLAG,TINC,H,IFORCE)
C
C    output
    CALL PRINT(T0,HOLD,X10,z10,a10,X20,z20,a20,x30,z30,a30,x40,Z4,
   $SIDE,IPRINT,IFORCE)
    IF(SIDE.NE.' ') SIDE=' '
C
C     call solution routine for next time step (t=T0+H)
20  CALL RK4(M1,M2,M3,C1,C2,C3,C4,K1,K2,K3,K4,T0,H,Z10,X10,Z20,X20,
   $Z30,X30,Z1,X1,Z2,X2,Z3,X3,IFLAG,TINC,IFORCE)
C
C    check for impact damper (through m4)
IF(M4.LE.0.0) GO TO 21
    X4=X40+Z4*H
C
C    check for impact on left wall
IF((B-D/2)+(X4-X3).LT.0.0.AND.IFLAG.NE.1) THEN
        IFLAG=1
        SIDE='L'
        H=H/2.0
        START=0.0
        FINISH=H
        GO TO 20
    END IF
C
C    check for impact on right wall
IF((C-D/2)+(X3-X4).LT.0.0.AND.IFLAG.NE.1) THEN
        IFLAG=1
        SIDE='R'
        H=H/2.0
        START=0.0
        FINISH=H
        GO TO 20
    END IF
C
C     check for convergence of a collision if the two masses are located to be 0.00001*D,
C     assume that the contact has established
IF(IFLAG.EQ.1) THEN
```

```
      IF( (DABS((B-D/2)+(X4-X3)).LE.0.00001*D) .OR.
     +    (DABS((C-D/2)+(X3-X4)).LE.0.00001*D)    ) THEN
C
C     The next 3 statements determine the velocities of the vibration
C     absorber [Z3] and of the impact damper [Z4].  The dummy variable,
C     [ZZ2] is only an intermediate variable because the velocity of the
C     vibration absorber before the impact is required to determine the
C     mass of the impact damper.
C
C     the following conditions are obtained from the conservation of
C     linear momentum and the coefficient of restitution.
                    ZZ2=(M4*Z4+M3*Z3-M4*E*(Z3-Z4))/(M3+M4)
                    Z4=E*(Z3-Z4)+ZZ2
                    Z3=ZZ2
C
C     CHECK FOR CHATTER. IF FOUND, GO TO SUBROUTINE CARRY
                CCOUNT=CCOUNT+1
                IF(CCOUNT-DCOUNT.GT.20) GO TO 23
                T0=T0+H
                HOLD=H
                H=TINC-H
                IFLAG=2
                GO TO 22
      END IF
    END IF
C
C     call bisect to determine impact instant, if convergence has not been satisfied yet
    IF(IFLAG.EQ.1.AND.SIDE.EQ.'L') THEN
      CALL BISECT(START,FINISH,H,(B-D/2)+(X4-X3),-1)
      GO TO 20
    END IF
C
    IF(IFLAG.EQ.1.AND.SIDE.EQ.'R') THEN
      CALL BISECT(START,FINISH,H,(C-D/2)+(X3-X4),-1)
      GO TO 20
    END IF
C
C     increment time
21  T0=T0+H
IF(IFLAG.EQ.0) HOLD=H
      DCOUNT=CCOUNT
C     RESTORE THE CONTROL PARAMETERS AFTER COMPLEMENTING THE
C     FULL STEP
      IF(IFLAG.EQ.2) THEN
                HOLD=H
                H=TINC
                IFLAG=0
```

```
      END IF
C
 22   Z10=Z1
      X10=X1
      Z20=Z2
      X20=X2
      Z30=Z3
      X30=X3
      X40=X4
C
      IF(T0.LT.TTOTAL) GO TO 15
      GO TO 25
23    CONTINUE
C
C     20 COLLISIONS HAVE BEEN DETECTED WITHIN ONE TIME STEP.
C     THIS SITUATION IS INTERPRETED TO BE "CHATTER"
C     THIS SECTION OF THE PROGRAM ASSUMES THAT THE IMPACT DAMPER
C     m4 AND MASS m3 WOULD WANT TO MOVE TOGETHER.
      CALL CARRY(M1,M2,M3,M4,K1,K2,K3,K4,C1,C2,C3,C4,T0,H,TINC,X1,Z1,
     $X2,Z2,X3,Z3,SIDE,B,C,D,IPRINT,IFORCE)
      Z4=Z3
C
      IF(SIDE.EQ.'L') THEN
          X4=X3-B+D/2
      ELSE
          X4=X3+C-D/2
      END IF
C
      T0=T0+H
      HOLD=H
      H=TINC-H
      IFLAG=2
      GO TO 22
25  continue
close(7)

      write(6,'(a,e14.7)')
     $'d1 = ',(b+c-d),
     $'x1 = ',sqrt(RMSX1),'v1 = ',sqrt(RMSV1),'a1 = ',sqrt(RMSA1),
     $'x2 = ',sqrt(RMSX2),'v2 = ',sqrt(RMSV2),'a2 = ',sqrt(RMSA2),
     $'x3 = ',sqrt(RMSX3),'v3 = ',sqrt(RMSV3),'a3 = ',sqrt(RMSA3),
     $'x4 = ',sqrt(RMSX4),'v4 = ',sqrt(RMSV4),'f1 = ',sqrt(RMSF),
     $'X1 = ',XMAX1,'X2 = ',XMAX2,'X3 = ',XMAX3,'X4 = ',XMAX4,
     $'F1 = ',XMAXF
C
          WRITE(6,'(a)')
C
```

```
      if(dmin.lt.dmax) then
                  dmin=dmin+dinc
          t0=0.0
          x10=0.0
          z10=0.0
          x20=0.0
          z20=0.0
          x30=0.0
          z30=0.0
          h=tinc
          go to 11
      end if

C*********************
C
C     INCREMENT FOR THE MASS RATIO  IN FOUR STEPS
IMASS = IMASS+1
      IF(IMASS.LT.5.AND.ID.EQ.1) GO TO 9

STOP
      END
C
C=============================================================
      SUBROUTINE CARRY(M1,M2,M3,M4,K1,K2,K3,K4,C1,C2,C3,C4,T0,H,TINC,
     $X1,Z1,X2,Z2,X3,Z3,SIDE,B,C,D,IPRINT,IFORCE)
C
      IMPLICIT REAL*8 (A-H,O-Z)
      REAL*8 M1,M2,M3,M4,K1,K2,K3,K4
      CHARACTER*1 SIDE
      COMMON FORCE, IFORC
      DIMENSION FORCE(20000)
      COMMON FOLD,FNEW,FNOW
      COMMON RMSX1,RMSV1,RMSX2,RMSV2,RMSX3,RMSV3
      COMMON RMSF,RMSA1,RMSA2
      COMMON RMSX4,RMSV4,RMSA3,XMAX4
      COMMON XMAX1,XMAX2,XMAX3,XMAXF
C
      IF(SIDE.EQ.'L') THEN
          X4=X3-B+D/2
      ELSE
          X4=X3+C-D/2
      END IF
C
      OLDM3=M3
      M3=M3+M4
      IFLAG=2
      T0=T0+H
```

```
      HOLD=H
C
C     COMPLEMENT THE TIME STEP COMING FROM CHATTER
C
      IDUMMY=T0/TINC
      H=(IDUMMY+1)*TINC-T0
Z10=Z1
      X10=X1
      Z20=Z2
      X20=X2
      Z30=Z3
      X30=X3
5  continue
C
C     EVALUATE THE ACCELERATION
A10=F1(M1,K1,K2,C1,C2,T0,Z10,X10,Z20,X20,
     $4,IFLAG,TINC,H,IFORCE)
      A20=F3(M2,K2,K3,C2,C3,T0,Z10,X10,Z20,X20,Z30,X30,
     $4,IFLAG,TINC,H,IFORCE)
      A30=F5(M3,K3,K4,C3,C4,T0,Z20,X20,Z30,X30,
     $4,IFLAG,TINC,H,IFORCE)
C
      CALL PRINT(T0,HOLD,X10,z10,a10,X20,z20,a20,X30,z30,a30,x4,z30,
     $SIDE,IPRINT,IFORCE)
C
C     SOLVE FOR T0+H
10 CALL RK4(M1,M2,M3,C1,C2,C3,C4,K1,K2,K3,K4,T0,H,Z10,X10,Z20,X20,
     $Z30,X30,Z1,X1,Z2,X2,Z3,X3,IFLAG,TINC,IFORCE)
      ACCEL=F5(M3,K3,K4,C3,C4,T0+H,Z2,X2,Z3,X3,
     $4,IFLAG,TINC,H,IFORCE)
C
C     CALCULATE THE POSITION OF THE IMPACT DAMPER :
      IF(SIDE.EQ.'L') THEN
         X4=X3-B+D/2
      ELSE
         X4=X3+C-D/2
      END IF
C
C     CHECK FOR SEPARATION
      IF(SIDE.EQ.'L') THEN
         IF(ACCEL.LT.0.0.AND.IFLAG.NE.1) THEN
                IFLAG=1
                H=H*ABS(A30)/(ABS(A30)+ABS(ACCEL))
                START=0.0
                FINISH=H
                GO TO 10
         END IF
```

```
      ELSE
         IF(ACCEL.GT.0.0.AND.IFLAG.NE.1) THEN
                  IFLAG=1
                  H=H*ABS(A30)/(ABS(A30)+ABS(ACCEL))
                  START=0.0
                  FINISH=H
                  GO TO 10
         END IF
      END IF
C
IF(IFLAG.NE.1) GO TO 15
C
      IF(DABS(ACCEL).LE.0.000001) GO TO 20
C
      IF(SIDE.EQ.'L') THEN
         CALL BISECT(START,FINISH,H,ACCEL,-1)
         GO TO 10
      ELSE
         CALL BISECT(START,FINISH,H,ACCEL,1)
         GO TO 10
      END IF
C
 15   T0=T0+H
      IF(IFLAG.EQ.0) HOLD=H
      IF(IFLAG.EQ.2) THEN
         HOLD=H
         H=TINC
         IFLAG=0
      END IF
C
      Z10=Z1
      X10=X1
      Z20=Z2
      X20=X2
      Z30=Z3
      X30=X3
      GO TO 5
C
 20   M3=OLDM3
C
      RETURN
      END
C
C=============================================================
      SUBROUTINE RK4(M1,M2,M3,C1,C2,C3,C4,K1,K2,K3,K4,T0,H,Z10,X10,
     $Z20,X20,Z30,X30,Z1,X1,Z2,X2,Z3,X3,IFLAG,TINC,IFORCE)
C
```

```
      IMPLICIT REAL*8 (A-H,O-Z)
      REAL*8 M1,M2,M3,K1,K2,K3,K4
      REAL*8 K1Z1,K1X1,K1Z2,K1X2,K1Z3,K1X3,K2Z1,K2X1,K2Z2,K2X2,K2Z3,
     $K2X3,K3Z1,K3X1,K3Z2,K3X2,K3Z3,K3X3,K4Z1,K4X1,K4Z2,K4X2,K4Z3,K4X3
      COMMON FORCE, IFORC
      DIMENSION FORCE(20000)
      COMMON FOLD,FNEW,FNOW
      COMMON RMSX1,RMSV1,RMSX2,RMSV2,RMSX3,RMSV3
      COMMON RMSF,RMSA1,RMSA2
      COMMON RMSX4,RMSV4,RMSA3,XMAX4
      COMMON XMAX1,XMAX2,XMAX3,XMAXF
C
C       fourth order runge kutta integration subroutine
C       statements (200 - 300)
C
 200  CONTINUE
C
      K1Z1=F1(M1,K1,K2,C1,C2,T0,Z10,X10,Z20,X20,
     $1,IFLAG,TINC,H,IFORCE)
      K1X1=F2(Z10)
      K1Z2=F3(M2,K2,K3,C2,C3,T0,Z10,X10,Z20,X20,Z30,X30,
     $1,IFLAG,TINC,H,IFORCE)
      K1X2=F4(Z20)
      K1Z3=F5(M3,K3,K4,C3,C4,T0,Z20,X20,Z30,X30,
     $1,IFLAG,TINC,H,IFORCE)
      K1X3=F6(Z30)
C
      K2Z1=F1(M1,K1,K2,C1,C2,T0+H/2.0,Z10+H/2.0*K1Z1,
     $X10+H/2.0*K1X1,Z20+H/2.0*K1Z2,X20+H/2.0*K1X2,
     $2,IFLAG,TINC,H,IFORCE)
      K2X1=F2(Z10+H/2.0*K1Z1)
      K2Z2=F3(M2,K2,K3,C2,C3,T0+H/2.0,Z10+H/2.0*K1Z1,
     $X10+H/2.0*K1X1,Z20+H/2.0*K1Z2,X20+H/2.0*K1X2,
     $Z30+H/2.0*K1Z3,X30+H/2.0*K1X3,
     $2,IFLAG,TINC,H,IFORCE)
      K2X2=F4(Z20+H/2.0*K1Z2)
      K2Z3=F5(M3,K3,K4,C3,C4,T0+H/2.0,Z20+H/2.0*K1Z2,
     $X20+H/2.0*K1X2,Z30+H/2.0*K1Z3,X30+H/2.0*K1X3,
     $2,IFLAG,TINC,H,IFORCE)
      K2X3=F6(Z30+H/2.0*K1Z3)
C
      K3Z1=F1(M1,K1,K2,C1,C2,T0+H/2.0,Z10+H/2.0*K2Z1,
     $X10+H/2.0*K2X1,Z20+H/2.0*K2Z2,X20+H/2.0*K2X2,
     $3,IFLAG,TINC,H,IFORCE)
      K3X1=F2(Z10+H/2.0*K2Z1)
      K3Z2=F3(M2,K2,K3,C2,C3,T0+H/2.0,Z10+H/2.0*K2Z1,
     $X10+H/2.0*K2X1,Z20+H/2.0*K2Z2,X20+H/2.0*K2X2,
```

```
     $Z30+H/2.0*K2Z3,X30+H/2.0*K2X3,
     $3,IFLAG,TINC,H,IFORCE)
      K3X2=F4(Z20+H/2.0*K2Z2)
      K3Z3=F5(M3,K3,K4,C3,C4,T0+H/2.0,Z20+H/2.0*K2Z2,
     $X20+H/2.0*K2X2,Z30+H/2.0*K2Z3,X30+H/2.0*K2X3,
     $3,IFLAG,TINC,H,IFORCE)
      K3X3=F6(Z30+H/2.0*K2Z3)
C
      K4Z1=F1(M1,K1,K2,C1,C2,T0+H,Z10+H*K3Z1,
     $X10+H*K3X1,Z20+H*K3Z2,X20+H*K3X2,
     $4,IFLAG,TINC,H,IFORCE)
      K4X1=F2(Z10+H*K3Z1)
      K4Z2=F3(M2,K2,K3,C2,C3,T0+H,Z10+H*K3Z1,
     $X10+H*K3X1,Z20+H*K3Z2,X20+H*K3X2,
     $Z30+H*K3Z3,X30+H*K3X3,
     $4,IFLAG,TINC,H,IFORCE)
      K4X2=F4(Z20+H*K3Z2)
      K4Z3=F5(M3,K3,K4,C3,C4,T0+H,Z20+H*K3Z2,
     $X20+H*K3X2,Z30+H*K3Z3,X30+H*K3X3,
     $4,IFLAG,TINC,H,IFORCE)
      K4X3=F6(Z30+H*K3Z3)
C
      Z1=Z10+H/6.0*(K1Z1+2.0*K2Z1+2.0*K3Z1+K4Z1)
      X1=X10+H/6.0*(K1X1+2.0*K2X1+2.0*K3X1+K4X1)
      Z2=Z20+H/6.0*(K1Z2+2.0*K2Z2+2.0*K3Z2+K4Z2)
      X2=X20+H/6.0*(K1X2+2.0*K2X2+2.0*K3X2+K4X2)
      Z3=Z30+H/6.0*(K1Z3+2.0*K2Z3+2.0*K3Z3+K4Z3)
      X3=X30+H/6.0*(K1X3+2.0*K2X3+2.0*K3X3+K4X3)
C
 300  CONTINUE
      RETURN
      END
C
C=============================================================
      FUNCTION F1(M1,K1,K2,C1,C2,T,Z1,X1,Z2,X2,
     $ICOUNT,IFLAG,TINC,H,IFORCE)
C
C     function subprogram for the velocity (Z1) of the primary mass
C
      IMPLICIT DOUBLE PRECISION (A-H,O-Z)
      REAL*8 M1,K1,K2
      COMMON FORCE, IFORC
      DIMENSION FORCE(20000)
      COMMON FOLD,FNEW,FNOW
      COMMON RMSX1,RMSV1,RMSX2,RMSV2,RMSX3,RMSV3
      COMMON RMSF,RMSA1,RMSA2
      COMMON RMSX4,RMSV4,RMSA3,XMAX4
```

```
      COMMON XMAX1,XMAX2,XMAX3,XMAXF
C
IF(IFORCE.EQ.1.OR.IFORCE.EQ.4.OR.IFORCE.EQ.5.OR.IFORCE.EQ.7)THEN
      F1=1.0/M1*(RANDF(T,ICOUNT,IFLAG,TINC,H)-
     $(C1+C2)*Z1+C2*Z2-(K1+K2)*X1+K2*X2)
      ELSE IF(IFORCE.EQ.8.OR.IFORCE.EQ.11.OR.IFORCE.EQ.12.OR.
     $IFORCE.EQ.14) THEN
      F1=1.0/M1*(FORCE1(T)-
     $(C1+C2)*Z1+C2*Z2-(K1+K2)*X1+K2*X2)
      ELSE
      F1=1.0/M1*(-(C1+C2)*Z1+C2*Z2-(K1+K2)*X1+K2*X2)
      END IF
C
      RETURN
      END
C
C=============================================================
      FUNCTION F2(Z1)
C     function subprogram for the displacement (X1) of the primary mass
C
      IMPLICIT REAL*8 (A-H,O-Z)
      F2=Z1
C
      RETURN
      END
C
C=============================================================
C
      FUNCTION F3(M2,K2,K3,C2,C3,T,Z1,X1,Z2,X2,Z3,X3,
     $ICOUNT,IFLAG,TINC,H,IFORCE)
C     function subprogram for the velocity (Z2) of the secondary mass
C
      IMPLICIT REAL*8 (A-H,O-Z)
      REAL*8 M2,K2,K3
      COMMON FORCE, IFORC
      DIMENSION FORCE(20000)
      COMMON FOLD,FNEW,FNOW
      COMMON RMSX1,RMSV1,RMSX2,RMSV2,RMSX3,RMSV3
      COMMON RMSF,RMSA1,RMSA2
      COMMON RMSX4,RMSV4,RMSA3,XMAX4
      COMMON XMAX1,XMAX2,XMAX3,XMAXF
C
      IF(IFORCE.EQ.2.OR.IFORCE.EQ.4.OR.IFORCE.EQ.6.OR.IFORCE.EQ.7)THEN
      F3=1.0/M2*(RANDF(T,ICOUNT,IFLAG,TINC,H)-
     $(C2+C3)*Z2+C2*Z1-(K2+K3)*X2+K2*X1+C3*Z3+K3*X3)
      ELSE IF(IFORCE.EQ.9.OR.IFORCE.EQ.11.OR.IFORCE.EQ.13.OR.
     $IFORCE.EQ.14) THEN
```

```
      F3=1.0/M2*(FORCE2(T)-
     $(C2+C3)*Z2+C2*Z1-(K2+K3)*X2+K2*X1+C3*Z3+K3*X3)
      ELSE
      F3=1.0/M2*(-(C2+C3)*Z2+C2*Z1-(K2+K3)*X2+K2*X1+C3*Z3+K3*X3)
      END IF
C
      RETURN
      END
C=============================================================
C
      FUNCTION F4(Z2)
C     function subprogram for the displacement (X2) of the
C     secondary mass
C
      IMPLICIT REAL*8 (A-H,O-Z)
      F4=Z2
C
      RETURN
      END
C
C=============================================================
C
      FUNCTION F5(M3,K3,K4,C3,C4,T,Z2,X2,Z3,X3,
     $ICOUNT,IFLAG,TINC,H,IFORCE)
C     function subprogram for the velocity (Z3) of the mass of the
C     vibration absorber
C
      IMPLICIT REAL*8 (A-H,O-Z)
      REAL*8 M3,K3,K4
      COMMON FORCE, IFORC
      DIMENSION FORCE(20000)
      COMMON FOLD,FNEW,FNOW
      COMMON RMSX1,RMSV1,RMSX2,RMSV2,RMSX3,RMSV3
      COMMON RMSF,RMSA1,RMSA2
      COMMON RMSX4,RMSV4,RMSA3,XMAX4
      COMMON XMAX1,XMAX2,XMAX3,XMAXF
C
      IF(IFORCE.EQ.3.OR.IFORCE.EQ.5.OR.IFORCE.EQ.6.OR.IFORCE.EQ.7)THEN
      F5=1.0/M3*(RANDF(T,ICOUNT,IFLAG,TINC,H)-
     $(C3+C4)*Z3+C3*Z2-(K3+K4)*X3+K3*X2)
      ELSE IF(IFORCE.EQ.10.OR.IFORCE.EQ.12.OR.IFORCE.EQ.13.OR.
     $IFORCE.EQ.14) THEN
      F5=1.0/M3*(FORCE3(T)-
     $(C3+C4)*Z3+C3*Z2-(K3+K4)*X3+K3*X2)
      ELSE
      F5=1.0/M3*(-(C3+C4)*Z3+C3*Z2-(K3+K4)*X3+K3*X2)
      END IF
```

```
C
      RETURN
      END
C=============================================================
C
      FUNCTION F6(Z3)
C     function subprogram for the displacement (X3) of the mass of the vibration absorber
C
      IMPLICIT REAL*8 (A-H,O-Z)
      F6=Z3
C
      RETURN
      END
C
C=============================================================
C
      FUNCTION FORCE1(T)
C     function subprogram for forcing on the primary mass
C
      IMPLICIT REAL*8 (A-H,O-Z)
      FORCE1=1.0*DSIN(1.80245*t)
C     FORCE1=0
C
      RETURN
      END
C
C=============================================================
C
      FUNCTION FORCE2(T)
C     function subprogram for forcing on the secondary mass
C
      IMPLICIT REAL*8 (A-H,O-Z)
      FORCE2=1.0*DSIN(1.80245*t)
C
      RETURN
      END
C
C=============================================================
C
      FUNCTION FORCE3(T)
C     function subprogram for forcing on the mass of the vibration absorber
C
      IMPLICIT REAL*8 (A-H,O-Z)
      FORCE3=1.0*DSIN(1.80245*t)
C
      RETURN
      END
```

```
C
C=============================================================
C
      SUBROUTINE BISECT(START,FINISH,DT,CHECK,I)
C     Subroutine subprogram to iterate by bisection.
C     If the control flag I is negative, CHECK<0 means mass 4 has
C     exceeded the required limit for bisection, and vice versa.
C
      IMPLICIT REAL*8 (A-H,O-Z)
      INTEGER I
C     REAL START,FINISH,DT,CHECK
      IF(I.LT.0) GO TO 5
C
      IF(CHECK.GT.0.0) THEN
      DT=DT-(FINISH-START)/2.0
      FINISH=DT
      ELSE
      DT=DT+(FINISH-START)/2.0
      START=FINISH
      FINISH=DT
      END IF
      GO TO 10
C
    5 CONTINUE
      IF(CHECK.LT.0.0) THEN
      DT=DT-(FINISH-START)/2.0
      FINISH=DT
      ELSE
      DT=DT+(FINISH-START)/2.0
      START=FINISH
      FINISH=DT
      END IF
C
   10 RETURN
      END
C=============================================================
C
      FUNCTION RANDF(T,ICOUNT,IFLAG,TINC,H)
C     CONTROLLER SUBROUTINE TO PROVIDE A SEQUENCE OF RANDOM
C     NUMBERS WITH A GAUSSIAN DISTRIBUTION (WHITE)
C     SEE MARK DOLATA'S THESIS FOR REFERENCE
IMPLICIT REAL*8 (A-H,O-Z)
      COMMON FORCE, IFORC
      DIMENSION FORCE(20000)
      COMMON FOLD,FNEW,FNOW
      COMMON RMSX1,RMSV1,RMSX2,RMSV2,RMSX3,RMSV3
      COMMON RMSF,RMSA1,RMSA2
```

```
      COMMON RMSX4,RMSV4,RMSA3,XMAX4
      COMMON XMAX1,XMAX2,XMAX3,XMAXF

C     READ IN THE FORCE VECTOR FOR EVERY 20000 FULL TIME STEP
C
      IF(IFORC.EQ.1.AND.ICOUNT.EQ.1) THEN
C     write(*,'(a,i5)') 'IFORC = ',IFORC,
C     $' GOING TO THE DATA FILE TO READ SOME FORCE '
      DO 10 II=1,20000
      READ(7,*,END=11) FORCE(II)
   10 CONTINUE
      GO TO 12
   11 write(*,'(a)') 'end of data file encountered '
   12 CONTINUE
      END IF
C
C     A NEW FORCE IF THERE IS NOT A COLLISION
C     ELSE, INTERPOLATE FOR THE FORCE
C
      IF(IFLAG.EQ.0.AND.ICOUNT.EQ.1) THEN
C
C     A NEW FORCE FOR ADVANCING BY A CONSTANT TIME STEP
C  **** NOTE :
C       THIS SECTION WHICH READS IN THE FORCING NEEDS
C        MODIFYING TO ACCOMODATE MULTIPLY FORCED CASES
C
C     F=RAND1(T,N,WU,SOWK,ix,iy,iz)
      F=FORCE(IFORC)

C     CHECK IF END OF THE FORCE VECTOR (20000). IF SO,
C     INITIALIZE THE INDEX TO READ IN NEW FORCE
IF(IFORC.EQ.20000) THEN
      IFORC=1
      ELSE
      IFORC=IFORC+1
      END IF
C
      FOLD=FNOW
      FNEW=F
      FNOW=FNEW
ELSE IF(IFLAG.EQ.1.AND.ICOUNT.EQ.1) THEN
C     ADJUST THE UPPER LIMIT OF THE FORCE DURING ITERATION
FNOW= FOLD+(FNEW-FOLD)/TINC*H
ELSE IF(IFLAG.EQ.2.AND.ICOUNT.EQ.1) THEN
C     USE THE FIRST UPPER LIMIT WHICH DID NOT GET USED DUE TO
C     ITERATIONS
FOLD=FNOW
```

```
      FNOW=FNEW
   END IF
   C
   C     PROVIDE THE FOUR-STEP FORCE FROM FOLD TO FNOW TO USE IN RK4
   C
      IF(ICOUNT.EQ.1) RANDF=FOLD
      IF(ICOUNT.EQ.2) RANDF=FOLD+(FNOW-FOLD)/2.0
      IF(ICOUNT.EQ.3) RANDF=FOLD+(FNOW-FOLD)/2.0
      IF(ICOUNT.EQ.4) RANDF=FNOW
   C
   C     write(*,'(a,i5)') 'IFORC = ',IFORC,
   C    $' RETURNING TO THE CALLING PROGRAM       '
    20  RETURN
      END
   C
   C=============================================================
   C
      SUBROUTINE PRINT(T,H,X1,V1,A1,X2,V2,A2,X3,V3,A3,X4,V4,SIDE,
     $IPRINT,IFORCE)
      IMPLICIT REAL*8 (A-H,O-Z)
      CHARACTER*1 SIDE
      COMMON FORCE, IFORC
      DIMENSION FORCE(20000)
      COMMON FOLD,FNEW,FNOW
      COMMON RMSX1,RMSV1,RMSX2,RMSV2,RMSX3,RMSV3
      COMMON RMSF,RMSA1,RMSA2
      COMMON RMSX4,RMSV4,RMSA3,XMAX4
      COMMON XMAX1,XMAX2,XMAX3,XMAXF
   C
   C     T : present time
   C     H : last time step
   C
      if(t.eq.0.0) go to 10
   C
      RMSX1=(RMSX1*(T-H)+X1**2*H)/T
      RMSV1=(RMSV1*(T-H)+V1**2*H)/T
      RMSX2=(RMSX2*(T-H)+X2**2*H)/T
      RMSV2=(RMSV2*(T-H)+V2**2*H)/T
      RMSX3=(RMSX3*(T-H)+X3**2*H)/T
      RMSV3=(RMSV3*(T-H)+V3**2*H)/T
      RMSX4=(RMSX4*(T-H)+X4**2*H)/T
      RMSV4=(RMSV4*(T-H)+V4**2*H)/T
      RMSF =(RMSF *(T-H)+FNOW**2*H)/T
      RMSA1=(RMSA1*(T-H)+A1**2*H)/T
      RMSA2=(RMSA2*(T-H)+A2**2*H)/T
      RMSA3=(RMSA3*(T-H)+A3**2*H)/T
      IF(ABS(X1).GT.ABS(XMAX1)) XMAX1=X1
```

```
      IF(ABS(X2).GT.ABS(XMAX2)) XMAX2=X2
      IF(ABS(X3).GT.ABS(XMAX3)) XMAX3=X3
      IF(ABS(X4).GT.ABS(XMAX4)) XMAX4=X4
      IF(ABS(FNOW).GT.ABS(XMAXF)) XMAXF=FNOW
C
   10 continue
C
      IF(IFORCE.EQ.1)  F=FNOW
      IF(IFORCE.EQ.2)  F=FNOW
      IF(IFORCE.EQ.3)  F=FNOW
      IF(IFORCE.EQ.4)  F=FNOW
      IF(IFORCE.EQ.5)  F=FNOW
      IF(IFORCE.EQ.6)  F=FNOW
      IF(IFORCE.EQ.7)  F=FNOW
      IF(IFORCE.EQ.8)  F=FORCE1(T)
      IF(IFORCE.EQ.9)  F=FORCE2(T)
      IF(IFORCE.EQ.10) F=FORCE3(T)
      IF(IFORCE.EQ.11) F=FORCE1(T)+FORCE2(T)
      IF(IFORCE.EQ.12) F=FORCE1(T)+FORCE3(T)
      IF(IFORCE.EQ.13) F=FORCE2(T)+FORCE3(T)
      IF(IFORCE.EQ.14) F=FORCE1(T)+FORCE2(T)+FORCE3(T)
C
C     WRITE(6,'(a,i2,a,e10.3)') 'IFORCE = ',IFORCE,'  F = ',F
C     WRITE(6,'(A,e10.3)') 'FORCE3(T) = ', FORCE3(T)

C     if(iprint.eq.1) WRITE(6,16)T,X1,V1,X2,V2,X3,V3,X4,V4,F,SIDE
C     if(iprint.eq.2) WRITE(6,17)T,sqrt(RMSX1),sqrt(RMSV1),
C    $sqrt(RMSX2),sqrt(RMSV2),sqrt(RMSX3),sqrt(RMSV3),sqrt(RMSX4),
C    $sqrt(RMSV4),sqrt(RMSF),SIDE
C   16 FORMAT(F7.3,9(1X,E9.2),A)
C   17 FORMAT(F7.3,9(1X,E9.3),A)
      if(iprint.eq.1) WRITE(6,16)T,X1,X2,X3,X4,V4,F,SIDE
      if(iprint.eq.2) WRITE(6,17)T,sqrt(RMSX1),
     $sqrt(RMSX2),sqrt(RMSX3),sqrt(RMSX4),
     $sqrt(RMSV4),sqrt(RMSF),SIDE
   16 FORMAT(F8.3,6(1X,E10.3),A)
   17 FORMAT(F8.3,6(1X,E10.3),A)
   20 RETURN
      END
```

2. EXAMPLE OF INPUT DATA FILE[2]

```
force.out[3]
  10.0              m1
   1.0              m2
   0.1              m3
   0.4              c1
   0.04             c2
   0.0              c3
   0.0              c4
  40.0              k1
   4.0              k2
   0.4              k3
   0.0              k4
   0.0              t0
   0.5              H
300.0               Ttotal
   0.0              x10
  10.0              z10
   0.0              x20
   0.0              z20
   0.0              x30
   0.0              z30
   0.3              e
  30.0              dmin; if negative, incremented from the program
   0.0              dmax
  10.0              dinc
   0.025            m4
   1                IPRINT (1:TIME VARIATION; 2:RMS VARIATION)
   0                IFORCE (0: NO FORCE;
                        1 : F1;
                        2 : F2;
                        3 : F3;
                        4 : BOTH F1 & F2;
                        5 : BOTH F1 & F3;
                        6 : BOTH F2 & F3;
                        7 : F1, F2 & F3;
                        8 : sine on 1;
                        9 : sine on 2;
                        10: sine on 3;
                        11: sine on both 1 & 2;
```

---

[2]This example is for the structure excited by an initial velocity on the primary system.
[3]A file contains radom data is needed for the simulation of random excitation.

12: sine on both 1 & 3;
13: sine on both 2 & 3;
14: sine on 1, 2 & 3;)

3. EXAMPLE OF OUTPUT DATA FILE

```
m1   0.1000000E+02
m2   0.1000000E+01
m3   0.1000000E+00
k1   0.4000000E+02
k2   0.4000000E+01
k3   0.4000000E+00
k4   0.0000000E+00
c1   0.4000000E+00
c2   0.4000000E-01
c3   0.0000000E+00
c4   0.0000000E+00
t0   0.0000000E+00
ttotal  0.3000000E+03
H    0.5000000E+00
x10  0.0000000E+00
x20  0.0000000E+00
v10  0.1000000E+02
v20  0.0000000E+00
x30  0.0000000E+00
v30  0.0000000E+00
e    0.3000000E+00
dia
c
b
m4   0.2500000E-01
IPRINT  1
IFORCE  0
     t        x1            x2            x3            x4            v4          F(t)
-------------------------------------------------------------------------------------------
  0.000  0.000E+00  0.000E+00  0.000E+00  0.000E+00  0.000E+00
  0.500  0.404E+01  0.865E+00  0.417E-02  0.000E+00  0.000E+00
  1.000  0.411E+01  0.417E+01  0.106E+01  0.000E+00  0.000E+00
  1.500  0.570E+00  0.658E+01  0.502E+01  0.000E+00  0.000E+00
  2.000 -0.286E+01  0.327E+01  0.987E+01  0.000E+00  0.000E+00

  ... ...
```

```
 297.500  0.181E-02  0.922E-02  0.247E-01 -0.102E+02  0.107E+00
 298.000 -0.910E-03 -0.218E-02  0.672E-03 -0.101E+02  0.107E+00
 298.500 -0.287E-02 -0.119E-01 -0.257E-01 -0.101E+02  0.107E+00
 299.000 -0.298E-02 -0.143E-01 -0.387E-01 -0.100E+02  0.107E+00
 299.500 -0.137E-02 -0.837E-02 -0.287E-01 -0.994E+01  0.107E+00
d1 =  0.3000000E+02
x1 =  0.3619602E+00
v1 =  0.6889547E+00
a1 =  0.1553189E+01
x2 =  0.9958209E+00
v2 =  0.1903709E+01
a2 =  0.4304667E+01
x3 =  0.3036091E+01
v3 =  0.5267406E+01
a3 =  0.1249212E+02
x4 =  0.9978499E+01
v4 =  0.7187268E+01
f1 =  0.0000000E+00
X1 =  0.4111829E+01
X2 = -0.9562503E+01
X3 =  0.2795332E+02
X4 = -0.3946021E+02
F1 =  0.0000000E+00
```